



HAL
open science

Excitability and laser localized structures in semiconductor microcavities

Margherita Turconi

► **To cite this version:**

Margherita Turconi. Excitability and laser localized structures in semiconductor microcavities. Other [cond-mat.other]. Université Nice Sophia Antipolis, 2013. English. NNT: 2013NICE4021 . tel-00866115

HAL Id: tel-00866115

<https://theses.hal.science/tel-00866115>

Submitted on 26 Sep 2013

HAL is a multi-disciplinary open access archive for the deposit and dissemination of scientific research documents, whether they are published or not. The documents may come from teaching and research institutions in France or abroad, or from public or private research centers.

L'archive ouverte pluridisciplinaire **HAL**, est destinée au dépôt et à la diffusion de documents scientifiques de niveau recherche, publiés ou non, émanant des établissements d'enseignement et de recherche français ou étrangers, des laboratoires publics ou privés.

UNIVERSITE DE NICE-SOPHIA ANTIPOLIS-UFR Sciences

Ecole Doctorale

Sciences Fondamentales et Appliquées

THESE

pour obtenir le titre de

Docteur en Sciences

de l'Université de Nice - Sophia Antipolis

Discipline : PHYSIQUE

présentée et soutenue par

Margherita TURCONI

**Excitability and Laser Localized
Structures in Semiconductor
Microcavities**

Thèse dirigée par: Stéphane BARLAND

soutenue le 12 Avril 2013

Jury :

M. Alejandro GIACOMOTTI	-	Rapporteur
M. Franco PRATI	-	Rapporteur
M. Damià GOMILA	-	Examineur
M. Massimo GIUDICI	-	Examineur
M. Philippe GRELU	-	Examineur
M. Stéphane BARLAND	-	Directeur

Acknowledgments

First of all, I am especially grateful to my supervisor, Stéphane Barland, for the patient guidance, the support and the advices he has provided throughout my thesis. I feel honoured to have worked with such a passionate and brilliant researcher. Second of all, I am keen to thank Giovanna Tissoni, who has supervised the numerical work of this thesis and who has been a good friend. Her calm and positive attitude was contagious and motivational for me. Moreover I must acknowledge Bruno Garbin for working with me on the control of excitable pulses in an optically injected laser.

I would also like to thank the referees and all the jury members for the careful reading of this manuscript and for the useful comments that helped to improve it.

A lot of people, who have shared these three years with me at INLN, have contributed to make my PhD experience pleasant and enriching. Some people helped me with french language, some of them shared the silence and the darkness of the hours before the last bus, some of them gave me a lift to the closest train station when the last bus was missed, some others made me discover beautiful beaches and mountains, some of them became good friends, someone made me laugh, someone made me coffee... Among these people I am keen to mention the Ph.D students and post-docs whom I met at INLN through the last years: Florence, Marta, Marianne, Maryvonne, Nicolas, Tom, Louis, Laurent, Jean-François, Julien, Xiaoli, Riad, Quentin, Axel, Raouf, Alessio, Matthieu, Francesco, Mathias, Dong, Pippou, Taha, François, Bruno...

I would also like to thank my flatmates and friends who made my life in Nice so nice: Noémie, Guillaume, Catherine, Linda, Nicolas, Yaser, Anvar, Vinciane, LP, Michele, Silvia, Daniele, Sébastien, Garibaldi, Laurene, Clara, Pauline, Giorgio, Danila, Aria...

I can not forget to thank my friends in Italy who have supported me at distance and who have been always available and enthusiastic to see me during the weekends I could spend back home: Mara, Marta, Laura, Chiara, Michela, Monica, Eli, la Clé, Eleonora, Claudio Luca e Chiara.

There are some special people who, consciously or unconsciously, made a lot for me: Paul “the Great”, Marto and “dough”.

Lastly, but not least, I would like to thank my family for all their love and encouragement, I would not have contemplated this road if not for my parents.

I sincerely thank all of you.

Contents

1	Introduction	1
1.1	Localized Structures	1
1.1.1	Localized structures in optics	2
1.2	Excitability	4
1.2.1	Classification	5
1.2.2	Excitability in optics	8
1.3	Motivations and contents	9
2	Laser Localized Structures	11
2.1	Our cavity soliton laser	11
2.2	Properties of laser localized structures	14
2.2.1	Phase profile	16
2.2.2	Modal behaviour	17
2.3	Mutual coherence	22
2.3.1	Incoherent solitons	23
2.3.2	Coherent and interacting solitons	25
2.4	Conclusions	30
3	Response to an External Perturbation	31
3.1	Experimental Set-Up	32
3.2	Switch-On	36
3.2.1	Writing beam wavelength	37
3.2.2	Writing beam power	39
3.2.3	Writing beam polarization	41
3.3	Switch-Off	43
3.3.1	Erasing beam polarization	44
3.4	Injection Below the Bistability Region	44
3.4.1	Looking for excitable LCS	46
3.5	Conclusions	49
4	Drift-Induced Excitable Localized Structures	51
4.1	Influence of alignment on the system dynamics	52
4.2	Single point dynamics	54
4.2.1	Analysis of the bifurcation	55
4.3	Spatially resolved measurements	58
4.3.1	Drift-induced excitable localized structures	61
4.3.2	Oscillating localized structures	63
4.4	Conclusions	64

5	Excitable Localized Structures: Numerical Simulations	67
5.1	Model and dynamical equations	68
5.2	Self-pulsing cavity solitons	69
5.2.1	Characteristics of the dynamics	71
5.3	Excitable localized structures	72
5.3.1	Response to different perturbations	77
5.4	Conclusions	78
6	Control of excitable pulses	81
6.1	Experimental Set-up	82
6.2	Response to a perturbation	83
6.3	Threshold-like behaviour	85
6.4	Conclusions	86
7	Conclusions and Perspectives	89
A		93
A.1	Resonant Saturable Absorber Mirror	93
	Bibliography	95

Introduction

Contents

1.1 Localized Structures	1
1.1.1 Localized structures in optics	2
1.2 Excitability	4
1.2.1 Classification	5
1.2.2 Excitability in optics	8
1.3 Motivations and contents	9

This manuscript is centered on localized structures and excitability. Both topics are of general interest since they are phenomena that are observed and studied in different systems. Among those, optical systems are particularly interesting because of the possibility of future applications in the all-optical processing of information. This introduction aims to remind the main features of these phenomena and to illustrate the contents of the present manuscript.

1.1 Localized Structures

Localized structures refer to self-organization of a physical quantity in one or more isolated regions surrounded by a homogeneous and qualitative different state. This phenomenon occurs in spatially extended and dissipative systems and they are also called dissipative solitons or autosolitons. Localized structures were probably first remarked by Faraday in the nineteenth century during his studies on pattern formation in liquids in contact with vibrating surfaces [Faraday 1831], then they have widely been studied both theoretically and experimentally since the 1980's [Koga 1980, Laughlin 1983, Rosanov 1990, Kerner 1994]. Localized structures have been observed in a large variety of systems, for instance: in vertically vibrated granular media [Umbanhowar 1996] (Fig 1.1a) where they look like isolated heaps of sand, in colloidal suspensions where they look like localized oscillations (also called oscillons) of the colloid level respect to the background level [Lioubashevski 1999] (Fig. 1.1b), and in gas discharge experiments where they appear as isolated current filaments [Astrov 1997] (Fig 1.1 c). In the following we will focus on localized structures in optics.

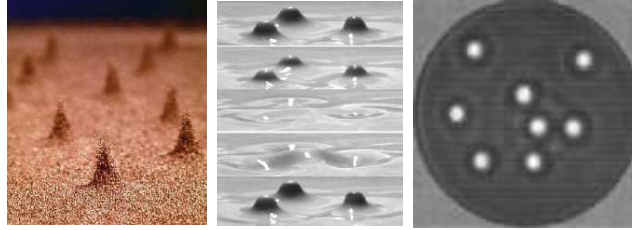


Figure 1.1: Localized structures in different systems: a) vertically vibrated granular medium (taken from [Umbanhowar 1996]), b) vertically vibrating colloids (taken from [Lioubashevski 1999]), c) gas discharge experiments (taken from www.uni-muenster.de).

1.1.1 Localized structures in optics

In optics, localized structures look like high(low) intensity peaks on a homogeneous and darker (brighter) background in the transverse plane perpendicular to the propagation direction. They are also known as cavity solitons (CS). In this thesis both appellations are used. The term “soliton” was first introduced to describe solitary waves that propagate without changing shape in conservative systems, where their formation is understood in terms of compensation between diffraction and nonlinearity. The term “cavity” describes the dissipative character of the system where these solitons form, because of the compensation of diffraction and nonlinearity and of energy input and energy output. An analogous mechanism can occur along the propagation direction in non spatially extended systems, in this case the non linearity compensates the chromatic dispersion, giving birth to temporal cavity solitons [Grelu 2012].

Cavity solitons, or Localized structures, possess very interesting properties:

- i) their size and shape do not depend on the boundary conditions but they are well determined by the balance between energy input and losses and between nonlinearity and diffraction;
- ii) they can exist in several positions of the transverse plane;
- iii) they are bistable which means that the bright spots are stable for the same parameters as the homogeneous dark state;
- iv) they can be independently manipulated which means that one LS can be switched-on and -off (because of the bistability) by a local perturbation without affecting a neighbouring localized structure;
- v) they can move spontaneously or they can be moved by applying an external gradient.

In virtue of these properties, CSs can be used as optical binary bits that can be processed in parallel. The position of cavity solitons can be fixed by introducing a spatial modulation in one parameter of the system, so that the CSs result trapped in the desired points of the space, under the action of opposite gradients. In this way,

an optical memory array, whose pixels are the CSs, can be realized. The potential of CSs for optical storage and parallel processing of information was recognized and stressed in [Firth 1996, Brambilla 1997, Coulet 2004].

Applications require compact and fast devices. Therefore, semiconductor microcavities represent a good candidate among all the optical systems where CS have been realized. The first experimental evidence of localized structures in semiconductor microcavities is reported in [Barland 2002]. The experimental set-up consists in a broad-area Vertical Cavity Surface Emitting Laser (VCSEL) pumped below threshold and driven by a holding beam. VCSELs are semiconductor microcavities composed of two high-reflectivity distributed Bragg reflectors, the active medium consists of quantum well structures which can be pumped electrically or optically. The cavity length is of few microns and the broad-area emitting surface has a diameter of 200 μm . In [Barland 2002] and [Hachair 2004], the authors show that CS can be manipulated independently by an external optical perturbation with a suitable phase with respect to the holding beam. In [Pedaci 2006], the phase of the holding beam was spatially modulated and the optical memory array was realized.

Other applications, which exploit the CS motion induced by gradients, were experimentally realized with the same set-up: an optical delay line [Pedaci 2008] and the mapping of inhomogeneities of the microcavity hosting the CS [Pedaci 2005].

1.1.1.1 Cavity soliton lasers

The experiment, which we reported on above, requires a driving beam of high spatial and temporal coherence. Now, it seems to be attractive, for applications, to remove the necessity of such holding beam and to deal only with inexpensive incoherent sources like an electric power supply or a high-power laser diode of low coherence. This implies going from a driven system to a laser, i.e. an active device where emission is self-sustained. A laser device able to host localized structures is called Cavity Soliton Laser (CSL). That is a laser which, although homogeneously pumped over its transverse section, emits isolated beams (the cavity solitons) surrounded by regions of pure spontaneous emission. These laser localized structures (or laser cavity solitons) differ from the localized structures in driven systems, whose polarization and frequency is locked to the one of the holding beam. A laser localized structure is like a microlaser and, as any laser, it has the freedom to choose its phase because it originates from a spontaneous symmetry breaking. Moreover, assuming that the cavity is sufficiently isotropic and broadband, the output frequency and polarization are also undetermined including the possibility of multi-frequency operation which could result in irregularly or regularly self-pulsing localized structures [Ackemann 2009]. Therefore in a CSL, every single CS within the laser aperture should have the freedom to chose between all these possibilities. This gives exciting new opportunities for fundamental studies as well as applications.

Three cavity soliton lasers based on two different physical mechanisms have been realized with semiconductor materials.

The two physical mechanisms that allowed to realize a Cavity soliton laser are:

the frequency-selective feedback from a Bragg grating and the saturable absorption. The experiment, exploiting the frequency-selective feedback, is described in [Tanguy 2008a]. In the case of saturable absorption, two different experimental setups were adopted: two mutually coupled VCSELs, one of which is pumped above transparency (the amplifier), and the other below transparency (the saturable absorber), in a face-to-face configuration [Genevet 2008]; and an optically-pumped monolithic VCSEL with integrated saturable absorber [Elsass 2010b].

1.2 Excitability

Excitability is defined by the response of the system to perturbations: perturbations below a certain threshold decay to the initial stable state, while perturbations overcoming the threshold result in the system running through a large and well defined excursion in phase space before returning to its original state. The time that passes before the system can be excited again is called refractory-time.

Excitability was initially introduced in physiology, to describe the spiking activity of neurons [Hodgkin 1952] (i.e. the generation of an abrupt and transient change of the membrane potential) then it has been extended to many other systems which are able to present this well-calibrated threshold-like response. Besides the neuron, among the paradigmatic examples we find the cardiac tissue and the bromate-malonic acid chemical reactions (Belousov-Zhabotinsky (BZ) reaction [Belousov 1959, Zhabotinsky 1964]). In a spatially extended excitable system (excitable medium) each elementary part of the system possesses the property of excitability, so by means of a spatial coupling mechanism a local excitation is transmitted in the neighbouring regions without decrement. In the above examples, the coupling is the diffusion.

In one-dimensional media one observes traveling waves as, for instance, neural spikes propagating along the axon. As the dimensions are increased the effects of this nonlinear phenomenon are more spectacular. In two-dimensional media such as a thin layer of an unstirred solution with a BZ reaction, one can observe rotating spiral waves [Winfree 1972, Zhabotinsky 1973] (see Fig. 1.2a). When the solution is unstirred, local oscillations of concentration can be ignited by pacemakers (inhomogeneities or external local perturbation) and then propagate in concentric rings. These propagating waves are described as fronts of excitation followed by refractory zones (see Fig. 1.2b). When two waves generated by two different pacemakers collide, they mutually annihilate as we can see on the top left corner of Fig. 1.2b). Because of the constant propagation velocity, the waves created by the faster pacemaker (the central one in Fig. 1.2b) will spread over the whole space, forming a target pattern. The spiral waves are originated from the break of an expanding excitation front caused by a defect or a local perturbation. Spirals waves together with their three-dimensional counterparts, the scroll waves [Winfree 1973], have also been found in the heart muscle in association with cardiac pathologies such as tachycardia and arrhythmia [Davidenko 1992, Gray 2012].

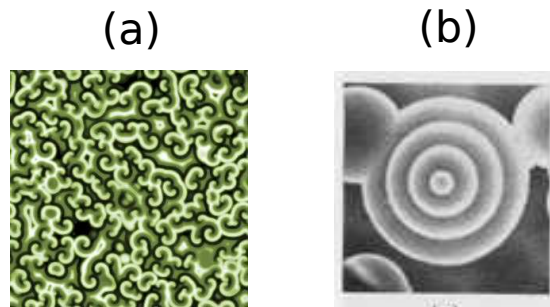


Figure 1.2: Snapshots of concentration waves in two-dimensional Belousov-Zhabotinsky reaction. (a) spiral waves (numerical simulation taken from wikimedia.org); (b) concentric wave propagation resulting in a target pattern (from scholarpedia.org).

These are some examples that give a hint on the richness of the phenomena linked to excitability and on their importance. For instance excitability describes the behaviour of some of the most vital parts of our body: heart and neurons. The latter are responsible for the transmission and processing of information. These computational properties can be exploited in other contexts. For instance BZ-like reaction have been used to find the minimum-length paths in complex labyrinths [Steinbck 1995], for image processing [Kuhnert 1989] and for constructing logic gates [Gorecka 2006].

In the next sections we will describe the different kinds of excitability and report on excitability in optics.

1.2.1 Classification

Excitable systems do not behave all the same: different excitable systems can react differently to the same perturbation and possess different properties. It is therefore important to know which stimulus is able to trigger the excitable response and how this response looks like in order to understand and to eventually exploit the computational properties of the system.

The first classification of excitability aimed to distinguish different kinds of neurons and it was done by Hodgkin. He injected steps of current into the axons membranes and looked at the resulting firing activity as function of the current amplitude. This method can be seen as the precursor of the bifurcation analysis . A Bifurcation is a qualitative change in the dynamics of a system upon variation of its parameters. In dynamical systems, the bifurcation analysis is a powerful tool for understanding complex non-linear phenomena even without knowing all the details of the system. Excitability is one of the phenomena that has been explained by this theory.

We present in what follows the classification resulting from the study carried out by Hodgkin and from the bifurcation theory. Both are currently used to describe excitable systems.

1.2.1.1 Hodgkin classification

Hodgkin was the first to perform a study on the bifurcation mechanism of excitability. His work is based on the analysis of the response of different squid axons in the resting state to a sudden application of constant current with various amplitudes [Hodgkin 1948]. He could distinguish three kinds of responses:

- *Class I.* The generated spiking state can have an arbitrary low frequency depending on the amplitude of the applied current.
- *Class II.* Spikes are generated within a certain frequency band which is relatively insensitive to changes in the strength of the applied current.
- *Class III.* Only a single spike is generated; repetitive spiking may occur only for very strong currents.

Neurons belonging to different classes have different computational properties. For example *Class I* neurons may encode the strength of a constant input into the frequency of the output while *Class II* neurons can act as threshold elements and reveal when the input is above a certain value.

1.2.1.2 Bifurcations

Dynamical system theory explains that, no matter the nature of the examined system, excitability appears close to a bifurcation that leads to the emergence (or disappearance) of a limit cycle. Such bifurcations are three:

- i) *saddle-node on invariant circle bifurcation* that occurs when a stable equilibrium and an unstable one merge and annihilate each other on an invariant circle, giving rise to a limit cycle of infinite period;
- ii) *saddle-loop bifurcation* when the limit cycle becomes an homoclinic orbit to the saddle point and its period becomes infinite;
- iii) *supercritical Andronov-Hopf bifurcation* that consists in the loss of stability of a stable focus giving birth to a limit cycle;

The phase portraits corresponding to the above bifurcations are illustrated in Fig. 1.3. The system is excitable when, before (or after) the bifurcations, only one steady state results stable (right column of Fig. 1.3).

The shape of the excitable response is defined by the limit cycle close to the bifurcation (left column of Fig. 1.3). When a perturbation above threshold is applied, the system undergoes a trajectory (thick line) that passes in the proximity of this limit cycle. In the cases i) and ii) the threshold is well defined: it consists in the stable manifold of the saddle (white circle in the figures). Hence an all-or-none behaviour is observed. Conversely in the Hopf bifurcation the threshold is not so well-defined, a small deviation from the resting state results into a short trajectory while a large deviation produces a large excursion corresponding to the excitable response (the two

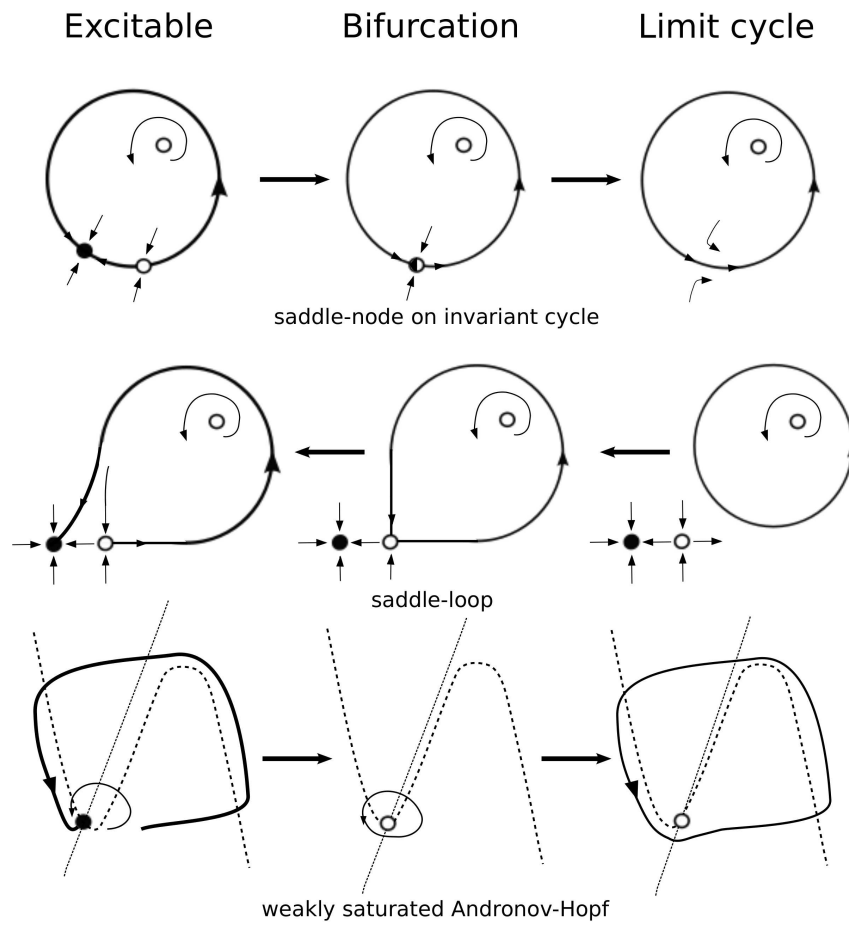


Figure 1.3: Three bifurcations leading to excitability. The thick arrows show the direction of the bifurcation parameter change. Stable nodes and focuses are represented by black circles while saddle points and unstable focuses by white circles. Stable limit cycles have solid lines while unstable one have dashed lines.

trajectories are sketched in the last excitable portrait of Fig. 1.3). Between the two trajectories there is a region which is referred to as a threshold-set [Izhikevich 2007] and which consists of trajectories corresponding to not-full amplitude responses. When the Hopf bifurcation is weakly saturated (iii), this threshold-set is very narrow (in real systems it can be even smaller than the noise level) so the system exhibits an effective all-or-none behaviour.

According to the Hodgkin classification, since at the *saddle-node on invariant circle bifurcation* and *saddle-loop bifurcation* the limit cycle has infinite period, the resulting excitability belongs to the *Class I*. On the other hand, the *Weakly saturated Hopf bifurcation* gives birth to a limit cycle which has a certain non-zero frequency thus the corresponding excitability is a *Class II*.

1.2.2 Excitability in optics

Among other systems in physics, optical systems can also exhibit excitable behaviour. Both classes of excitability has been observed.

On one hand Class I has been found in lasers with optical feedback [Giudici 1997] and laser with optical injection [Goulding 2007] (saddle node on invariant cycle bifurcation) or in laser with saturable absorber [Plaza 1997] (saddle-loop bifurcation). On the other hand Class II has been observed in optical amplifiers [Barland 2003] (Hopf bifurcation) and in active photonic crystals [Brunstein 2012].

Excitable optical systems were proposed for applications such as optical switch, since they react only in response to sufficiently large input signals, and pulse-reshaping, since a noisy and dispersed pulse which is sufficiently powerful can generate a well-contrasted and strong pulse.

The above-mentioned systems have very small spatial extension therefore the observed excitable behaviour has a global character and no propagation of excitable waves has been observed. Instead propagation could be observed in a vertical-cavity semiconductor optical amplifier, a device that can be described as a two-dimensional excitable medium [Marino 2005]. In [Marino 2005] authors report on an interesting dynamical scenario that involves both wave propagation and stationary patterns by showing that the excitable wave propagation is confined on a Turing pattern.

More studies involve extended optical system and are situated at the intersection between excitability and phenomena of self-organization [Gomila 2005, Jacobo 2008]. These studies are numerical, no experiment has been done yet. In [Gomila 2005] authors demonstrate the existence of excitable localized structures in a paradigmatic model for a Kerr cavity. The excitability described in [Gomila 2005] is locally confined since it is a property of the localized structure while the medium that hosts the structure (the Kerr cavity) is not excitable. Therefore, this kind of structures could be found in any other system supporting LSs provided that there is a mechanism able to induce oscillations of the LS amplitude that eventually bifurcate to excitable dynamics. The concept of excitable localized structures opens new perspectives in terms of applications in the information processing by combining the computational properties of excitable systems and the parallelism of localized structures. Logical

operations have been already realized numerically [Jacobo 2012].

1.3 Motivations and contents

My work aimed to study laser localized structures and excitability in semiconductor laser systems and to investigate the possibility of the intersection of both phenomena: the excitable localized structures. Both LS and excitability in optics, especially in fast materials like semiconductors, are interesting for application in the all-optical information processing. Excitable localized structures is a recent concept rising from numerical studies that would offer appealing perspectives for more functional applications. In this thesis we report on the first experimental investigation of this innovative topic. Properties of Laser localized structures (included excitability) have been studied in a system composed of two coupled broad-area semiconductor-microcavities in a LSA (Laser with Saturable Absorber) configuration [Genevet 2008]. Using a model of a VCSEL (Vertical Cavity Surface Emitting Laser) with intracavity saturable absorber [Bache 2005], we have also performed numerical simulations in order to look for excitable localized structures in this kind of system. A different system without spatial dependence is used to look experimentally for the mere excitable dynamics: a small-area VCSEL with optical injection.

The manuscript is structured as follows. In Chapter 2 we report on the characteristics of the observed laser localized structures and on their interaction. In Chapter 3 the response to an external local perturbation is analyzed. The characteristics of the perturbation that allow to control the stable stationary LSs in our system are investigated. Moreover, we study the response to a perturbation applied to the homogeneous non-lasing state for parameters out of the LS bistability in order to look for excitable localized structures.

In Chapter 4 we analyze the bifurcation occurring at the onset of lasing when a localized structure nucleates on a defect and then drifts because of gradients, showing that such a bifurcation possesses the characteristics of a bifurcation that describes excitable dynamics. In Chapter 5 we report on the numerical results about excitable localized structures in a semiconductor LSA. In Chapter 6 the experimental results about excitability in a small-area optically injected VCSEL are illustrated.

Laser Localized Structures

Contents

2.1	Our cavity soliton laser	11
2.2	Properties of laser localized structures	14
2.2.1	Phase profile	16
2.2.2	Modal behaviour	17
2.3	Mutual coherence	22
2.3.1	Incoherent solitons	23
2.3.2	Coherent and interacting solitons	25
2.4	Conclusions	30

In this chapter the cavity soliton laser based on saturable absorption, which we studied experimentally, will be briefly illustrated. Then coherence properties of laser localized states will be pointed out. Eventually some observations about interaction between different localized structures in guise of phase synchronization and of non-local coupling will be reported.

2.1 Our cavity soliton laser

A scheme of the experimental set-up is reported in Fig. 2.1. For a detailed description of the system and its working principles see [Genevet 2008, Genevet 2009b, Genevet 2009a], here we will point out important aspects for our purpose. The physical system correspond to the portion that is highlighted by a red rectangle and it is composed of two semiconductor laser resonators L_1 and L_2 , a beam splitter BS, two collimators C whose focal length is 8 mm and two lenses L whose focal length is 5 cm. The rest is the detection system.

L_1 and L_2 are two nominally identical broad area (200 μm) Vertical Cavity Surface Emitting Lasers (VCSEL), both of them are equipped with temperature and current control, respectively T_1 , I_1 and T_2 , I_2 . They are placed face-to-face at distance of about 30 cm.

The coupling strength between the two devices is given by the beam-splitter BS placed in external cavity, its transmission depends on the polarization: 80% for p-polarization and 60% for s-polarization. The polarization symmetry¹ is then broken

¹ VCSELs, unlike edge emitter semiconductor lasers, support both linear polarization and their combination (circular, elliptical). This is due to the circular symmetry of the VCSEL cavity.

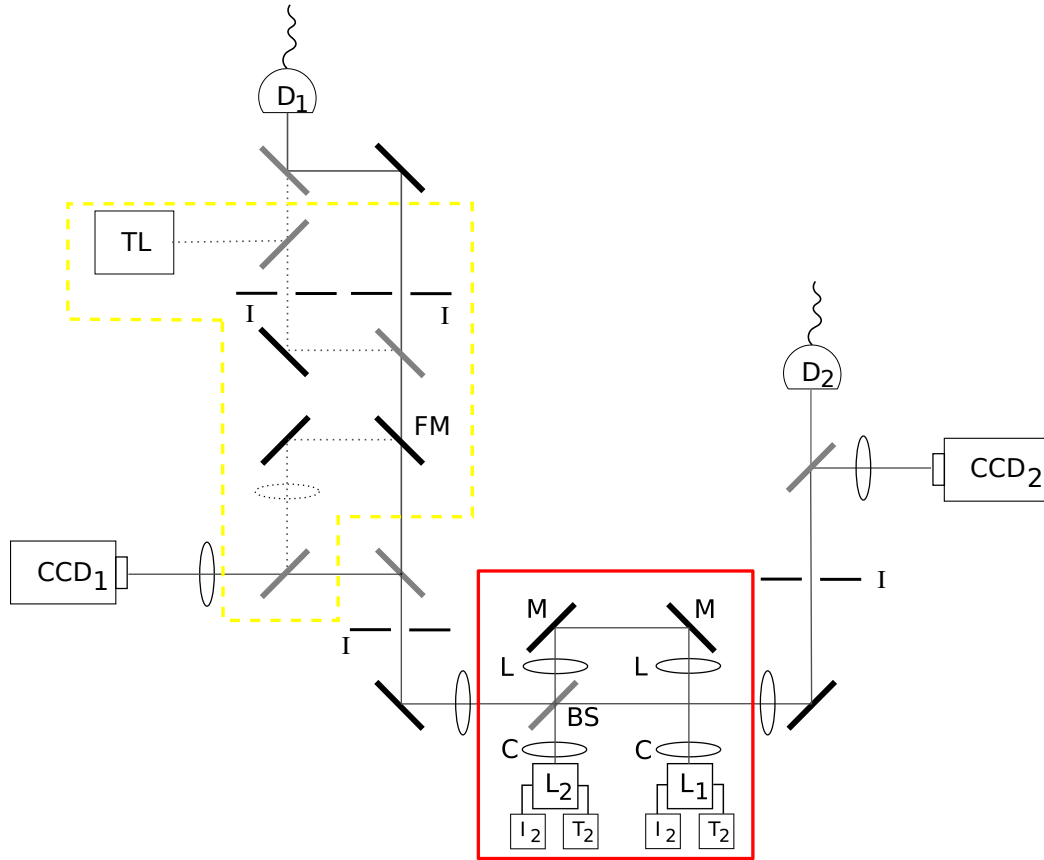


Figure 2.1: Schematic of the experimental set-up. The physical system is encircled in red. L_1 , laser above transparency; L_2 , laser below transparency; C , aspherical collimator (focal length = 8 mm); L , lenses (focal length = 5 cm); BS (and all grey slashes), beam splitters; M (and black slashes), mirrors. Outside the red square we have the detection system. $CCD_{1,2}$, Charged Couple Device camera (20 Hz); $D_{1,2}$, fibre-coupled amplified photo-detector (8 GHz); I , iris diaphragm. The yellow dashed-line part is added for the analysis of the coherence properties of localized structures and it is discussed in section 2.2. FM , flipping mirror; TL , tunable laser.

and radiation in the cavity ends up being p-polarized since losses are smaller for this polarization. The 20% reflected light goes for detection. Two branches are available: one collecting light from the amplifier L_1 and the other from the absorber. In both branches a CCD camera monitors the time-averaged near field emission and a 8GHz fibre-coupled amplified photo detector (D_1 and D_2) enables for time resolved measurements. An iris, positioned on a plane conjugated to the CCD's plane, is used to select the spatial region which we want to monitor. We used a multi-mode fibre for the temporal measurements and we checked that the area selected by the iris is smaller than the area which is coupled into the fibre.

By means of the collimators C and lenses L , the near-field of one resonator is imaged onto the plane of the near-field of the other one with magnification equal to one (1 to 1 self imaging configuration). The alignment procedure is done biasing both

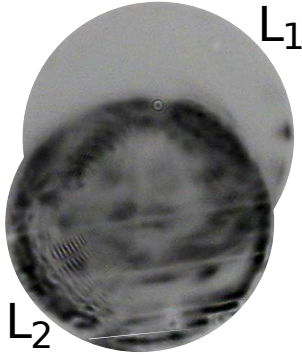


Figure 2.2: Near field image on the plane of the L_1 when self-imaging is accomplished (dark areas correspond to high intensities). We observe the spontaneous emission of L_1 which is biased at few mA and the image of L_2 which is reflected by the exit mirror of L_1 (the reflection also partially occurs on the substrate of L_1 since the two lasers are not perfectly superimposed). L_2 is biased at more than one hundred mA and it is lasing because of feedback provided by the exit mirror of L_1 and its substrate .

lasers and by looking at their emitted radiation on the cameras. The self-imaging is achieved when the round emitting faces of the two VCSELs appear clear on both camera with the same size like in Fig. 2.2.

The self imaging configuration compensates diffraction occurring during propagation in the external cavity, keeping the Fresnel number high. Large Fresnel number is a condition required for the existence of localized states together with bistability [Lugiato 2003]. Bistability is provided by the mechanism of saturable absorption. More precisely L_1 is biased above transparency ($I_1 \approx 200 - 300$ mA) and it plays the role of amplifier while L_2 is kept below transparency ($I_2 \approx 10$ mA) and it behaves as an absorber [Genevet 2008]. For the saturable absorption to be effective, the cavity-resonances of L_1 and L_2 have to overlap, otherwise the two devices will see each other as mere mirrors. Resonance matching is achieved by setting properly the temperatures of the two devices.

Temperature influences the refraction index of the semiconductor medium and so the effective cavity length of the resonator. The cavity-resonance change of our VCSELs has been measured as 0.114 nm/ $^{\circ}$ C [Genevet 2009b]. A similar effect is given by the bias current because of Joule heating. The corresponding cavity-resonance change is of 0.005 nm/mA. Therefore, the temperature of the two devices should be set in order to compensate the wavelength mismatch due to the different biasing ($I_1 > I_2$). Supposing the two devices are the same (same wavelength in the same operating conditions), the temperature difference should be: $T_2 - T_1 \approx 8^{\circ}$ C. See [Genevet 2009b] for a detailed analysis of the parameter region for the correct functioning of the cavity soliton laser.

Once the good parameters are settled, the evolution of the near field shows well defined features as the current of the amplifier I_1 is increased from zero [Genevet 2008]. First of all we observe an increase of the global intensity because of the feedback due to reflexion on L_2 exit mirror. Feedback reduces losses in the compound system that eventually starts lasing.

Then the increasing Joule heating makes L_1 approach the resonance with L_2 and the two devices start interacting, so the global intensity decreases due to the absorption from L_2 . Most of the compound system is not lasing anymore, we are in the off-state where the very weak radiation emitted is spontaneous emission. In this conditions

some bright spots can arise abruptly as we keep increasing the current I_1 and they persist as the current is decreased again. The hysteresis cycle observed in the best conditions is about 5 mA and it can be reduced down to tenths of mA in the worst cases.

These bright spots are compatible with the definition of cavity solitons: they have very well defined size (15 μ m of diameter), they are surrounded by a homogeneous dark back-ground and they are stable for a certain range of parameters where the background is also stable (within the hysteresis cycle mentioned above); furthermore they can be switched on and off independently [Genevet 2008].

Our cavity solitons laser is working.

Moreover, it is worth to point out that, compared to their counterparts born in driven systems, these cavity solitons arise from spontaneous emission as any free-running lasers and thus they have the freedom to choose their own phase. They are then called laser cavity solitons. Laser cavity solitons are only a part of the family of laser localized structures (LLS). Other LLS have been observed in our system: multi-peaked structures (clusters of LCS) and ring structures with phase singularity (vortices)[Genevet 2010a].

In the following we are going to analyze the coherence properties of laser localized structures and their interactions.

2.2 Properties of laser localized structures

We've already mentioned that the phase of LLS is arbitrary, we should also say that the lasing frequency can be chosen by the system between the modes of the external cavity that lie in the gain bandwidth. A single VCSEL usually operates in a single longitudinal mode because of the short resonator length (of the order of μ m). Two consecutive longitudinal modes result very far away and only one lies within the gain curve. The distance between two consecutive longitudinal modes in a Fabry-Perot resonator is called Free Spectral Range: $FSR = c/(2L)$.

When we add an external cavity, the corresponding cavity modes become accessible. The external cavity length (i.e. the distance L_1 - L_2) considered in this chapter is $L = 32$ cm that corresponds to a free spectral range $FSR = c/(2L)$ of 465 MHz. Due to the presence of several modes under the gain curve, the lasing process can be affected by multi-mode emission, and frequency multi-stability. In this section we will report observations about the coherence properties of LLS focusing on the spectral properties of the emission and on the extension of the phase profile. Our observations are mainly based on interferometric and spectral measurements.

We built a Mach Zehnder-like interferometer by taking the beam directed towards the fast detector D_1 with a flipping mirror and readdressing it onto the camera CCD1 (see Fig. 2.1) in such a way that the two near fields perfectly overlap. In a regular Mach Zehnder interferometer, the two beams are perfectly aligned in order to measure their exact phase difference. We leave voluntarily a tilt between the two beams in order to get a fringes pattern and study qualitatively the frequency and

phase emission of laser solitons.

It is worth to remind the mathematical expression of the two wave interference in order to understand what we can work out from observations of the interference pattern.

Let us consider two monochromatic waves U and U' coming from the same coherent source and arriving on the plane of the camera. Each point of the space is described by the vector \vec{x} , U comes from the reference arm of the interferometer while U' comes from the other arm and it accumulates a phase delay ϕ during propagation:

$$U(\vec{x}, t) = A(\vec{x})e^{i(\vec{k}\cdot\vec{x}-\omega t)} \quad U'(\vec{x}, t) = A'(\vec{x})e^{i(\vec{k}'\cdot\vec{x}-\omega t+\phi)}$$

$A(\vec{x})$ and $A'(\vec{x})$ are the space-dependent amplitudes; k and k' the wave vectors, ω and the angular frequency. The observable intensity in a point \vec{x} resulting from the interference of the two waves is given by:

$$I(\vec{x}) = |A(\vec{x})|^2 + |A'(\vec{x})|^2 + 2A(x)A'(x)\cos\left(\frac{c}{\lambda}(\hat{r} - \hat{r}') \cdot \vec{x} + \phi\right) \quad (2.1)$$

where $\vec{k} = \frac{c}{\lambda}\hat{r}$ and $\vec{k}' = \frac{c}{\lambda}\hat{r}'$. The first two terms on the right hand side of eq. 2.1 correspond to the intensities of the single waves and the third one is the interference term. The interference term consists in periodic fringes perpendicular to the difference of the two wave vectors. The fringes period depends on the wavelength. The visibility of the fringes is defined as:

$$Visibility = \frac{\max(I(\vec{x})) - \min(I(\vec{x}))}{\max(I(\vec{x})) + \min(I(\vec{x}))}$$

The maximum value of the visibility is 1 and it is reached when the amplitudes of the two waves coincides: $A(\vec{x}) = A'(\vec{x})$. We can think that U and U' describe LCSs in our interferometer. If they are monochromatic, the visibility on the camera will be high, otherwise, the visibility will decrease. In fact, if LCSs are polychromatic the interference pattern results in the sum of different cosine terms (as in eq. 2.1) that have different periods and amplitudes, so the global visibility will be affected. An example of this kind of interferometric measurements is reported in Fig 2.3.

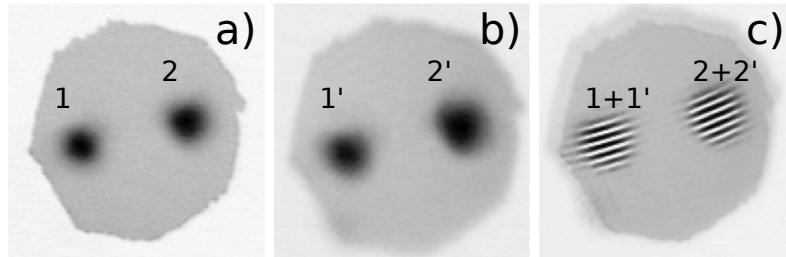


Figure 2.3: Spatial intensity distribution of the near field coming from the one arm of the interferometer (a), from the other (b). (c) is the interferogram resulting from the superposition of the two arms. System parameters are the same: $I_1 = 188.8$ mA, $I_2 = 11.1$ mA.

We name with integers the localized structures of interest that are observed in the near field image of the first branch of the interferometer (the one that goes directly to CCD1 after the beam splitter) and with primed integers the same structures coming from the other branch. When the two beams (Fig. 2.3 a) and b)) are superimposed, a fringed pattern appear (Fig. 2.3 c)). The fringes are visible only on the bright region occupied by the laser solitons, this means that the emission of both structures is coherent while the one of the background is not. Moreover the fringes are well contrasted so probably the laser solitons are emitting on a single longitudinal mode. This supposition can be confirmed by spectral measurements.

In order to perform the spectral analysis we flip-on the flipping mirror in such a way that the output beam can reach the optical fibre (D_1 in the set-up scheme Fig. 2.1). Then the optical fibre may be put in an optical spectral analyzer or in a detector connected to a power spectrum analyzer. The power spectrum will allow to study the modal composition of a structure within a bandwidth from 9 kHz to 8 GHz (limit given by the detector) while the optical spectrum will be used for a coarse analysis (the resolution bandwidth of OSA hp86142 is 60 pm that corresponds to approximately 20 GHz at 980 nm).

It is worth to underline that when the two devices are interacting (necessary condition in LS regime), there is no qualitative difference between the near-field profile observed in the plane of L_1 (on CCD1) and the near-field profile observed in the plane of L_2 (on CCD2) [Genevet 2008]. Hence the choice to base our analysis on measurements made on the detection branch 1 does not neglect any important aspects.

2.2.1 Phase profile

We observe experimentally that the spatial range of coherence of a localized structure is broader than its area. This is because the phase profile of a localized structure has a diameter much larger than the one of intensity profile. This characteristic was theoretically found in solitary waves generated in general dissipative systems with subcritical instability [Fauve 1990] and more recently it has been pointed out in [Vahed 2011] in the case of semiconductor laser with saturable absorber. In [Vahed 2011], the spatial extension of the phase profile is responsible for interaction among cavity solitons which we will talk about in section 2.3.

The general method to analyze the phase profile of an electromagnetic beam is based on interference between the electromagnetic beam and a reference coherent plane wave. This reference beam can be obtained in our system by modifying slightly the interferometer previously described by adding a short focal-length lens in one branch of the interferometer (see dotted lens in Fig. 2.1). This operation allows to expand a coherently-emitting region of the output beam (for example a CS) such that it is much larger than the global output beam waist of the system. The reference beam and the output beam are then recombined on the CCD camera.

With this method we will measure the phase profile of a LCS. We select an area of the near field where at least one LCS is stable (Fig. 2.4 a) one structure is

expanded in one arm of the interferometer to form the reference beam (Fig. 2.4 b). The result of the interferometer is a fringe pattern (Fig. 2.4 c). The shape of the fringes is due to the tilt between the two beams and on the phase profile of the reference beam (probably not completely flat but parabolic because of the lens).

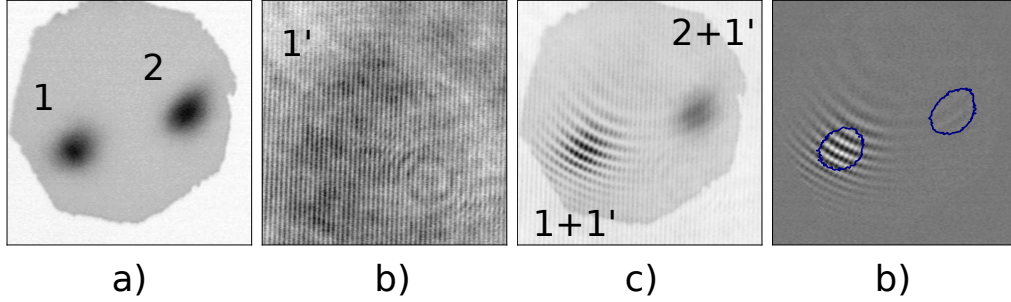


Figure 2.4: Two localized structures appear on the near field intensity distribution (a). Structure 1 is expanded to form a reference beam (b). Combining (a) and (b) on the camera we obtain the interference pattern (c). Fringes are visible on structure 1 (c)-(d) and they occupy a wider region of space compared to the structure diameter (blue line in (d)). (d) is the elaboration of images (a)(b)(c) in order to highlight the interference fringes: $d = c - (a + b)$. System parameters are: $I_1 = 185.8$ mA $I_2 = 9.9$ mA (left).

The interference pattern can be isolated for a better clarity by mathematical operation between the intensity matrices of images (a),(b) and (c). In order to work out the interference term from eq. 2.1, we should subtract the sum of the single beam intensities from the total intensity $I(\vec{x})$. In this way we obtain Fig. 2.4 (d): $d = c - (a + b)$. Then we compare the size of the interference pattern with the size of the cavity soliton (Fig. 2.4 d). The fringes are visible over an area that has a diameter three times the diameter of the soliton. Therefore the phase is well defined even in the surrounding of the cavity soliton where the emission is very weak (at noise level). These experimental observations are compatible with the results of the numerical work [Vahed 2011] even though we did not delve deeper, studying for example the shape of the phase profile. The phase profile plays a key role in formation of clusters [Genevet 2010c] and in interactions with different solitons [Vahed 2011].

2.2.2 Modal behaviour

In our system LCSs that have been observed so far are essentially monochromatic and they can undergo mode hopping. That is a sudden switch to another resonator mode under some external perturbation. Mode hops are possible since cavity solitons lasing at different frequencies share part of their stability domain. Then the final lasing frequency depends on the history of the system and it can be swapped by some perturbations as described theoretically and experimentally in [Genevet 2010b]. Possible causes of mode hops are: drift of temperature, noise or small vibrations of the optics that form the resonator.

Here we demonstrate that LCS can be multi-mode and that monochromatic and multi-mode LCSs can coexist on the transverse plane of the system for the

same range of parameters. Then we will show that mode hopping is a general phenomenon happening to different localized structures hosted in our system. Eventually we will say a little bit more about multi-mode laser solitons.

Fig. 2.5 displays the intensity distribution of the superposition of the two near fields upon decrease of the current I_1 within the bistability region. Four bright

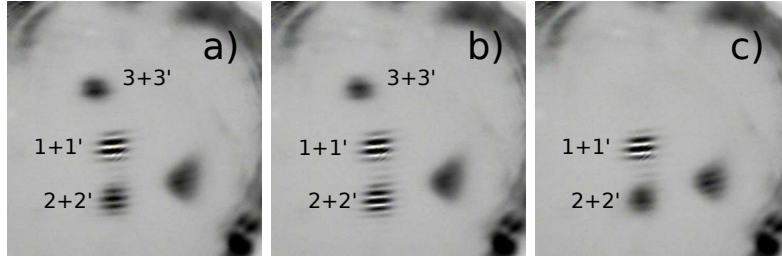


Figure 2.5: Intensity distribution of the interferogram obtained splitting the output beam into two beams and then recombining the two near-field images on the camera (dark areas correspond to high intensities). Fringes visibility of structure 2 changes upon decrease of the amplifier bias within the bistability domain. (a) $I_1 = 197.8$ mA: structures 1, 2 and 3 just switched on. (b) $I_1 = 197.3$ mA. (c) $I_1 = 196.1$ mA: structure 3 just switched off. Structures 1 and 2 are stable until $I_1 = 195.6$ mA. For all the three cases $I_2 = 9.5$ mA.

spots are visible in figure 2.5 (a), structures 1, 2 and 3 have just switched on simultaneously² (within the integration time of the camera) for $I_1 = 197.8$ mA while the structure on the side is not bistable thus it can't be classified as LS.

We will focus our attention on the evolution of the fringes of structures 1 and 2, for this reason we also show and compare the intensity profile along a line perpendicular to the fringes in Fig. 2.6.

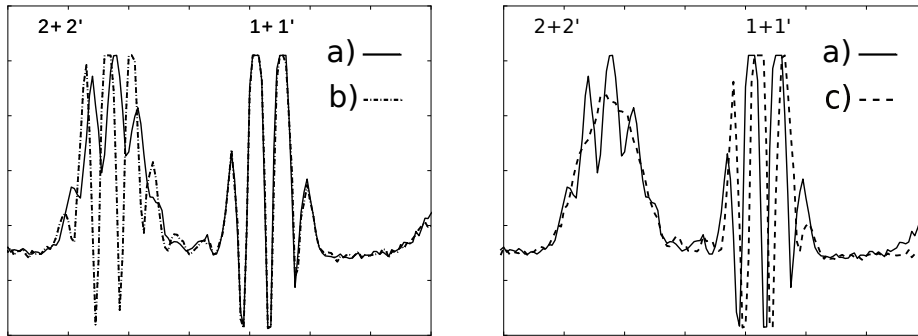


Figure 2.6: Intensity profiles obtained from a cut of the interferograms of the pictures 2.5 along a line perpendicular to the fringes. Left: comparison between the interference fringes in situation (a) and (b) of 2.5. Right: between (a) and (c).

In (a) fringes appear well contrasted on structure 1 while they are less clear on

²This phenomenon of simultaneous switching is not usual since the system parameters are slightly different all over the transverse surface because of spatial disorder. Either the three structures rise in spatial islands where the parameters are the same or a non local interaction exist between them, this topic will be discussed later in section 2.3

structure 2. As the current is decreased (b)-(c), the fringes on 1 do not lose contrast while fringes on 2 evolve becoming more visible in (b) or fading away (c). We can gather that Cavity soliton 1 (CS1) is always monochromatic while CS2 is monochromatic in (b) and polychromatic in (a) and (c). In (a) fringes are still visible while in (c) they completely disappear suggesting that several spectral components are present. The power spectrum of the case (c) is illustrated in Fig. 2.7.

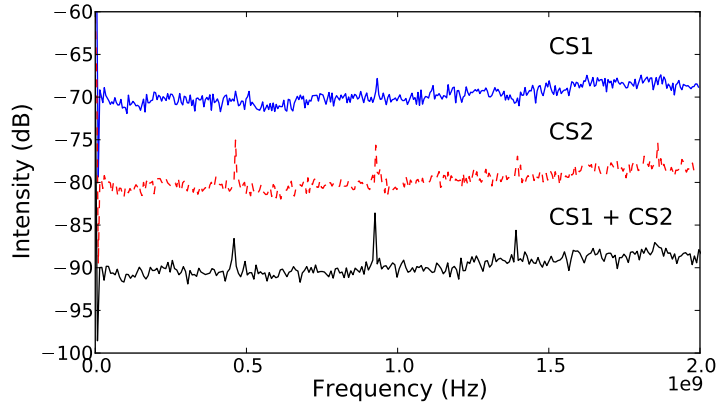


Figure 2.7: Power spectrum of laser solitons depicted in figure 2.5 (c). The structure named 1 (CS1) is essentially monochromatic while the one named 2 (CS2) is multimode: the spectrum shows several peaks at intervals equal to the FSR. The spectrum of the overlap of both structures do not differ from the one of CS2 indicating that the mode emitted by CS1 is part of the spectrum of CS2. Traces are vertically shifted for clarity.

Furthermore in Fig. 2.6 we also remark a spatial shift of the fringes maxima from (a) to (c) for structure 1, and from a) to b) for structure 2.

This shift of the interference pattern can be explained in terms of phase hopping: the laser source (i.e. the LCS) changed abruptly its phase. That is equivalent to adding an additional phase in the cosine argument of eq. 2.1 which relocates the maxima. For CS2 the phase hop occurs together with the hop from multi-mode to single-mode regime.

In the following we will show that mode hops may occur to all LLS. In Fig. 2.8 is depicted a near field and the corresponding interferograms. Two single-humps, a ring and a complex structure appear.

From the interferogram we notice that the single-hump structures are coherent while the complex structure pass from being incoherent to being coherent upon a small perturbation (knock on the optical table). We focus our attention on the ring, its emission is coherent: fringes are well contrasted and the power spectrum is flat. The interferogram also reveals a dislocation of the fringe pattern that is a typical signature of phase defects. The ring structure is an optical vortex. In order to monitor its emitted frequency, we perform an heterodyne detection: radiation from

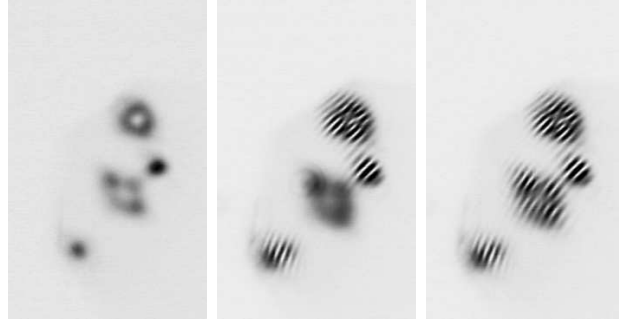


Figure 2.8: Spatial intensity distribution of the near field coming from one branch of the interferometer (left) and of the interference of the two branches (centre and right). System parameters are the same $I_1 = 206.1$ mA, $I_2 = 7.5$ mA.

the vortex is selected by the iris and mixed with a beam coming from a tunable laser (TL in Fig. 2.1) in the detector D_1 in order to eventually analyze the beat frequency. We first tune the external laser by looking at the optical spectrum (Left of Fig. 2.9) and then we perform measurements on the power spectrum (Right of Fig. 2.9).

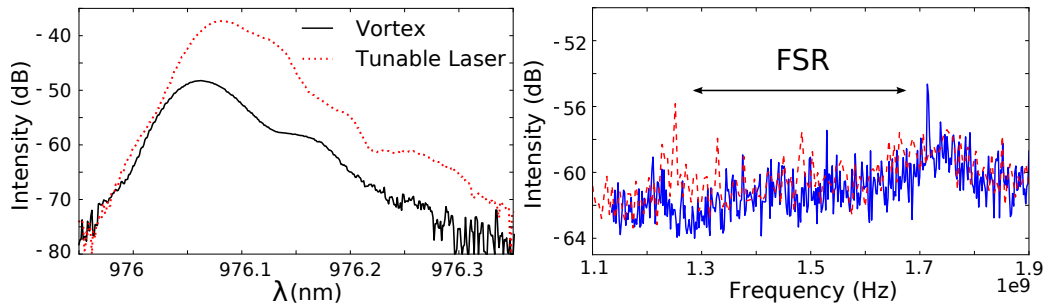


Figure 2.9: Left: Optical spectra of the Vortex and of the tunable laser obtained by a Optical Spectrum Analyzer with a mono-mode fibre input. Right: Power spectrum of the beat between the vortex and the tunable laser. The two power spectra correspond to the same set of parameters. The beat peak spontaneously jumps from one value to the other upon a small mechanical perturbation (a knock on the optical table). The frequency difference matches the free spectral range of the external cavity.

While the power spectra of the tunable laser and of the vortex looked separately are flat, the power spectrum of their superposition shows a peak. This peak moves in a discrete way as a perturbation is applied Fig. 2.9 and the frequency shift corresponds to a FSR.

2.2.2.1 Multimode laser cavity solitons

Multi longitudinal mode operation of LCS is very interesting because it opens possibilities for mode-locked LCS i.e. three dimensional localization of light. In partic-

ular our experiment is a good candidate for this aim since saturable absorption is a way to reach passive mode-locking in laser systems (see [Keller 2006] and references therein). For mode-locking to occur, a fixed phase relationship between the different modes is necessary. The sum of all modes will then result in a periodic train of pulses whose period is the cavity round trip time.

Observations of cavity solitons that can operate in multiple longitudinal mode have already been reported in [Tanguy 2008b] in case of a cavity soliton laser with frequency selective feedback. In this work it is shown that even though the power spectrum of a cavity soliton appears flat, its optical spectrum can display side modes. The authors explain this observation in terms of mode competition: the different modes intensity would be oscillating in anti-phase. This phenomenon is typical of multimode semiconductor lasers [Yacomotti 2004]. As described in [Yacomotti 2004], the anti-phase dynamics allows a compensation in the total output: the intensity of each mode displays amplitude oscillations in the megahertz range but the global intensity remains practically constant in time.

In the previous section we have already discussed multi-mode operation of LCS in our system. We described it through low visibility in the interferograms and the presence of peaks at frequencies that are multiple of the FSR in the power spectrum. We have not said anything about the temporal behaviour.

Here we report observation of two- and multi- mode temporal dynamics in LCSs. When the LCS is in two-mode operation, the time trace shows a periodic oscillation around a non-zero value that corresponds to the average intensity of single-mode LCS (left hand side of Fig. 2.10). Hence the two mode are not competing but they have comparable constant intensity. The period of the oscillation corresponds to the difference between the modes frequencies: 2 FSR for Fig. 2.10.

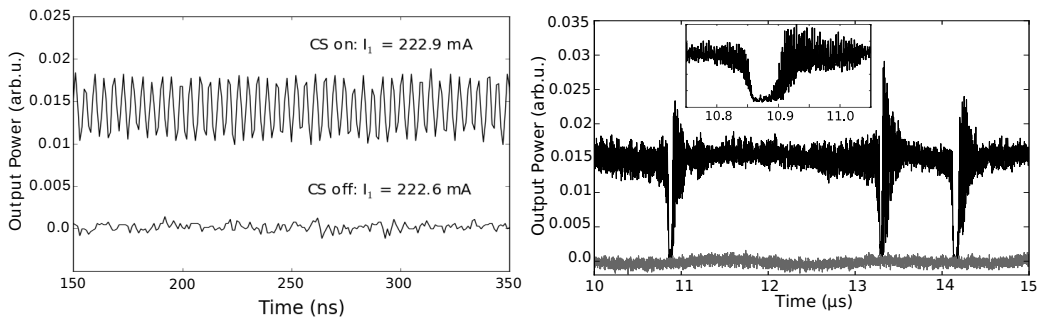


Figure 2.10: Time trace of a multi-mode laser soliton compared with the non-lasing one. Left: A two-mode LCS; the oscillating period correspond to a beat note between two modes distant twice a FSR; the bistability region is $222.6 < I_1 < 222.9$ mA for $I_2 = 4.3$ mA. Right: a multi-mode LCS that presents intensity dropouts as if it had switched off and then on again; insert is a zoom of the first dropout; $I_1 = 252.5$ mA and $I_2 = 0.6$ mA.

Two-mode LCSs aren't very robust, the two-mode operation is often a transient regime: it occurs upon variation of the current I_1 within the bistability region like the multi-mode regime that we discussed previously (for CS2 in Fig 2.5). It is anyway possible to get LCSs that switch on in two-mode operation and that keep

the same modal behaviour for all the bistability range, even for several realizations. But in these cases the stability range is very narrow (tenths of mA) as the example displayed in Fig. 2.10.

Multi-mode operation is more frequently observed. This means that, when not flat, the power spectrum often shows more than one peak like CS2 in Fig. 2.7. We noticed that the position and the number of peaks fluctuates, there is thus a sensitivity to parameter variation and to external perturbations.

The time trace do not show neither periodic pulses (phase locked regime) nor a completely constant emission (antiphase competition). It presents complex fluctuations around the single mode LCS intensity that are due to multi-mode interference. Moreover the temporal dynamics presents intensity dropouts as if the structure had switched off and then switched on again (Right hand side of Fig. 2.10). A zoom of one dropout is displayed in the insert. The residence time in the off-state last around 50 ns and it is followed by the emission of series of pulses that bring the system to the on-state. This transient is analog to the transient of the switch-on process of LCS that have already been studied [Genevet 2009b, Genevet 2009a]. As the parameters approach the lower edge of the bistability region (i.e. close to the switch off), the frequency of dropouts increases as well as the residence time. The phenomenon could be inserted in the framework of noise-driven dynamics in bistable systems. This regime, however, was not matter of additional studies.

2.3 Mutual coherence

Another characteristic of laser cavity solitons that arose from previous works is the mutual incoherence. Thus they are independent micro lasers originated on the same device [Genevet 2010c]. The demonstration is illustrated in Fig. 2.11. Structures

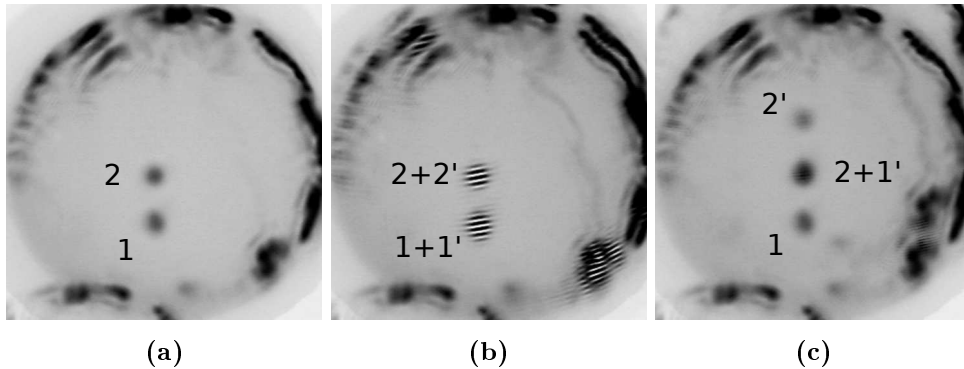


Figure 2.11: Spatial intensity distribution of the near field from the main arm of the interferometer (a). Laser solitons 1 and 2 have just switched-on. When the other arm of the interferometer is opened, 1 and 2 interfere with themselves (b), but not between each other: 2 and 1'(c). $I_1 = 199.1$ mA, $I_2 = 11.1$ mA.

1 and 2 are coherent because in the interferometer we observe well contrasted fringes when they interfere with themselves 2.11(b). But when one structure is

superimposed to the other one, we do not observe any fringes 2.11 so they are not mutually coherent. The possible reasons of the observed mutual incoherence are essentially two: (i) the lasing frequency is different, (ii) the frequency is the same but the phase is uncorrelated. Obviously (i) does not exclude (ii) and vice versa. For both cases the interference fringes between the two solitons would not be stationary and so they would be washed out by the integration time of the camera. In order to investigate for which reason two different solitons do not interfere, we analyzed LCSs properties for different system configurations. We call a configuration, a particular position of one resonator respect to the other.

We remind that localized structures theoretically arise from a homogeneous broad-area device which has translational symmetry, hence they can exist in every point of the transverse plane of the system and no energy is required to move them around (see [Ackemann 2009] for basic properties of localized structures). Despite that, in real systems the stable position of a localized structure depends on spatial inhomogeneities. In VCSELs these inhomogeneities arise from fluctuations during the epitaxial growth of semiconductor layers and they cause a local change of the cavity resonance. Investigations about the role of defects can be found in [Kuszelewicz 2000, Rosanov 2002, Caboche 2009].

In our system we have to deal with spatial defects of both the amplifier and absorber. Hence we expect that the relative alignment of L_1 and L_2 will influence LCS properties and position since different regions of L_1 are coupled with different regions of L_2 (see subsection 2.3.2).

During our analysis we ended up finding mutual coherent cavity solitons. In the following subsections, we will investigate the reasons of non mutual coherence, and we will study the the case of coherent and interacting solitons.

2.3.1 Incoherent solitons

The method that we have available to study interference between two independent laser beams is the analysis of the power spectrum (heterodyne measurements). In case of different lasing frequencies, we expect to see a peak at the beat note, otherwise in case of same lasing frequency we should see a broadening around zero Hz corresponding to the convolution of the two laser line-widths.

Experimentally we split the output beam that goes towards D_1 (see Fig. 2.1) in two beams. The output beam should contain at least two cavity solitons. We select a different cavity soliton from each of the two beams by means of an iris. Eventually we recombine the two solitons signals into the fibre-coupled detector.

We considered only the cases of supposed monochromatic solitons i.e. solitons whose power spectrum was flat.

Our observations ended up to be more complicated than what we expected.

Even though the two individual solitons had a flat power spectrum, the heterodyne spectrum could (i) show several peaks or (ii) none. In Fig. 2.12 we report an example of the first case: the interference between two solitons shows two peaks

in the power spectrum. The peak distance matches the free spectral range of the external cavity while the first peak is at around 6.2 GHz that is thirteen times the FSR. A reasonable interpretation is that one soliton is switching repeatedly from one longitudinal mode to the successive one while the other soliton is lasing at a frequency that is 6.2 GHz apart. The mode-switch is analogue to the antiphase mode dynamics reported in [Tanguy 2008b, Yacomotti 2004].

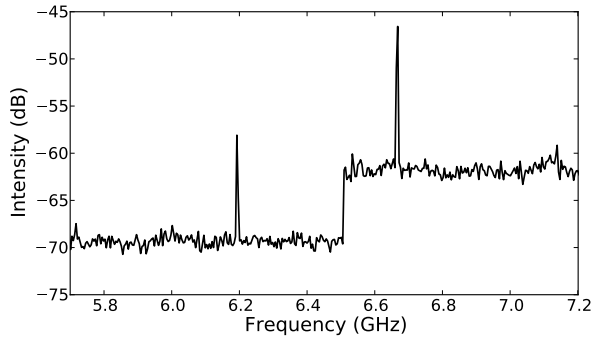


Figure 2.12: Averaged power spectrum of the superposition of two cavity solitons (average over 20 sweeps). Two beat frequencies show up while the spectrum of the single soliton is flat. This hints at two modes competition dynamics that had already been observed in [Tanguy 2008b]. The intensity step comes from the detection.

When the heterodyne power spectrum is flat, the two solitons could be lasing at the same frequency but a broadening at zero frequency was not visible. Then we looked at the optical spectrum. An example is displayed in Fig. 2.13. The peaks are separated by 0.1 nm that corresponds to a frequency difference of around 30 GHz at 976 nm. Therefore the two structures are lasing at two very far longitudinal modes. Since the detector bandwidth is 8 GHz, the beat note could not be perceived.

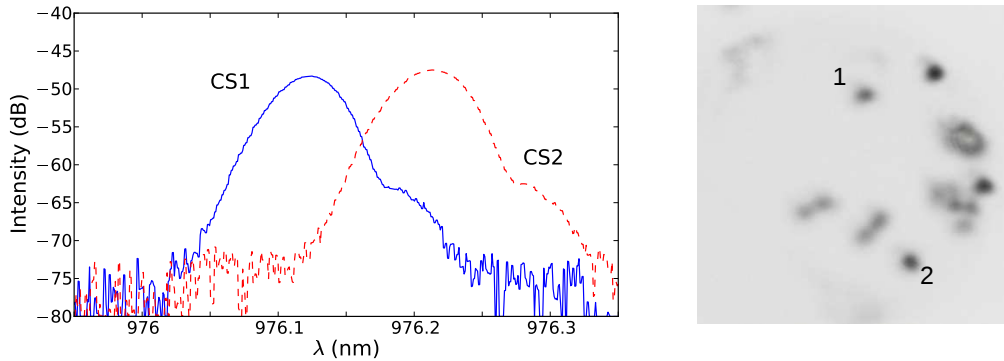


Figure 2.13: Optical spectra corresponding to the two laser solitons in the near field image on the right. Both optical spectra are obtained with a mono-mode fibre input. The spectrum of structure 1 differs from the one structure 2 by 0.1 nm that corresponds to a frequency difference of 30GHz.

In conclusion, our measurements demonstrate that, when the superposition of two different solitons do not show interference fringes, it is because their lasing frequencies are different or because at least one soliton undergoes mode switch. Besides, the lasing frequency of one CS resulted to be several FSR apart compared to the lasing

frequency of the other, so that the beat note was undetectable by our detection system (detector plus spectrum analyzer).

Nevertheless we remark that in the optical spectrum shown in 2.13, the spacing between the two peaks is bigger than the peak resolution of our OSA (60 pm). Sometimes, on the contrary, the two peaks could appear separated by a quantity smaller than the instrument resolution, thus making the measurements unreliable. In these cases the hypothesis of the same lasing frequency with uncorrelated phase should be reconsidered. Precise measurements of the optical spectrum by means of a Fabry-Perot interferometer could clarify this point.

2.3.2 Coherent and interacting solitons

Theoretically and numerically the interaction and formation of bound states was first studied in the case of slightly overlapping localized structures. In [Vladimirov 2001], the authors show that stable bound states can be formed if the phase difference between the two localized structures is 0 or π . We demonstrated experimentally the existence of two humps structure that exhibits phase locking or a phase mismatch of π between the two humps [Genevet 2010c], as illustrated in Fig. 2.14.

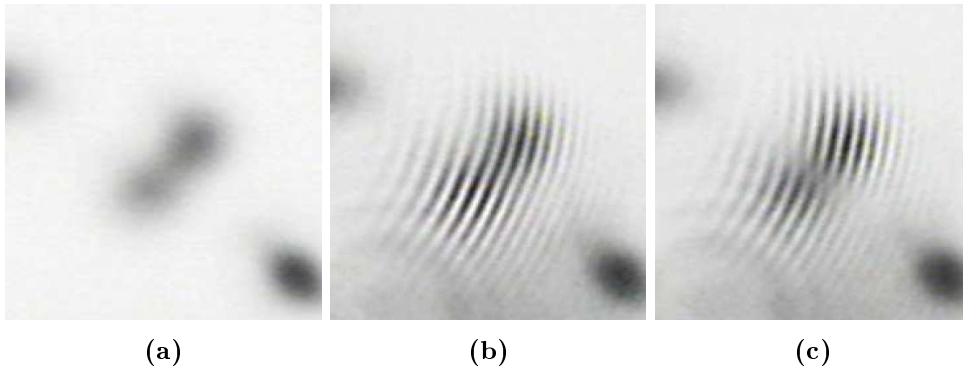


Figure 2.14: (a) Near field intensity distribution showing a two-humps cluster coexisting with a single hump laser soliton. $I_1 = 212.9$ mA, $I_2 = 7.5$ mA. (b) Interference pattern of the (a) with a reference beam obtained from one of the two humps of the cluster. Fringes appear over all the cluster and they look continuous, indicating that the two contiguous solitons are coherent and locked in phase. (c) Same as in (b) but for $I_1 = 213.7$ mA. White (dark) fringes become dark (white) when passing from one hump to the other, indicating that the two contiguous solitons have a π phase difference.

Here we focus our attention on interaction between laser solitons whose distance is greater than their diameter.

Numerically, phase-mediated interaction among laser solitons has been shown in a semiconductor laser with saturable absorber [Vahed 2011]. Since the phase profile is much broader than the intensity profile, the interaction can occur at distance much greater than the soliton intensity diameter. The interaction depends on

the initial distance and results in an adjustment of the soliton relative position and a phase locking. Authors show that for a certain range of initial distances, the relative phase oscillates around a π value. For larger distances, the phase is completely locked at 0 value.

In real systems though, solitons are not free to move around, they are pinned on defects. In the cavity soliton laser with frequency selective feedback, frequency and phase locking have been studied both numerically and experimentally taking into account the pinning role of defects [Paulau 2012]. Defects induce a shift in LCS frequency since they affect the cavity resonance. In [Paulau 2012], it is shown that LCSs lock by an Adler mechanism. The locking phase depends on the relative detuning between the two solitons, for equal defects (zero detuning), it is π .

In Fig. 2.15, six different near field images of the amplifier L1 for which the LCSs properties have been studied are depicted.

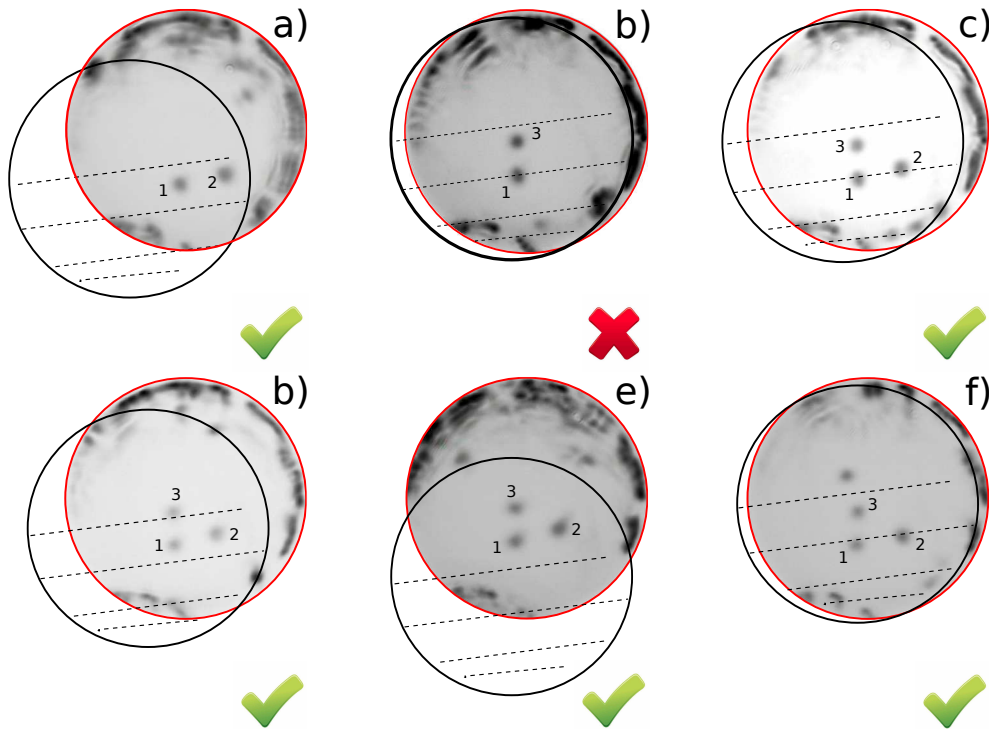


Figure 2.15: Near field images of the amplifier L_1 (red circle) for different relative alignments of the absorber L_2 (black circle). Dotted lines on L_2 are the main defects of the absorber (visible in Fig. 2.2). Since the alignment is different, the parameter region for bistable LCS slightly changes: (a) $I_1 = 191.1$ mA, $I_2 = 11.1$ mA (b) $I_1 = 197.8$ mA, $I_2 = 11.2$ mA (c) $I_1 = 202.6$ mA, $I_2 = 11.1$ mA (d) $I_1 = 195.9$ mA, $I_2 = 10.8$ mA (e) $I_1 = 187.7$ mA, $I_2 = 11.1$ mA (f) $I_1 = 206.9$ mA, $I_2 = 11.2$ mA. Yes and No tags tell if at least two structures are coherent.

They correspond to six different alignments of L_2 (black circle) respect to L_1 (red circle). The system can work as a cavity soliton laser only in the areas where the two lasers are superimposed.

First of all, we notice that the structures appearing in the near field have approximately the same position respect to L_1 . For example the three solitons (labeled 1, 2, and 3) in the configuration (c) can be found also in (d), (e) and (f) while in (a) and (b) we see only two of them. This means that the inhomogeneities of the amplifier have a predominant role in choosing the position of the cavity solitons.

On the other hand, we will show that the coherence properties of the solitons are influenced by the big spatial defects of L_2 (see dashed lines in Fig. 2.15). In fact, even though the distance between the solitons 1, 2 and 3 of Fig. 2.15 is short enough that one could expect a phase-mediated interaction³, only two LSs are mutually coherent in each configuration of Fig. 2.15 except configuration (b), where the two LSs are incoherent. In this configuration, we notice that the structure 1 lies on a defect line of L_2 while the structure 3 is not. Because of the big defect, the characteristics of the system may vary significantly through the two solitons positions. This variation could prevent interaction and synchronization [Paulau 2012]. Two solitons in the same positions (1 and 3) but in configuration (e) are mutually coherent. In this case the defects on L_1 that give rise to the solitons are coupled with a part of L_2 that is rather homogeneous. The interaction between solitons is then possible. In (a), (c), (d) and (f) the solitons, which are mutually-coherent, are the ones labeled 1 and 2. They either lie on the same defect line (c,f) or in between two lines (a,d).

We studied the phase relationship between coherent LCSs. In order to do that we modified the set-up in such a way that we could measure the far field of the two coherent structures in analysis. We found phase differences of either π or 0. Examples are shown in Fig. 2.16 and Fig. 2.17.

The first one corresponds to configuration (e) of Fig. 2.15. In panel (a) we observe the near field of two LCS. The interference (b) between the near field and the expansion of the soliton on the bottom displays fringes on both structures which indicates mutual coherence. The two lobes with a central minimum in the far field (c) demonstrates the π difference between the two LCSs.

Fig. 2.17 corresponds to configuration (c) of Fig. 2.15. The near field in panel (a) displays three LCSs. The interference (b) shows that only two of them are coherent. From the far field (c) we deduce that the two coherent solitons are locked in phase. We believe that, differently from the case of phase mediated interaction described in [Vahed 2011], the value of the phase locking (0 or π) does not depend on the distance between the position of the localized structures, since the two interacting structures in Figs. 2.16 and 2.17 can show both values of phase locking. We also observed a switch from 0 to π that followed a small parameters change or a mechanical perturbation.

Another kind of long-range interactions that can not be explained by the previously described mechanisms (phase mediated and Adler synchronization) have been

³We remind that the phase profile of a CS has a diameter that is three times the one of the intensity profile. Thus a long-range interaction between two different CSs is expected when their distance is short enough for their phase profiles to overlap.

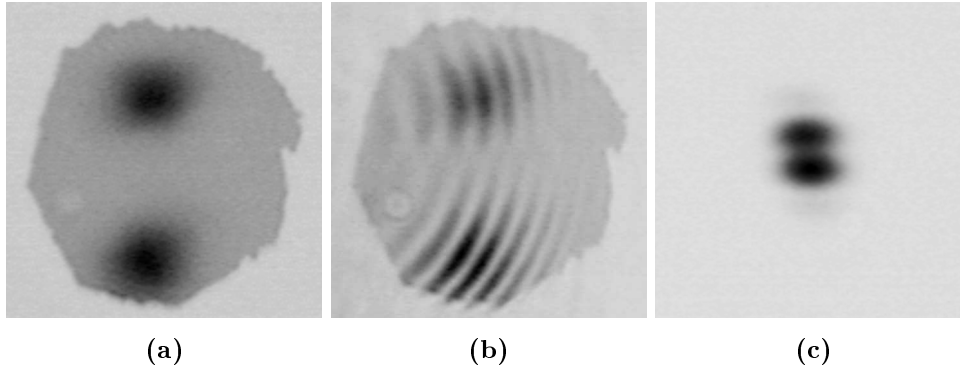


Figure 2.16: Spatial intensity distribution of the near field where two localized structures appear (a). (b) Interference between the near field and a reference beam obtained from the structure on the bottom. The fringes appear over both structures indicating that they are coherent. (c) Far field of both structures. The presence of two lobes with a central minimum indicates an antiphase locking $I_1 = 186.3$ mA, $I_2 = 9.9$ mA

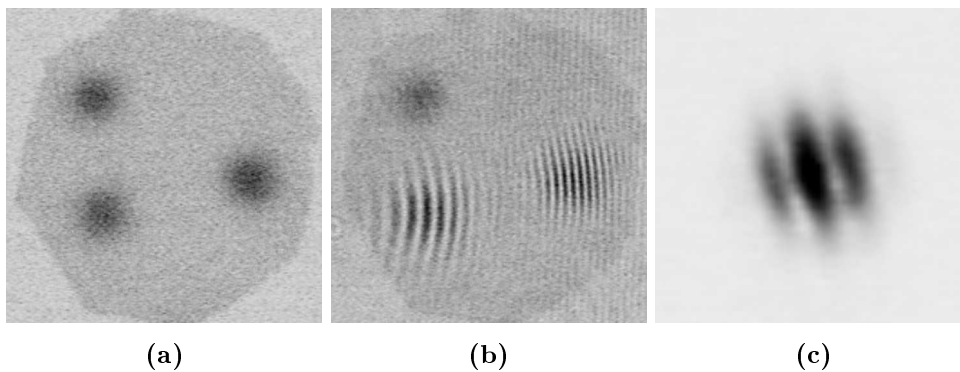


Figure 2.17: Spatial intensity distribution of the near field where three structures appear (a); (b) interferogram of the near field and the expansion of the structure on the bottom left hand side. Fringes appear also on the structure on the right hand side, indicating that it is coherent with the structure on the bottom. (c) far field of both structures. The central maximum indicates that the two structures are locked in phase. $I_1 = 204.9$ mA, $I_2 = 11.1$ mA.

observed. It becomes evident at the switch of localized structures: the switch of a localized structure could induce the switch of a close one. In Fig. 2.18 we report a sequence of near field images where we control two cavity solitons by means of an external writing beam. In (a) the system is in the nonlasing state (white area). In (b) a writing beam is applied to create a laser soliton. Surprisingly another structure about $30\mu\text{m}$ below the writing beam switches on at the same time (within the integration time of the CCD camera). When the writing beam is moved away, both laser solitons persist, which indicates their bistability. When the control beam is moved back (d) and then removed (d), the soliton is switched off while the one below remain on, which demonstrates their independence.

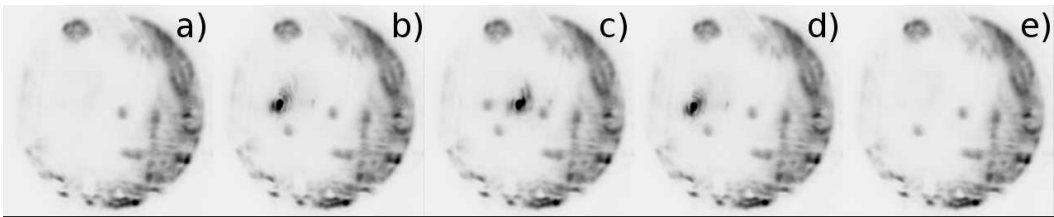


Figure 2.18: Near field intensity distributions in bistability parameters region. When the system is in the nonlasing state (white area in frame (a)), a perturbation applied in a certain location (b) can nucleate two localized structures which persist when the perturbation is moved elsewhere in (c). When one localized structure is destroyed (d), the other one persists (e) .

A similar mechanisms can be observed in the switch-off. Fig. 2.19 illustrates the temporal dynamics of a portion of the near field that includes two structures separated by about $30\mu\text{m}$. The time trace starts from a constant value equal to twice the

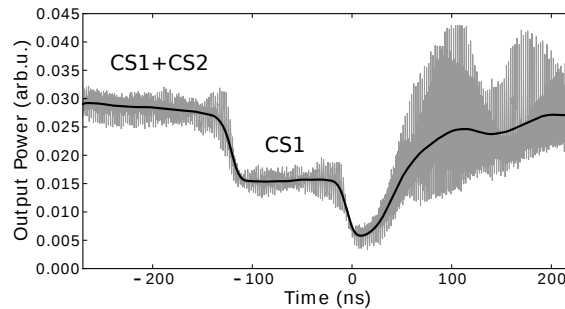


Figure 2.19: Temporal dynamics of the output power corresponding to an area of the near field which includes two cavity solitons. Both solitons exhibit a dynamics analog to the one depicted in the right hand side of Fig. 2.10. Moreover the dropouts are synchronized: First CS2 switches off and then CS1 switches off after 100 ns) .

single cavity soliton intensity. Then the global intensity drops down towards zero in two steps and subsequently comes back to its original value. The value reached after the first step corresponds to the single CS intensity. Therefore we are observing two structures presenting intensity dropouts as the ones that we have already seen

in Fig. 2.10 and whose dropouts are synchronized. The intensity of the structure that we called CS1 drops down after 100 ns after the switch-off of CS2. The two structures also re-switch on together but we can not recognize a delay time from these data because of the switch-on transients. A typical switch-on transient last few hundreds of ns. So when two of them overlap, they are impossible to distinguish.

2.4 Conclusions

In this chapter, we have experimentally investigated the properties of laser localized structures arising in mutually coupled semiconductor resonators in a laser with saturable-absorber configuration. Mode hopping and phase hopping induced by small fluctuations of the system parameters have been observed. We also report on observations of multi-mode localized structures.

Interactions between different structures have been studied. Interferometric measurements show that LSs can be either mutually incoherent or coherent.

On the one hand, we found that two localized structures result mutually incoherent because they have different frequency emission or because one of them continuously jumps from one mode of emission to another one (mode hopping).

On the other hand, two structures result mutually coherent because they emit on the same dominant frequency, and a well-defined phase relationship is established between them. Our measurements of phase coupling in clusters revealed a in-phase or an anti-phase locking between the two structures of the cluster, which fulfill the theoretical predictions. The same in-phase and anti-phase locking has been measured between two separate localized structures.

We believe that the spatial inhomogeneities of the system play a crucial role in this long range interaction. Infact, the mutual coupling occurs when the pinning position of the two structures are close enough for their phase profiles to overlap provided that the pinning sites are located on the same defect or in a homogeneous region of the space.

We remark another long range interaction: the switch-on and the switch-off of one structure can be induced respectively by the switch-on and the switch-off of a neighbouring one.

Response to an External Perturbation

Contents

3.1	Experimental Set-Up	32
3.2	Switch-On	36
3.2.1	Writing beam wavelength	37
3.2.2	Writing beam power	39
3.2.3	Writing beam polarization	41
3.3	Switch-Off	43
3.3.1	Erasing beam polarization	44
3.4	Injection Below the Bistability Region	44
3.4.1	Looking for excitable LCS	46
3.5	Conclusions	49

An external perturbation is essential to investigate the features of a dynamical system. In a bistable system, a perturbation can make the system switch from a state to the other, while in excitable system, if a certain threshold is overcome, it causes a deterministic response of the system that eventually comes back to the original state.

An appealing feature of cavity solitons is the bistability: the CS state and the homogeneous background state are stable for the same region of parameters. An external perturbation can switch a CS -on or -off provided that it is stronger than a certain threshold. The threshold is fixed by the unstable branch of the CS solution which connects the stable background and the stable CS branch.

The control of CSs is fundamental for applications. The switch-on and switch-off duration determines the speed at which information can be written and processed. Because of their rapid response, semiconductor devices may allow for fast manipulations of cavity solitons. For this reason, the switching of CSs in semiconductor devices has been object of several studies. The switching techniques that have been proposed may differ according to the considered system.

In semiconductor microcavities with coherent injection (holding beam HB), two kinds of switching techniques had been studied: coherent and incoherent. In the coherent switching, part of the HB is used as a control beam [Barland 2002, Hachair 2004]. The control beam is locally injected in phase or out of phase in

order to write or erase the CSs. In the incoherent one, the perturbation does not have a stable phase relation with the HB and it acts, as an additional localized pumping, on the population inversion. Experimentally it was realized in optically pumped devices [Barbay 2006]. From a numerical point of view, both methods were analyzed [Brambilla 1996, Michealis 1998].

In cavity soliton lasers, phase, polarization and frequency are not fixed by the HB and therefore they are chosen freely by the system. The switching methods that have been proposed for cavity solitons laser can be called semi-coherent and incoherent. The principle of the incoherent switching is the same described above, while the semi-coherent consists in a perturbation of the electric field by the injection of an external laser beam whose phase is independent of the phase of the system.

The different techniques are described and compared numerically in the case of a VCSEL with intracavity saturable absorber in [Mahmoud Aghdami 2008]. Experimentally in an optically pumped monolithic VCSEL with intracavity saturable absorber [Elsass 2010b] solitons were repeatedly switched-on and -off at a repetition rate up to 80 MHz by incoherent switching. In our system, it has been shown that the switch-on occurs with a long transient (hundreds of ns) [Genevet 2008] that decreases upon reduction of the external cavity length. This transient limits the rapidity of our system compared to monolithic one.

Other theoretical and experimental studies on lasers with saturable absorber but without spatial degrees of freedom have demonstrated that a LSA can exhibit excitable behaviour [Dubbeldam 1999, Plaza 1997, Larotonda 2002, Barbay 2011].

The excitability is observed by applying an optical perturbation when the pump parameter is such that the non-lasing state is stable and the lasing state unstable and close to a transition to a self-pulsing regime.

We are going to apply a short optical perturbation in the bistability region in order to investigate the switch dynamics of CS. Moreover a perturbation is applied also for parameters below the bistability region where the non-lasing solution is stable and the CS solution is not. The aim is to investigate the possibility to find local excitable behaviour i.e. excitable localized structures.

3.1 Experimental Set-Up

In figure 3.1 a scheme of the setup with the injected laser is depicted.

The perturbation should be by preference shorter than any system-variable typical response. We first generated sub-nanosecond pulses by gain switching of a 10 mW power edge emitter laser diode. But the pulse energy wasn't enough to solicit a response from our system. Eventually the laser (LD in 3.1) that we used to generate the perturbation is a 100 mW edge emitter. Its current is modulated (MOD in Fig.3.1) with a pulse sequence provided by a waveform generator. The minimal duty cycle achieved is 0.1% of the sequence period plus 0.2 % of rise and fall time. Because of the big impedance of the LD, the minimal pulse duration that we could achieve is about 15 ns.

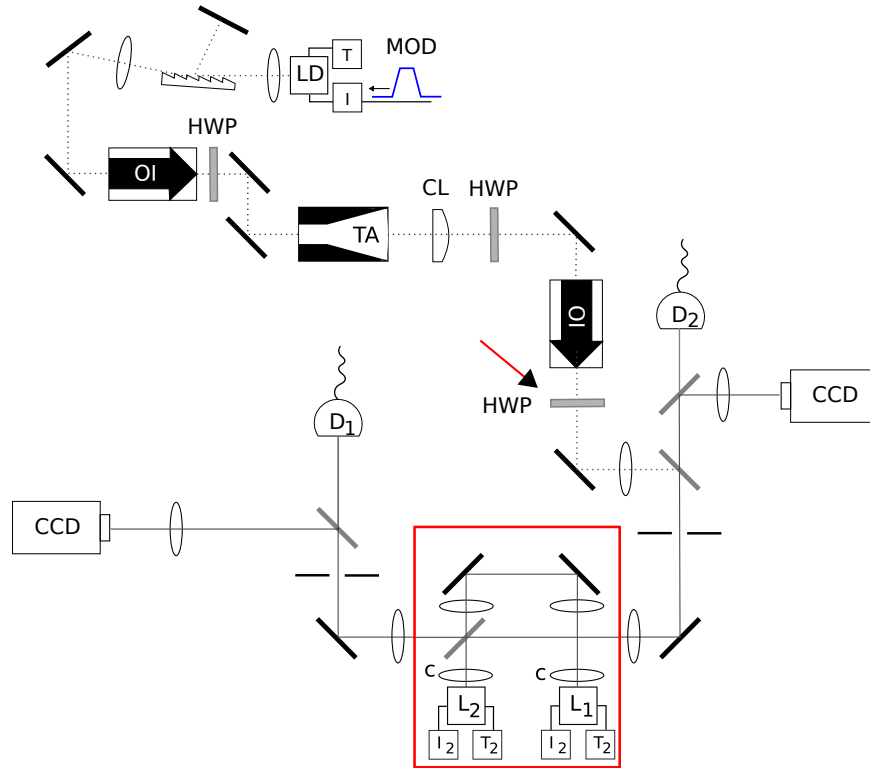


Figure 3.1: Schematic of the experimental set-up. The physical system is encircled in red and it is already been described in chapter 2. The control beam is generated by an edge emitter laser diode (LD) that has been modulated in current (MOD); LD emission frequency can be tuned twisting a mirror that couples LD and the diffraction grating (G); OI, optical isolator; TA tapered amplifier; CL, cylindrical lens to correct the beam astigmatism; HWP, half wave plate.

The wavelength emitted by LD is $\lambda_{WB} = 982$ nm. Since the usual wavelength of CSs (λ_{CS}) that switch on spontaneously in our system is around 976 nm, a diffraction grating is added in front of LD in order to tune its laser frequency in the proximity of λ_{CS} . The switching process is very sensitive to the perturbation wavelength as we will see below. The half wave plate highlighted in the scheme 3.1 allows us to change the polarization of the writing beam from parallel to orthogonal respect to the CS's one.

The injection is done on the absorber L_2 , in such a way that the perturbation pulse could locally saturate the absorption and start the lasing process. The same method is used in [Taranenko 1997, Genevet 2008]. The switching process is monitored through the fast detectors: D_1 and D_2 , the iris selects the area of interest. We remind that D_1 sees the system output coming from the amplifier L_1 while D_2 detects the radiation coming from the absorber L_2 . The control beam is injected locally in the absorber through reflection on the BS. During the injection D_1 receives the part of the pulses that is transmitted (60% or 80% according to the polarization) by the BS and that didn't enter in the system. After one round trip time from the beginning

of the injection it also starts receiving the effects of the injection on the system: the beam reflected on BS goes in L_2 then it is transmitted to L_1 and eventually reflected on the BS to go towards D_1 . Since the pulse duration is of the order of tens nanoseconds and the round trip time is 1.8 ns, the injected beam and its effects on the system overlap on D_1 . However, the system response is much weaker than the injected pulses because of the BS transmission-reflectivity ratio.

On the other hand D_2 receives only the system response to the injected pulses. The signal in D_2 has a delay of 3.5 ns compared to the signal in D_1 because of the optical path difference from the output BS to the fibre-coupled detectors. Moreover it is much weaker because of the two beam-samplers which the output beam passes through before reaching D_2 . In Fig. 3.2 and 3.3 we show an example of the signal detected by D_1 and D_2 , during a switch-on event. In the first figure λ_{WB} is not tuned

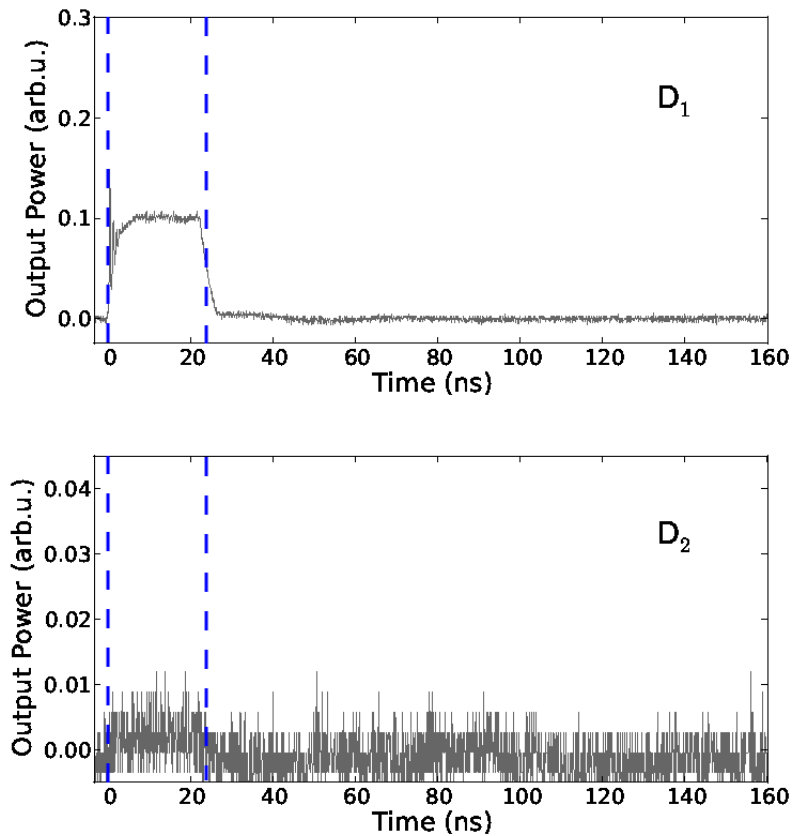


Figure 3.2: Example of temporal signal detected by the two detectors during an injection event when the feedback from the grating is cut. At the beginning the system is in the non lasing state, D_1 (top) and D_2 (bottom) detect the local system output (zero intensity). When the perturbation is injected (dashed blue lines), D_2 detects the effect of the perturbation on the system while D_1 sees the injected pulse together with the response of the system. In this case this perturbation is not effective and after the injection, the system is back to its initial state.

(the feedback from the grating was removed) while in the second one $\lambda_{WB} \approx \lambda_{CS}$. The signal in D_2 has been shifted to compensate the delay and re-scaled in such a way that it is at the same level of the signal in D_1 when both detectors look at the same cavity soliton. The spontaneous emission background is set at zero in both signals. At the beginning the system is in the non lasing state, D_1 and D_2 detect the local system output (zero intensity).

When the grating is removed, the writing pulse is not effective and the system stays in the non-lasing state after the injection (blue dotted lines in Fig. 3.2). The injected pulse (visible in D_1 trace) has a square shape. Relaxation oscillations are visible at its onset. The effect of this not tuned pulse on the system is almost imperceptible (see D_2 traces between the blue dotted lines).

On the other hand, if the injected pulse is appropriately ¹ tuned (Fig. 3.3), the

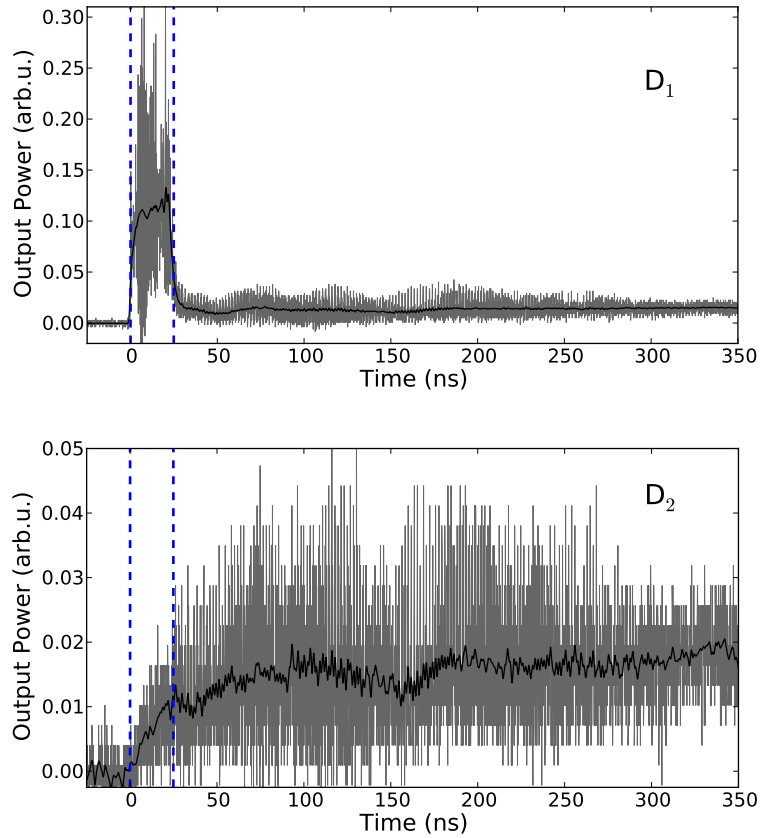


Figure 3.3: Example of temporal signal detected by the two detectors during one injection event when the injected pulse is tuned in proximity of the CS wavelength. The smoothed trace is overlapped (black line). At the beginning the system is in the non lasing state, D_1 (top) and D_2 (bottom) detect the local system output (zero intensity). When the perturbation is injected (dashed blue lines), D_2 detects the effect of the perturbation on the system while D_1 sees the injected pulse together with the weak response of the system. After the injection, a localized structure is switched on.

intensity grows in D_2 during the injection. After the injection, the output power undergoes to fast oscillations (grey trace) before reaching the stable LCS value. This switching transient last for around 250 ns and it is also visible in the trace D_1 . In D_1 we also observe that the injected pulse (grey trace between the two blue dotted lines) shows a complicated fast dynamics due to feedback instabilities from the grating. The black lines are the filtered traces (frequencies up to 1 GHz); the filter will be used in the next sections in order to better identify the instant at which the switch occur. A tapered amplifier (TA in Fig. 3.1) was added in a second time in order to amplify the perturbation and to explore the system response upon variation of the injected power.

3.2 Switch-On

In this section we investigate the influence on the switch-on dynamics of the writing beam (WB) parameters, such as wavelength and power and polarization. In particular we focus our attention on the critical energy for the switch to occur and on the switching time i.e. the delay between the rise of the injected pulse and the rise of the CS.

Because of fluctuations in the injected pulses (due to feedback instability) we decided to perform several realizations for the same injection and system parameters and to study the average behaviour. We analyze series of at least five hundreds switch-on events for different WB wavelengths and powers.

The system is prepared in the nonlasing state in the bistability region. The WB is addressed where a CS is known to arise pinning on a defect. The writing pulses are fired with a period of 2 ms. In order to bring back the system to the non-lasing state after a switch-on event, the current of the amplifier I_1 is modulated synchronically with the WB in such a way that it drops down below the bistability region some hundreds of microseconds after the injection. The delay between the modulation dropout and the following WB injection is chosen long enough to allow the stabilization of the system parameters.

In our analysis we distinguish successful switches from unsuccessful ones. A switch-on event is unsuccessful when the system remains in the non-lasing state after the WB injection, it is successful when the intensity grows and reaches the CS's value. Among the successful switches we also count CSs that are switched-on and that spontaneously switch-off after some time. The reasons of the spontaneous decay of the excited CSs will be discussed later in section 3.4.

The studies concerning wavelength and power are carried out by using a WB with orthogonal polarization respect to the CS. The WB wavelength is adjusted by tilting the mirror that couples LD to the grating while the pulse power is controlled with the pump current of the TA.

A comparison between on-switches with orthogonal and parallel polarization is discussed in the last subsection.

¹Discussion about the frequency tuning of the control beam will be broached in the next sections

3.2.1 Writing beam wavelength

The injected wavelength turned out to be critical for the switch-on to be successful. This criticality comes from the decision to keep the injected pulse duration as short as possible (below twenty nanoseconds) and from the constraint imposed by the maximum power² available (5 mW). In these conditions, the best results in terms of success rate (i.e. the number of successful on-switches over the total number of events) are obtained for WB wavelengths blue tuned of few tenths of nanometer compared to the CS's one. For longer pulses (microseconds) so for higher energies, a successful switch was possible for different wavelengths within a broader bandwidth around λ_{CS} (about 1 nanometer which is the resonance width of our devices).

The effect of the frequency detuning between the WB and the CS on the switching is rather complex and also difficult to measure because of the long realization time during which the system parameters might drift³. In the following, we will show some measurements that will illustrate the main consistent effects.

In Fig.3.4 we measure switch-on events at the maximum pulse power for two different wavelengths in order to directly compare the system response. The time traces acquired by the two detectors are displayed.

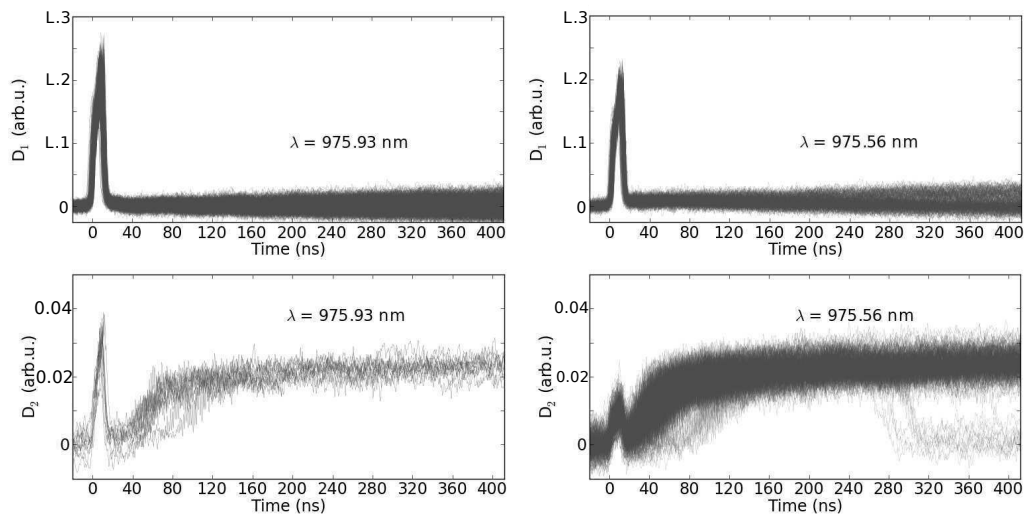


Figure 3.4: Superposition of filtered time traces detected by D_1 (upper row) and D_2 (lower row) corresponding to switch-on events at two injected wavelengths. Right column: fifteen hundreds WB pulses at $\lambda = 975.93$ nm (D_1), 15 of which were successful (D_2). Left column: five hundreds WB pulses at $\lambda = 975.56$ nm (D_1), 257 of which were successful (D_2). $\lambda_{CS} = 975.95$ nm.

² We consider the injected power as the power reflecting on the beam splitter and effectively reaching L_2 .

³The spontaneous switch-on threshold occurs for lower bias of the amplifier I_1 as the experiment is repeated several times. The efficiency of the WB pulses is sensitive to how far I_1 is from the threshold value. Moreover the I_1 value determines the cavity resonance. These two elements have an influence on our measurements.

In the top row we show the superposition of all the injection events detected by D_1 ; in the bottom row, we report only the successful events detected by D_2 . One wavelength matches λ_{CS} (left column) within the resolution of the optical spectrum analyzer (60 pm), the other is 0.4 nm blue tuned respect to λ_{CS} (right column). The success rate is much bigger for blue tuned WB. When the WB wavelength matches the CS's one, the success rate is only 0.01% while when it is blue tuned the success rate is of 0.51%.

We also observe that the peak power of the blue tuned injected pulses is slightly lower than the peak power of pulses at the wavelength of the CS. But the corresponding peaks in D_2 do not keep the same proportionality: the peak power of pulses at CS wavelength is twice the peak of the blue tuned ones. This means that the reflectivity on L_2 is lower for the blue tuned wavelength. In appendix A we report on a device analogous to a VCESL below transparency: the resonance saturable absorber mirror (RSAM). Its spectral reflectance curve (Fig. A.2) shows that the reflectivity reaches the minimum value at resonance. Hence we can conclude, from the observed difference in the reflectivity, that the cavity resonance of L_2 is blue-tuned respect to the cavity soliton frequency. For a different configuration, we have tried to switch on a CS with three different wavelengths: the CS one (λ_1) and two blue tuned ones ($\lambda_{2,3}$). The corresponding optical spectra together with the nonlasing state and CS spectrum are depicted in Fig.3.5.

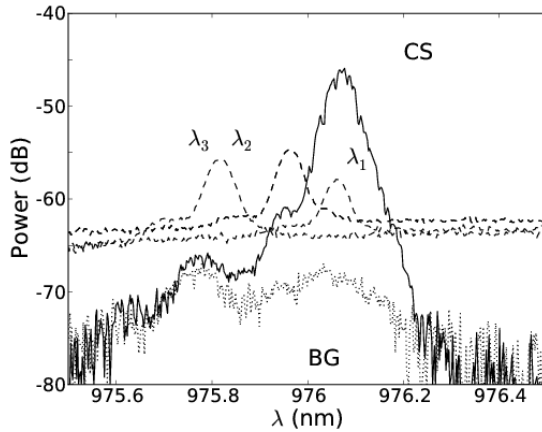


Figure 3.5: Optical spectra. The homogeneous nonlasing background (BG) spectrum (dotted line) is broader than the laser cavity soliton (CS) spectrum (solid line). Switch-on events have been measured for three different writing beam (WB) wavelengths: $\lambda_{1,2,3}$ (dashed line).

Before the injection, the system is in the nonlasing state, the spontaneous emission spectrum is broad (dotted line) compared to the laser CS spectrum (solid line) and the CS peak wavelength is red tuned compared to the non lasing hump (around 975.8 nm) still visible in the CS spectrum (confirming what observed in [Genevet 2008, Genevet 2009a]).

The switch-on of a CS was possible for the wavelength that matches λ_{CS} (λ_1) and for the most blue tuned one (λ_3) but not for intermediate case (λ_2) (spectra corresponding to the three different WB pulses are drawn in dashed lines).

The success rate is again higher for the blue tuned pulses which means that the threshold for the switch to occur is lower. Our observations are in agreement with

experimental studies about the wavelength influence on the switch-on process reported in [Tanguy 2007, Radwell 2010]. In these works the authors show that the minimal threshold occurs when the WB is about 0.1 nm blue tuned and that this wavelength corresponds to the cavity resonance.

Moreover the fact that the writing pulses at λ_2 are not effective suggests that the detuning should not be smaller than a certain amount (0.1 nm in the case of Fig.3.5).

3.2.2 Writing beam power

For each wavelength of Fig.3.5 we acquire series of five hundreds switch-on events for different writing pulse powers in order to find the minimal energy necessary for the switch and to study the evolution of the switching time. The pulse power is controlled by the bias current of the tapered amplifier (TA). In the following we show the results for λ_3 which is the wavelength that allowed for higher success rates.

The average pulse duration is 15.5 ± 0.4 ns.

For low current of the TA, i.e. for weak writing pulses, the system stays in the non-lasing state after each WB pulse. As the average pulse power increases, some of the pulses begin to be effective and they bring the system to the high power state: the LCS. For values of the current between 1.3 and 1.4, the number of successful events increases abruptly from 30% to 80% (see Fig.3.6). We locate the threshold

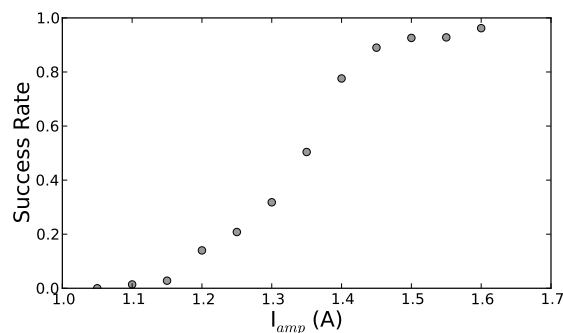


Figure 3.6: Switch-on success rate as function of the bias current of the WB amplifier. The success rate is calculated over 500 WB pulses whose length is $dt = 15.5 \pm 0.4$ ns.

for the switch between these two values. In energy, the threshold is about 25 pJ.

For higher value of the current, the success rate is very close to one.

Fig.3.7 shows the superposition of successful switch-on events together with the respective switching-times histogram for three different value of I_{amp} : 1.3 A (top), 1.5 A (centre), 1.6 A (bottom).

In average, the CS switches on in a shorter time as the injected power increases. This is in qualitative agreement with the phenomenon of non-critical slowing down. Besides the switching-time distribution shrinks although the uncertainty keep being quite high: of the order of ten ns.

A possible contribution to the spread of the switching-time distribution could come from the local heating of the device caused by the WB. Thermal changes are very sensitive to noise and they induce a slow displacement of the hysteresis cycle that would affect the threshold of the switching process as it has already been observed in [Barbay 2006].

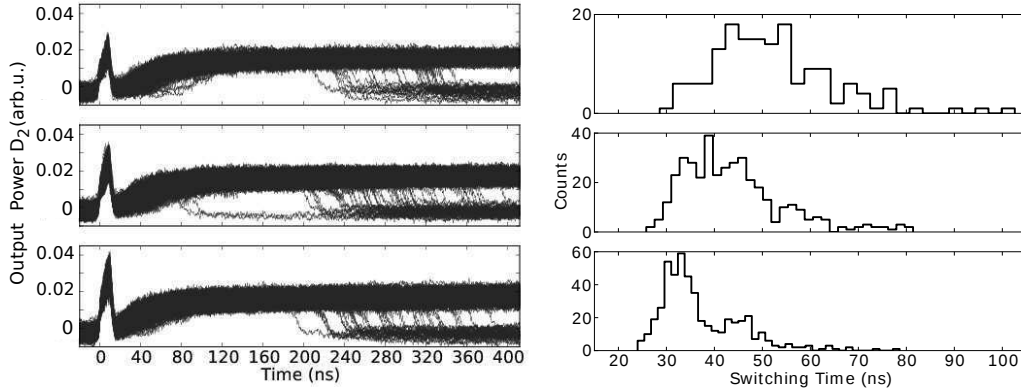


Figure 3.7: Overlapping of successful switch-on events at λ_3 for three different WB amplifications (left) and corresponding histograms of switching times (right). The switching-time is the time delay between the beginning of the injected pulse and the instant at which the power reaches half of the CS power. Top: $I_{amp} = 1.3$ A, success rate is 32% . Centre: $I_{amp} = 1.5$ A, success rate is 93%. Bottom: $I_{amp} = 1.6$ A, success rate is 96%.

In order to analyze the switch-on mechanism, we interrupt the coupling between L_1 and L_2 by putting an obstacle in the middle of the cavity and we study the reflection of the writing pulses on the mere absorber L_2 . We measure series of five hundreds pulses for the same WB amplification used to switch-on in Fig.3.6. A schematic of the experiment with the beams involved is drawn in the left hand side of Fig.3.8. In order to calculate the reflectivity we calculate the injected pulse energy E_{IN} and the reflected pulse energy E_{OUT} , using the full bandwidth time traces i.e. taking into account the fast dynamics of the injected pulses.

The energy of the injected pulse can be worked out from the signal D_1 while the reflected energy can be worked out from D_2 , given the reflectivity and transmission of BS (R,T).

We calibrate the signal detected by D_1 and D_2 in such a way that they correspond to the power measured just after the BS as in the schematic. The calibration for D_1 is trivial because we can easily measure the transmitted power of WB. While the calibration of D_2 is done when the system is working as a CSL, by measuring the power corresponding to the CS and to the background.

In the right hand side of Fig.3.8 we report the reflectivity of L_2 as function of the average input energy. Here the reflectivity is calculated as the average of the ratio of output energy to input energy. The error-bars corresponds to the standard deviation. As we can see in appendix A, reflectivity in RSAMs is linked to the absorption

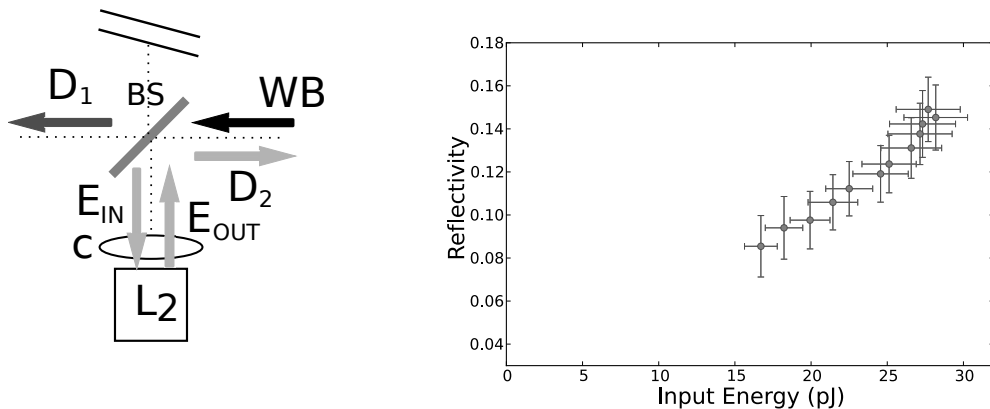


Figure 3.8: Left: schematic of the method used to measure the response of L_2 as function of the WB energy for the same parameter as in Figs. 3.6 and 3.7; $I_2 = 3.6$ mA, $dt = 15.5 \pm 0.4$ ns. Right: average reflectivity of the absorber L_2 as function of the injected energy. The error-bars correspond to the standard deviations.

saturation. The measured reflectivity of L_2 shows the effects of the nonlinear absorption since it is not constant: it passes from 8% to 15% as the injected energy increases. Moreover if we compare the trend of the right hand side of Fig. A.2 with our data Fig. 3.8, we observe that our data behaves qualitatively as the RSAM reflectance for low injected intensity.

We can conclude that the effect that our WB pulse has in the switching process is to partially saturate the absorption of L_2 . However the contribution of thermal effects can't be completely excluded.

3.2.3 Writing beam polarization

All CSs that we have analyzed are p-polarized. Two causes contribute to favour one specific polarization over the other. One is the fact that the beam-splitter which couples L_1 and L_2 has a lower reflection coefficient for p-polarized light than for s-polarized, which makes the p-polarized radiation experience less losses. The other one is the birefringence of the VCSELs. Birefringence is the frequency split of the two orthogonally polarized modes which, together with the frequency dependence of the gain and absorption, makes the two orthogonally polarized modes experience a different net gain. In VCSELs the birefringence is small: 5-10 GHz [van Exter 1997, Ackemann 2001].

The polarization of the writing beam is not crucial for the switch but it has an influence on the necessary switching energy and on the resulting switching-time. This subsection aim to evaluate the threshold difference.

The polarization of the WB can be changed by rotating the half wave plate pointed by the arrow in Fig. 3.1. Before reaching L_2 , the WB is reflected by two BSs. Because of the dependence of reflection coefficient of BSs on the polarization the WB power effectively injected in L_2 changes as the HWP is rotated. From the

known values of the reflection coefficients of the beam splitters, we can estimate that the injected power for p-polarized WB is one fourth of the injected power for s-polarization.

In figure 3.9 we show a superposition of switch-on events for the same experimental conditions except for the HWP orientation. The amplification of the WB is set at the maximum level ($I_{amp} = 1.7$ A) and the detuning of the WB respect to the CS is the optimal one for this case: $\lambda_{WB} = 975.82$ while $\lambda_{CS} = 976.02$ nm.

The signal from D_1 is normalized according to the transmission and reflection coefficients of the BSs which the WB pass through, so that it finally represents the injected signal E_{IN} (top row). The injected pulses for s-polarized WB are about four times bigger than the p-polarized pulses which matches our expectation. Despite the weaker injection, for p-polarization 100% of switch-on events are successful while for s-polarization WB the 90%. The filtered time traces corresponding to the successful events are displayed in the bottom row of Fig. 3.9. The vertical dashed line in the bottom figures represent the injection time.

For what concerns the switching time, we observe that it is shorter and more defined in the p-case (around 20 ns) while in the s-case, CSs start rising within a large time interval: between 20 and 80 ns.

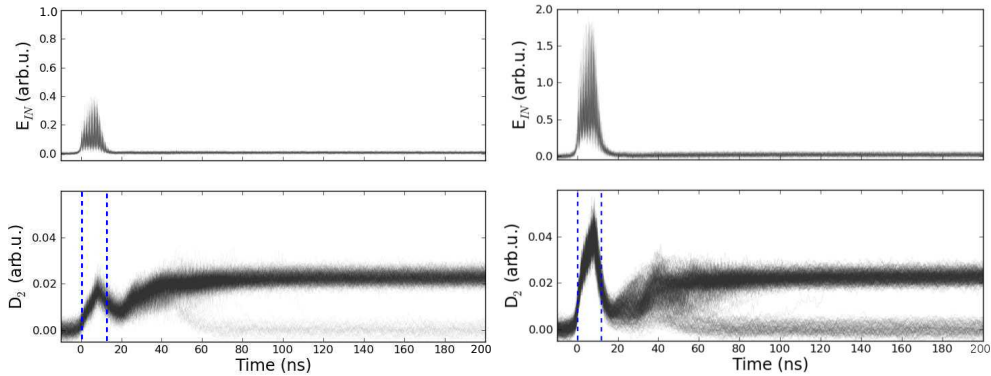


Figure 3.9: Superposition of time traces corresponding to full bandwidth signal of the injected pulses E_{IN} (top row) and to the filtered successful switches detected by D_2 (bottom row). Switch-on is performed for two WB polarizations: p-polarization (left) and s-polarization (right); the injected wavelength is $\lambda_{WB} = 975.82$ nm; the system parameters are $I_1 = 309.1$ mA and $I_2 = 10.6$ mA; $\lambda_{CS} = 976.02$ nm.

The success rate of the p-polarized switching remains quite high even decreasing the pulse amplification. It reaches the same value that we have obtained for the s-switching (90%) for $I_{amp} = 1250$ mA. For this amplification current, the peak power of the injected pulses is the 12% of the peak power of the s-polarized injected pulses depicted in Fig. 3.9. Hence we can estimate that for p-polarized switching, the threshold energy would reduce of the same amount. Since we found a threshold of 25 pJ for s-polarized switching, we would expect to be able to switch on CSs with few pJ using p-polarized switching at the same wavelength.

3.3 Switch-Off

In order to have a complete control of LCSs, once we have written them, it is important to be able to erase them. As we did for the switch-on process, we will study the parameters of the injected beam that allow to optimize the switch-off. Five hundreds injections are acquired for each set of parameters. The optimal conditions previously found do not apply in the switch-off process: p-polarized blue tuned pulses are not effective on the CS. However, once again, the wavelength is very important: the pulses must be as close as possible to the CS wavelength. In this case the CS is affected by the perturbation and its intensity drops down. For a given perturbation power, the effectiveness of CS switch-off depends on the distance, in terms of parameters, from the spontaneous switch-off. If we are far, the CS switches on again after some time as we see in Fig. 3.10. In the case reported in the figure, the CS is bistable for values of $306.6 \text{ mA} \leq I_1 \leq 311.1 \text{ mA}$ and the erasing beam polarization is orthogonal. The drop in intensity becomes deeper and the off-time is longer as the system get closer to the spontaneous switch-off ($I_1 = 306.6 \text{ mA}$). The complete switch-off occurs for $I_1 = 307.1 \text{ mA}$. For longer perturbation pulses

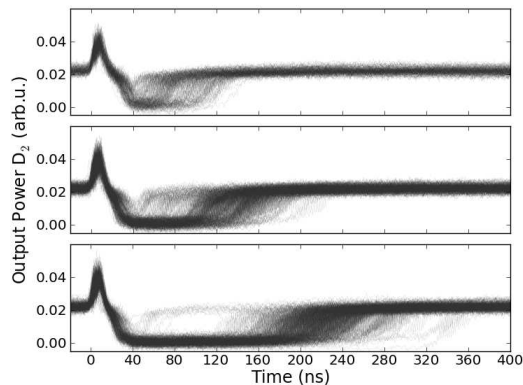


Figure 3.10: Effects of the erasing pulses on a CS for decreasing I_1 within the bistability region. Superposition of five hundreds events for $I_1 = 310.2 \text{ mA}$ (top), $I_1 = 309.2 \text{ mA}$ (centre), $I_1 = 308.7 \text{ mA}$ (bottom); $I_2 = 10.6 \text{ mA}$. The injected wavelength matches the CS one.

the switching off happens before (further from the switch-off point i.e. for higher I_1) than for shorter ones. This means that the necessary energy to switch-off decreases with the proximity to the lower edge of the bistability region as expected; and that with the available perturbation it is not possible to switch-off a CS within all the bistability region. We introduce a modulation in I_1 that would switch-on the CS again after every perturbation pulse, in order to evaluate the success rate and the threshold for a given value of I_1 .

The best result was obtained for the maximum amplification and for a value of I_1 closed to the spontaneous switch-off. The successful events are only the 10% of the total number of realizations and they are displayed in Fig.3.11. The switch-off is

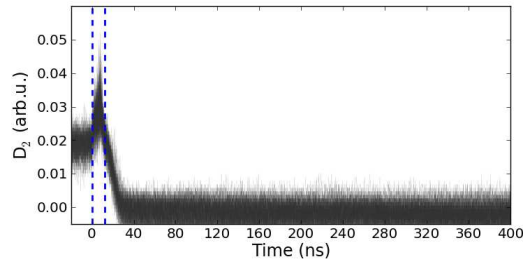


Figure 3.11: Superposition of successful switch-off events for $I_1 = 303.1$ mA, $I_2 = 10.6$ mA. The CS bistability domain is 302.7 mA $\leq I_1 \leq 307.1$ mA. The success rate is 10%.

sharper than the switch-on and it does not show a multimode dynamics, the power simply drops down to zero in 10 ns after the end of the erasing pulse (dashed lines).

3.3.1 Erasing beam polarization

The available perturbation seems to be inadequate to reach a high success rate and so to evaluate an average threshold for the CS erasing. Nonetheless we compare the effects of the perturbation when the polarization is parallel and orthogonal to the CS' one (Fig. 3.12). We notice that for both polarization, the CS shows an intensity

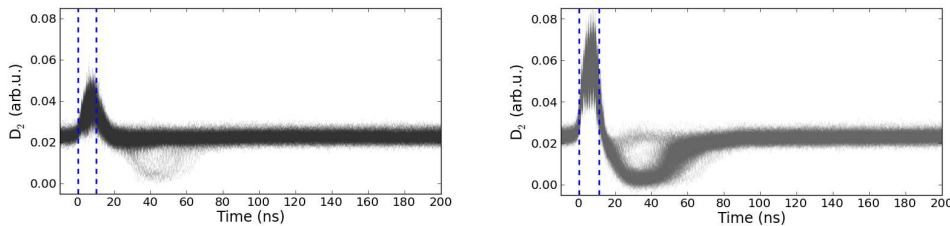


Figure 3.12: Superposition of filtered time traces corresponding to switch-off events for injection with parallel polarization (left) and with orthogonal polarization (right). The CS that we try to switch-off is the same of Fig. 3.10; the system parameters are the same: $I_1 = 310.7$ mA, $I_2 = 10.6$ mA.

dropout but it does not switch-off. For parallel polarization only few erasing pulses drop the power down to zero while for orthogonal polarization in most of the cases the CS switches-off and around 30 ns afterwards, it switches-on again.

3.4 Injection Below the Bistability Region

As we have seen in the switch-on section, from time to time a CS that is switched-on, switches-off spontaneously after some time. In this case, the observed CS lifetime⁴ goes from 40 to 350 ns (see time traces of Fig. 3.7).

The phenomenon can be described as an attempt to switch-on a CS that is unstable

⁴Time for which the system stays locally in the on-state

or as the switch-on of a stable CS very close to lower edge of the its stability domain (bistability region). In the first case the CS state is not fully attained and the system comes back to the non-lasing state in a time shorter than the switching transient (about 200 ns). In the second case, the CS state is reached but small perturbations like noise can switch the CS off. The lifetime shows then a stochastic component (see time traces of Figs. 3.7, 3.9). These CSs could be laser solitons with a different frequency which have different bistability domains and which result unstable for the present system parameters. Observations of CSs lasing at different frequencies and having different but overlapping bistability domains have been already reported in [Genevet 2010b].

In this section we focus our attention on these CSs which exhibit a short lifetime once they are excited. First, for a given perturbation, we evaluate the frequency of these events as function of the pump parameter I_1 and we compare it to the total number of successful switches. Later, in the next subsection, we analyze in detail the statistics of the switch-off times for I_1 below the bistability region.

In Fig.3.13, we report the total success rate (blue squares) and the fraction of the successful switches that corresponds to CSs with a short lifetime (red circles). The detected time-window for each event is 500 ns so CSs, that switch-off spontaneously after that time, are not counted. The used WB has s-polarization.

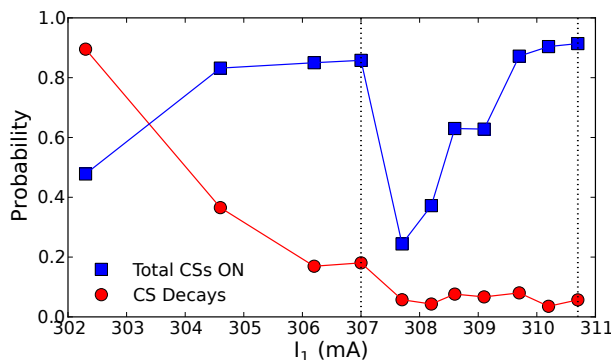


Figure 3.13: Ratio of successful switches to the total number of events (blue squares) and number of CSs that decay spontaneously over the switched-on ones (red circles) as function of I_1 for s-polarized injection. The CS bistability domain is marked by the black dotted lines.

Within the bistability region (delimited by the vertical dotted lines), the success rate (blue squares) passes from 90% to 20% as I_1 approaches the lower edge. This means that the energy necessary for the switching increases as I_1 moves away from the spontaneous-switching point. On the other hand the CSs with a short lifetime (red circles) are a small constant fraction of the total number of successful switches. Just below the lower bistability edge ($I_1 = 307$ mA), despite the fact that the CS solution is unstable, we observe an unexpected increase of the success rate. When we remove the train of writing pulses the CS persists for a time of the order of tens

of milliseconds and then it switches-off. Therefore the presence of the perturbation is responsible for the metastability observed in the CS. Given the time scale of the decay time, this phenomenon could have thermal origins. When we are sufficiently far from the bistability (for $I_1 = 302.3$ mA in Fig. 3.13), the success rate decreases again and almost the totality of the successful events switches-off within our detected time-window. So, in these conditions, the observed behaviour can be better described in terms of failed attempts to switch-on a state that is not stable. This is the regime that we study in the following.

3.4.1 Looking for excitable LCS

In order to test the local excitable behaviour of our system below the CS stability domain, we analyze in detail the temporal response to a short optical perturbation. The applied perturbation is not amplified so the injected pulse power is about one tenth of the previously used maximum power. In order to be able to excite the system response even at low power, the injected pulses are p-polarized, their duration is increased (at least 20 ns) and their wavelength is tuned to have the best success rate. The results reported below are obtained for $\lambda_{WB} = 975.70$ nm while $\lambda_{CS} = 975.82$ nm.

Furthermore the injected train of pulses have a strongly astigmatic spatial profile as we can see on the near field monitored by the camera (inside the dotted area of Fig.3.14). The horizontal dimension is larger than the profile of a localized structure, while the vertical dimension is narrower. Despite its shape, that does not match the CS one, the perturbation is able to trigger a response from the system. The time-averaged profile of the response have the shape of a localized structure (Fig.3.14 b)).

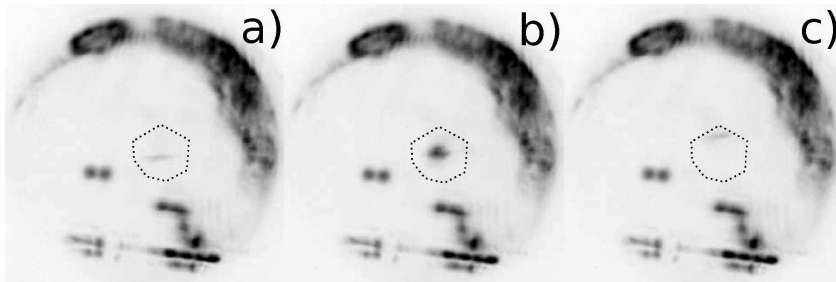


Figure 3.14: Time-averaged near field for injection below threshold (dark areas correspond to high intensities). The analyzed area is delimited by the dotted curve. The train of injected pulses appears as a weak and astigmatic bright spot (a), when it is moved on the known pinning position, it excites the response of the system that in average looks like a CS (b). When the beam is moved away, the system comes back immediately (within the integration time of the camera) to the nonlasing state. $I_1 = 260$ mA, $I_2 = 4.6$ mA.

We remind that the principal features of the excitability are:

- the existence of a threshold for the perturbation, below which the system linearly responds;

- once the threshold is overcome the system emits a deterministic nonlinear pulse, which does not depend on the perturbation, before coming back to the stable initial state.

We observe that our system reacts in two different ways.

i) When the pulses are not strong enough or the wavelength is not properly tuned, the system does not exhibit any visible response after the injected pulse (Fig. 3.15). In the figure we display the average of several time traces corresponding to this kind of events. The average allows to extract the system response from the time traces of D_2 which have a low signal to noise ratio. The response of the system to the injected pulse is linear, it acts qualitatively as a low-pass filter: from a square input pulse (D_1), we get a triangular output (D_2).

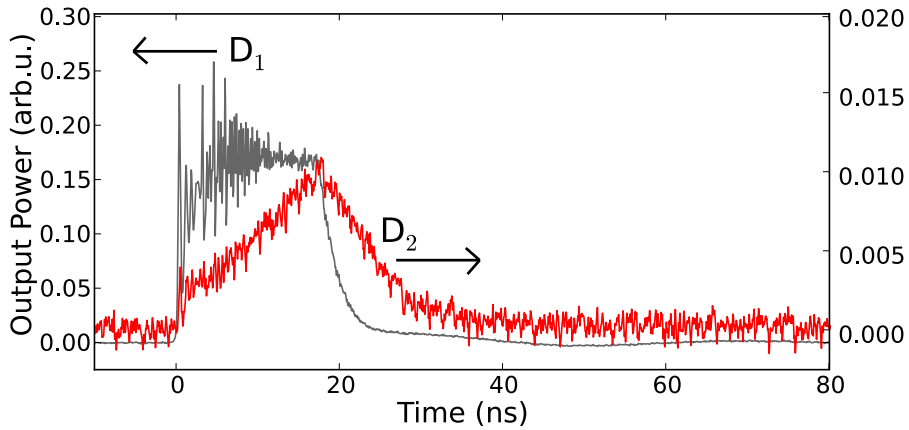


Figure 3.15: Average of hundreds of time traces acquired by D_1 and D_2 corresponding to unsuccessful events: the system stays in the nonlasing state after the injected pulse (D_1). The system (D_2) behaves as a low-pass filter during the injection: from 0 to 20 ns.

ii) When the pulses are strong enough and well tuned, the system emits light after the perturbation: the intensity grows and it returns back to zero after some time (see an example on the left of Fig. 3.16). The number of successful events for a given perturbation depends on how distant I_1 is from the bistability region. On the right hand side of Fig. 3.16 we show the success rate obtained with 20 ns long pulses whose average power is $300 \mu\text{W}$. The fact that the number of responses increases abruptly from 20% to 100% demonstrates the presence of a threshold to overcome in order to obtain a nonlinear response from the system.

The threshold-like all-or-nothing behaviour is demonstrated, the next step is to investigate the return trajectory (the way by which the system returns to its initial state) of the response. To this purpose, we analyze the filtered time traces of all the successful events for a set of parameters used to trace Fig.3.16 and we measure the return time (see Figs.3.17 and 3.18). We observe that all the response amplitudes are comparable with the CS one and that there are no events shorter than 100 ns. The measured on-state lifetime can go from the cutoff 100 to more than 800 ns (limit imposed by the detection time window). Nonetheless a deterministic

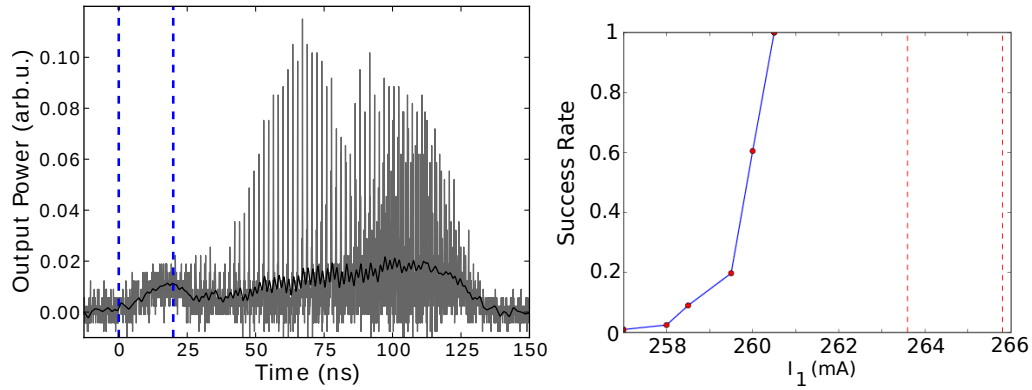


Figure 3.16: Left: example of the full-bandwidth time trace acquired by D_2 , corresponding to one successful event. The filtered trace is superposed in black. Right: success rate (red circles) calculated over 200 realizations for different values of I_1 . The injected pulses have a power of about $300 \mu\text{W}$ and p-polarization. The abrupt rise of the success rate as I_1 gets closer to the bistability region (dashed red lines), denotes the existence of a threshold in the response mechanism.

component shows up: most of the responses last about 125 ns.

This typical pulse duration is much longer than the excitable pulse width measured in a VCSEL with intracavity saturable absorber which is in the subnanosecond range [Barbay 2011]. It is also far from the known time scales of the system variables (of the order of nanoseconds for carrier lifetime). Its origin seems to be linked to the switching transient of a CS. If we look at the full bandwidth time trace in Fig.3.16, we notice that the dynamics is identical to the one observed in the switch-on of a cavity soliton [Genevet 2009a].

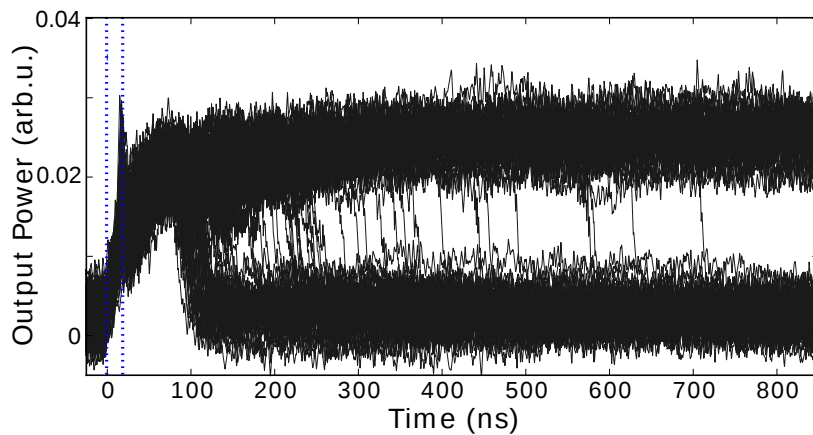


Figure 3.17: Superposition of time traces detected by D_2 corresponding to successful events. The system parameters are $I_1 = 260 \text{ mA}$, $I_2 = 4.6 \text{ mA}$.

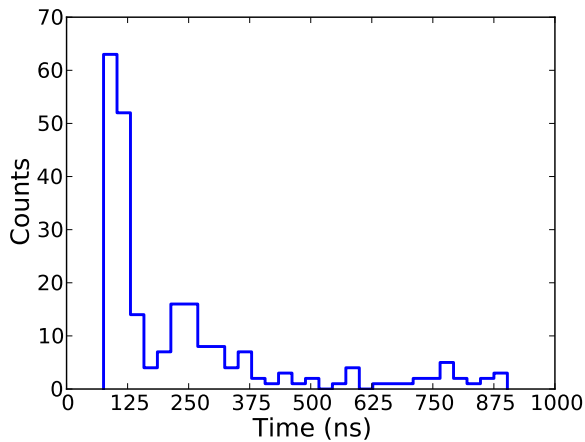


Figure 3.18: Histogram of the return time for the successful events depicted in Fig.3.17; the time is counted from the beginning of the injected pulse until the instant when the power drops down of half the CS value.

3.5 Conclusions

We have demonstrated that we are able to switch-on and -off localized structures. The optimal beam characteristics ended up to be different for the two processes. Switch-on prefers p-polarized pulses with wavelength blue tuned compared to the one of the structure that is addressed. Switch-off, on the other hand, is favored by s-polarization and a wavelength that matches the CS's one. The switch-on process, at our best, takes twenty nanoseconds to start and about two hundreds nanoseconds to be completed because of the dynamical transient while the switch-off, when successful, occurs in about twenty nanoseconds. The switch-off efficiency could be affected by the lack of power. The maximum injected energy is about 30 pJ for s-polarized pulses and about ten pJ for p-polarization. Moreover in [Mahmoud Aghdami 2008] the authors show that the efficiency of the switching depends on the control beam size. The spatial profile of the injected beam shape is hardly controllable experimentally. The difficulties encountered in the switch-off might be due to this constraint.

Besides we have studied the response of the system below the bistability region and found some elements peculiar to excitability such as a threshold-like behaviour and a certain determinism in the return trajectory (the way by which the system returns to its initial state). Indeed the majority of the responses has a duration of 125 ns and none lasts for a shorter time.

Moreover, the spatial profile of the time averaged response matches the one of the stable CS. These observations are encouraging experimentally excitable localized structures. Although the mechanism leading to excitability has still to be clarified as well as the presence of a stochastic component in some of the observed return trajectories.

Numerical works about excitable localized structures in kerr cavities, show the importance to apply a suitable perturbation. In a infinite-dimensional system, ex-

citability is found by applying a perturbation in a specific direction: the one the unstable LS [Gomila 2007]. Thus, once again it might be the perturbation shape that limits our results.

Drift-Induced Excitable Localized Structures

Contents

4.1	Influence of alignment on the system dynamics	52
4.2	Single point dynamics	54
4.2.1	Analysis of the bifurcation	55
4.3	Spatially resolved measurements	58
4.3.1	Drift-induced excitable localized structures	61
4.3.2	Oscillating localized structures	63
4.4	Conclusions	64

Since the demonstration of their existence in spatially extended optical systems, localized structures have been mainly studied in a context of bistability, in the interest of using them as optical bits for parallel information storage and treatment. On the other hand, excitability in optics has been observed and investigated in absence of spatial degrees of freedom.

In contrast to all of these studies excitability mediated by localized structures has been recently studied theoretically in a paradigmatic model for a nonlinear optical cavity with spatial dependence [Gomila 2005]. At the intersection between the phenomena of nonlinear light localization and excitability, excitable localized structures offer both the parallel mode of operation typical of localized states and the threshold-like response of excitable systems. Thus, they open novel perspectives for applications in information processing [Jacobo 2010]. They appear as well-calibrated pulses of light which are localized in space and after which the system returns to its initial quiescent state. In the case studied in [Gomila 2005], excitability arises from the collision of a stable limit cycle (oscillating localized state) with the unstable localized state branch, leading to a saddle loop bifurcation close to which the system shows excitable localized structures.

We have already studied localized structures out of the bistability context in sec. 3.4, in this chapter we analyze the behavior of localized structures subjected to external gradients.

We observe a local bifurcation from the nonlasing state to a periodic emission of pulses that has the same features of the one reported in [Gomila 2005] *i.e.* a finite amplitude and infinite period. Analysis of the spatio-temporal dynamics close

to the bifurcation reveals the presence of noise triggered excitable localized states and of localized states oscillating on the pinning position. We start presenting our work from experimental observations, then we report on the further measurements that allow the physical explication of the phenomenon. Conclusions are drawn to summarize the results.

4.1 Influence of alignment on the system dynamics

Alignment plays a crucial role in the dynamics of our system. In particular, for what concerns localized structures, it is known that their stable spatial location arises from an interplay of spatial inhomogeneities and gradient induced forces. In this section we show an example on how the alignment changes the near-field intensity distribution and its time-averaged dynamics as function of the parameters. First of all the parameters are set in such a way that the system is able to work as a cavity soliton laser and we monitor the evolution of the near field with the camera corresponding to L_2 when the mirror just in front of L_1 is rotated horizontally. Snapshots for different relative alignments are displayed in Fig.4.1. At the beginning (a-b) the intensity in the area of overlap is rather high and complex structures are visible, then the interaction between the two devices becomes more clear until we recognize bright localized structures surrounded by a dark homogeneous background (d). As the mirror is further tilted, the structures get blurred (e-f) until they become less contrasted and elongated (g). In h) all structures disappear and we observe only a dark background.

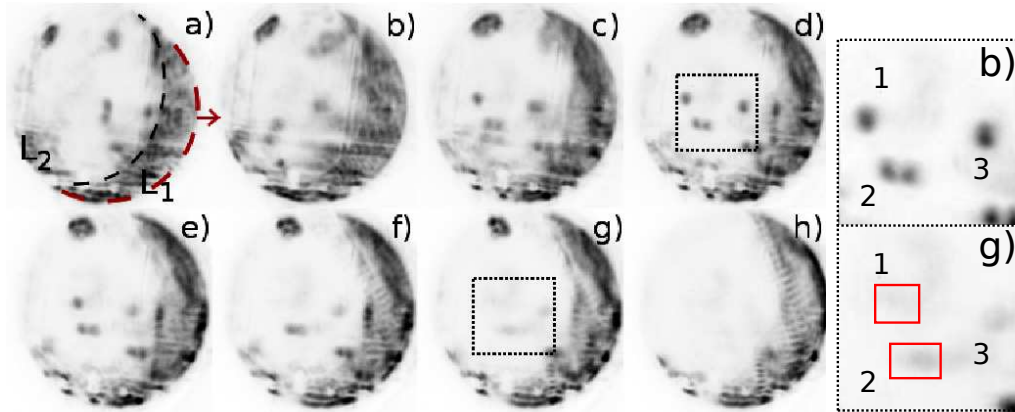


Figure 4.1: Evolution of the near-field intensity distribution as the alignment is changed (dark areas correspond to high intensities). Left: from a) to h) the profile of L_1 moves to the right with respect to L_2 . Right: zoom of snapshot d) and g). The red squares correspond to the areas analyzed in the following. $I_1 = 290$ mA, $I_2 = 11.7$ mA.

If we resolve in time the emission of the structures 1 and 2 in g), we will find a behavior like the one displayed in Fig.4.2. It consists in the emission of bursts rather similar to each other, whose duration is of the order of 15 ns. Each burst is composed of short pulses separated by the compound cavity round-trip time, that

is the time taken for the light to make twice the distance L_1-L_2 : 1.8 ns. Hence this fast dynamics is associated to the multiple-longitudinal-mode dynamics.

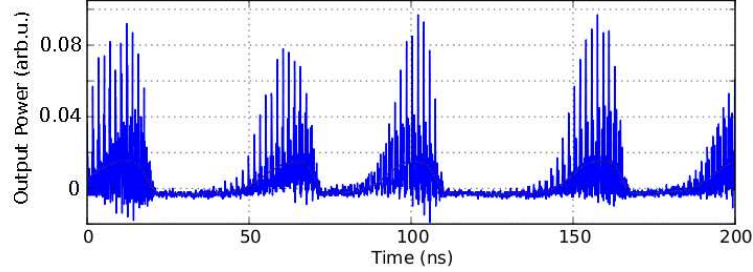


Figure 4.2: Time traces detected by D_1 corresponding to the emission coming from a weakly bright and elongated structure surrounded by nonlasing background, equivalent to structures 1 and 2 shown in Fig.4.1 g).

In a second time, the mirror is kept in the position g) and the current I_1 is scanned up and down. We compute the intensity of the areas 1 and 2 delimited by the red squares in Fig.4.1 g) as function of the current in order to trace the local LI curve. The aim is to understand how the pulsing structures form, if they are bistable and what is the link with stable localized structures.

In Fig.4.3 the LI curve 2 (dotted line) shows a hysteresis cycle at threshold (region B) while the spatial profile matches a typical CS profile (see inset B). The spatial profile change qualitatively entering in region D (see inset D), becoming a pulsing structure; bistability between the two spatial profiles is observed in region C. On the other hand, the LI curve 1 (straight line) does not show a hysteresis cycle and it overcomes the laser threshold in region D exhibiting a pulsing behavior.

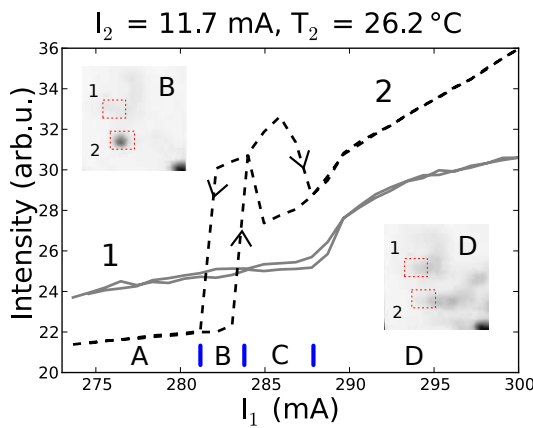
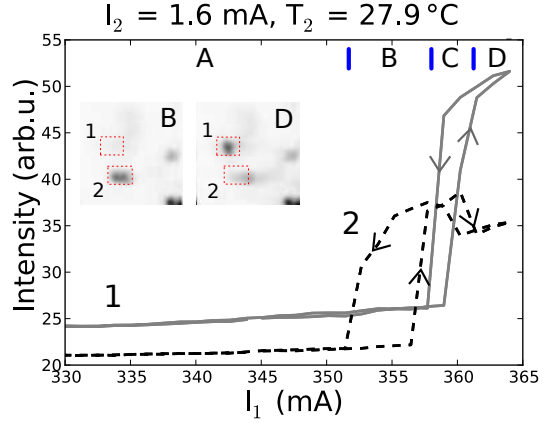


Figure 4.3: Time-averaged local LI curve for two points of the space (1 and 2 as in Fig. 4.1 g)). For low current, each point is in the nonlasing state (A); B corresponds to the bistability region of the bright spot 2 (see inset B); as the current is further increased, 2 passes in a lower intensity state whose near field profile is broader (D and inset D), at the same time 1 starts emitting; as the current is decreased a hysteresis cycle between the broader structure with lower intensity and the higher intensity localized spot appears in 2 (C) while 1 does not show any bistability.

In Fig.4.4 we show the same LI curves but diminishing the current of the absorber I_2 and increasing its temperature T_2 . The global effect is to increase the laser thresh-

old which occurs for higher I_1 . The curve 2 behaves like the previous one except for the fact that a two-lobes instead of a single-lobe structure is generated. On the other hand curve 1 shows a hysteresis cycle corresponding to a single-lobe LS.

Figure 4.4: Time-averaged local LI curve for same two points as in Fig 4.3) but for different current and temperature of the absorber. Four regions are distinguishable: A) both curves are below threshold; B) curve 2 shows a bistable two-lobes structure (inset B); C) curve 1 shows a bistable localized structure; D) the two-lobes structure in 2 becomes a less bright and broader structure while in 1 a non-bistable bright spot is visible (inset D).



Summarizing, in the same regions of the transverse plane where localized structures are known to be stable under optimal alignment conditions, a local pulsing behaviour appear when the alignment conditions are slightly changed. This local pulsing behaviour (Fig.4.2) can appear at the onset of the lasing process or beyond the bistability region of a localized structure (respectively curve 1 and 2 in Fig.4.3). For the same alignment conditions, the system can exhibit localized structure if the current of the absorber is reduced and its temperature slightly increased (curve 1 in Fig.4.4).

In the following we will analyze in detail the temporal and spatial dynamics of the pulsing regime at the onset of lasing.

4.2 Single point dynamics

For our analysis, we measure the temporal emission of a small region of the space, selected by the iris. The recorded area has a diameter of about $20 \mu\text{m}$ that is slightly larger than the typical diameter of a localized structure. We select a region where a localized structure is known to be stable (pinning on a defect) under optimal alignment conditions. For the alignment conditions considered in the following, the system behaves as in the curve 1 of Fig.4.3: the loss of equilibrium of the nonlasing solution occurs through emission of pulses. For a given current of the absorber I_2 , three regimes are distinguishable upon increase of I_1 , they are illustrated in Fig.4.5. At threshold, the pulses are emitted sporadically (a); then the time between two successive pulses (interspike time) decreases (b) and a clear periodicity appears (c). In the completely periodic regime, the time-averaged near field consists in a bright $40 \mu\text{m}$ long and $15 \mu\text{m}$ wide region surrounded by homogeneous dark background. The detector is placed on the brightest part of this region (see inset in Fig.4.5). Even though there is a certain interest in the fast dynamics, in this study, we focus

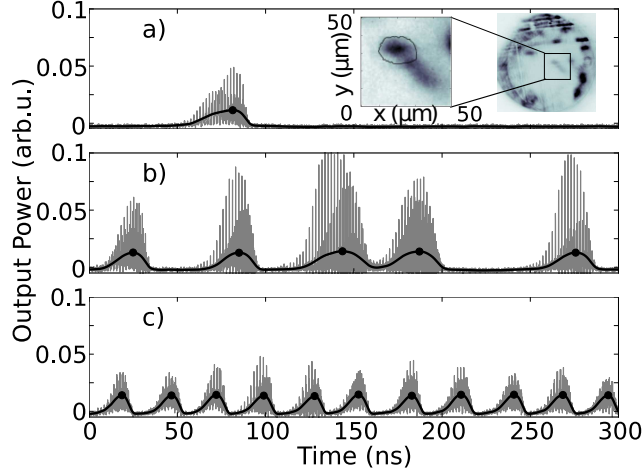


Figure 4.5: Full bandwidth (grey line) and filtered (black thick line) time traces of the power emitted by the small (~ 20 -microns diameter) region of space delimited by the black circle in the inset. The dynamics changes its characteristics as the pump I_1 is increased, it is: sporadic for $I_1 = 308.4$ mA (a); quasi-periodic for $I_1 = 310.9$ mA (b) and periodic for $I_1 = 315.4$ mA (c). $I_2 = 5.5$ mA.

our attention on the slow envelop of the pulses which we obtain by Fourier filtering the time series allowing only components below 1.3 GHz (thick line in Fig.4.5). Although the choice of the filter is arbitrary, we have checked that the observations reported below do not depend on the chosen width of the filter window, provided that it is sufficient to smooth out the details of the longitudinal mode dynamics. We acquire time traces for different value of I_2 and study the evolution of the dynamics upon variation of I_1 in order to characterize the bifurcation leading from the stable nonlasing state to the periodic pulsing regime. The interspike-times and the peak-amplitudes are measured by identifying the maximum of the pulses (black spots in Fig.4.5) and analyzed in the following subsection.

4.2.1 Analysis of the bifurcation

In the top panel of Fig.4.6 we show how the average time between pulses depends on I_1 , for four values of I_2 . The error bars correspond to the standard deviation. In all cases we observe that the loss of equilibrium of the nonlasing solution upon increase of I_1 occurs first via the mostly disordered emission of pulses, followed by a decrease of the average value of interspike time. The dispersion of the interspike time also strongly diminishes indicating that the dynamics is more and more periodic. If the current I_1 is increased further than the displayed values, the spatial profile becomes more complicated and the slow dynamics is overcome by the fast one. Thus we don't analyze this regime.

On the other hand, the amplitude of the pulses is very well defined in any case as shown on the bottom panel of Fig.4.6. This indicates that the trajectory followed by

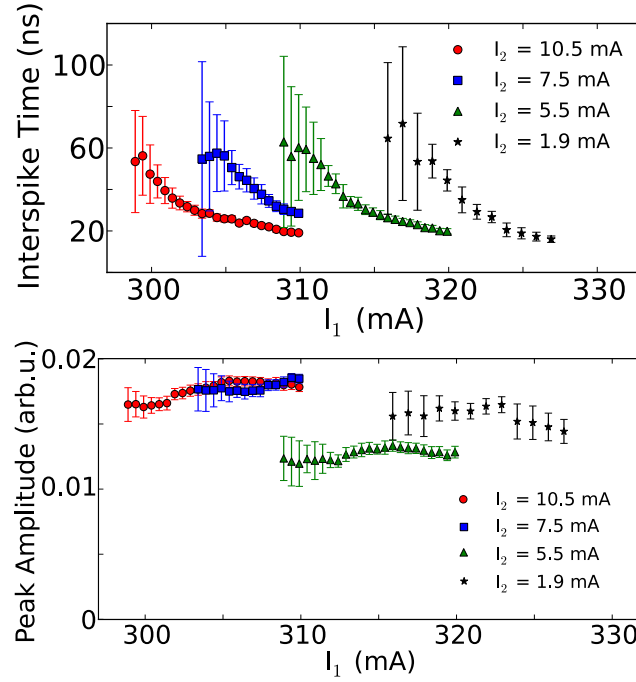


Figure 4.6: Top: mean value of interspike time as function of amplifier pump I_1 , for different values of the absorber current: $I_2 = 10.5$ mA (\bullet), $I_2 = 7.5$ mA (\square), $I_2 = 5.5$ mA (\triangle), $I_2 = 1.9$ mA (\star). Bottom: corresponding mean value of the peak amplitude. The error bars indicate the standard deviation.

the system in phase space is very well defined even when the temporal distribution is disordered.

The trend of all the interspike time curves in Fig.4.6 is compatible with the period of a limit cycle arising via a saddle-node on an invariant circle [Strogatz 1994] or via a saddle-loop [Gaspard 1990] bifurcations (both leading to excitability [Izhikevich 2007]). Both are infinite-period bifurcation. The period is proportional, respectively, to the inverse of the square root of $(I_1 - I_s)$ [Strogatz 1994] and to the logarithm of the same quantity [Gaspard 1990]. Where I_s represents the value of the control parameter at which the bifurcation occurs. The fit of one set of the experimental data with these functions is reported on Fig.4.7.

Moreover our system behaves like a noise-driven excitable system as we illustrate below. When we compute the coefficient of variation for the data reported in Fig.4.6 *i.e.* the ratio between the standard deviation and the average value (Fig.4.8), we find a maximum value of 0.9. This is an indication that the observed emission of pulses is close to be a Poissonian process, for which the coefficient is 1.

As we analyze the histograms of data corresponding to the three different regimes (see Fig.4.9 (left)). We remark that while the periodicity of the time series is very clear in case c), the other two histograms exhibit an exponential decay at long times. This indicates that the pulse emission process, when not periodic, can be described

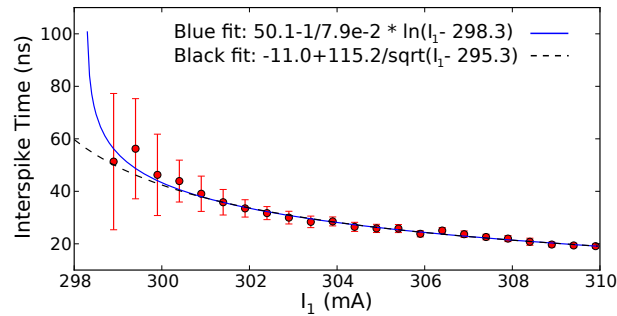


Figure 4.7: Average interspike time as function of I_1 for $I_2 = 10.5$ mA. The curve is fitted with the equation for the period of a limit cycle arising from a saddle-loop (blue straight line) and from a saddle-node bifurcation (dashed black line).

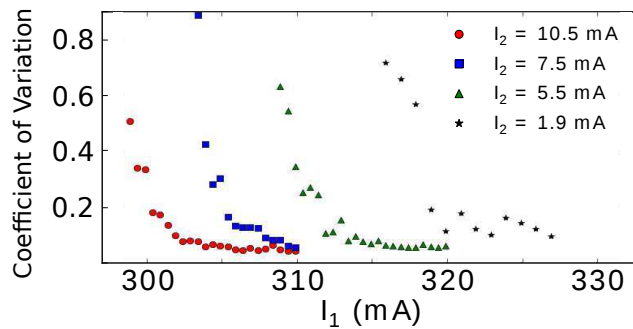


Figure 4.8: Coefficient of variation of the measured interspike time: standard deviation to average ratio.

as noise induced barrier crossing (see e.g. [Hänggi 1990, Kramers 1940]). On the other hand, a cut-off is present at short times: there are few events below twenty nanoseconds and none below ten nanoseconds. The same kind of distribution with exponential tail and a cut-off is observed for the interspike time of noise induced excitable pulses [Yacomotti 1999, Eguia 2000]. In this framework, the cut-off at short times which is visible in all these histograms is caused by the refractory time of excitable pulses.

The fact that the pulses are randomly triggered by noise is further confirmed by the return map of time intervals shown on the right panel of the figure. If the dispersion of the interspike time were due to simple fluctuations of the period of a limit cycle, an accumulation of points would be visible in the $y = x$ region of the return map. Since the distribution of points fills up the whole phase space, with exception of the refractory time, the origin of the time intervals is clearly random.

For the sake of completeness we point out that all the data used to obtain Figs. 4.6 (and figures related to it), have been obtained in the exact same configuration (alignment and spatial region) for consistency. The phenomenon is though observable for different combinations of the alignment and the detected spatial region.

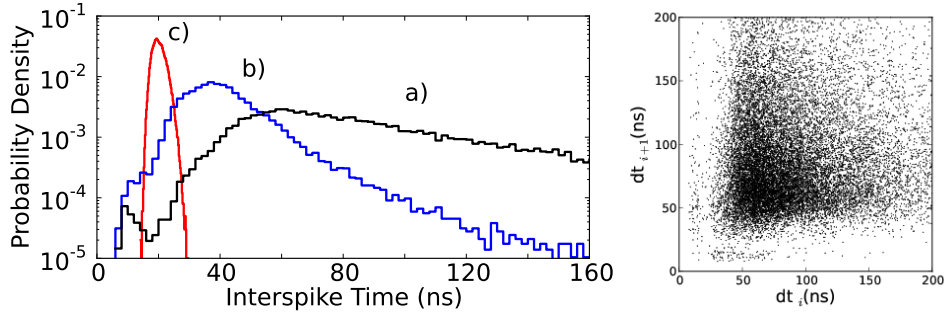


Figure 4.9: Left: histograms of interspike times in noise dominated (a), periodic (c) and intermediate regimes (b). Right: return map of time intervals corresponding to case (a). System parameters are: $I_1 = 343.9$ mA, $I_2 = 1.9$ mA (a), $I_1 = 333.6$ mA, $I_2 = 5.9$ mA (b), $I_1 = 343.4$ mA, $I_2 = 5.9$ mA.

That is the case for Fig.4.9. The qualitative evolution of the interspike time average and standard deviation is preserved but the absolute values of the parameters for which the dynamics occurs, change according to the configuration in which the measurements are performed. For this reason the parameters for which the histograms are obtained are not consistent with the data analyzed previously.

Independently on the physical origin of the observed dynamics, the system clearly presents a bifurcation from a stable fixed point to an infinite period and a finite amplitude limit cycle which is a situation leading to excitability. Therefore the observed random generated pulses are identifiable as noise triggered excitable pulses. In the next section we will investigate the physical mechanism that is behind the observed dynamics. To this purpose, we analyze in more detail the spatial dynamics of the system around this bifurcation.

4.3 Spatially resolved measurements

We acquire simultaneously times series from two different detectors in the spatial region of interest. The detectors are aligned along the elongated direction of the bright structure visible on the camera as shown in near field snapshot of Fig. 4.10. Each detector monitors a 20 microns diameter area, whose centers are separated by 23 micrometers. Typical time traces corresponding to the periodic regime are shown on Fig.4.10. In these cases the occurrence of a pulse in one region of space is followed by a pulse in the neighbouring region with a delay and the clear correlation (see Fig. 4.11) between the two traces demonstrates a propagation in the transverse dimension. In order to complete these measurements, we also show in Fig. 4.12 that the time lag between the two traces increases with the distance between the detectors.

The fact that the intensity emitted in the area monitored by D_2 increases only upon decrease of the intensity emitted in the area monitored by D_1 hints at an interpretation of the dynamics in terms of a localized state nucleated in front of

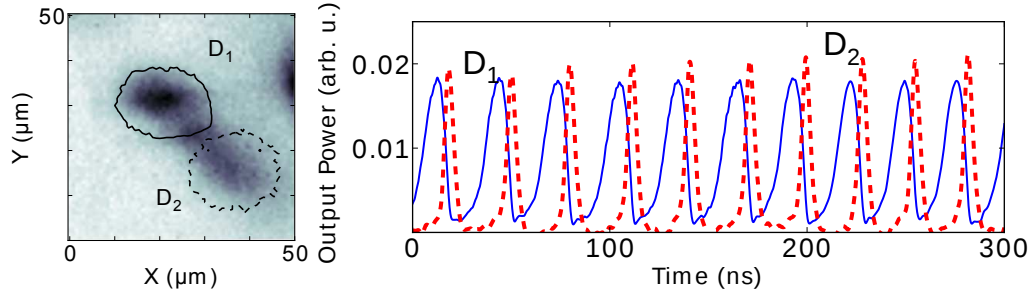


Figure 4.10: Left: near field intensity distribution showing the areas detected simultaneously by D_1 and D_2 . Right: time traces corresponding to the radiation emitted by the two regions monitored by D_1 (blue straight line) and D_2 (dashed red line). The dynamics is interpreted as localized states that periodically nucleate in D_1 and then drift towards D_2 . $I_1 = 302.9$ mA, $I_2 = 10.5$ mA .

D_1 which then drifts across the spatial region of interest. If detector D_2 is moved further away, no intensity is detected, which indicates that the structure has reached a spatial region where it can not exist due to spatial inhomogeneities [Caboche 2009].

The speed of the localized structure can be estimated from the time separation between the falling edges in D_1 and D_2 , *i.e.* when the structure leaves the area monitored by each detector. In Fig. 4.10 this lag is of 4.4 ns, which together with the distance between the two detectors edges (23 micrometers), leads to an estimated velocity of $5.2 \mu\text{m/ns}$ (without any assumption of the size of the propagating structure), a value close to the velocity of drifting localized structures measured in a different experimental system based on nominally identical devices [Caboche 2009].

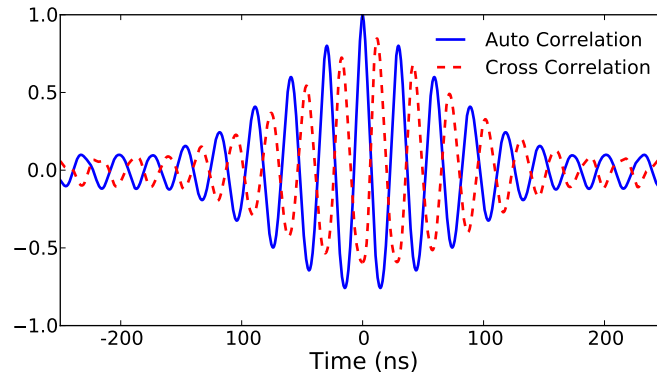


Figure 4.11: Zoom around zero delay of the auto-correlation of the signal D_1 (blue straight line) and of the cross-correlation of the signals D_2 and D_1 reported on Fig.4.10 (red dashed line). Signals are normalized subtracting the average value and dividing by the standard deviation. The auto-correlation shows that the signal has a correlation time of 200 ns, which reveals an imperfect periodicity. The cross-correlation looks like the auto-correlation. Its maximum peak is close to one and is shifted respect to the zero thus indicating the high correlation and the delay between the two signals.

This estimation can be checked against the duration at half maximum of the pulses measured in D_2 : assuming a size of the localized structure (FWHM) of 12 micrometers (as measured for stationary localized structures in this experimental arrangement), the center of the structure would drift about 32 micrometers during a pulse. The pulse duration of 6.6 ns then leads to an estimated velocity of $4.8 \mu\text{m}/\text{ns}$, which matches rather well the previous estimation.

The motion takes place along a well defined direction (along the elongated dimension of the bright structure) which critically depends on the alignment. For instance, the direction is tilted by a certain angle (about 45deg) in the case of the structure in the inset of Fig. 4.10 and it is horizontal in the case of structure 2 on Fig. 4.1 g). This suggests that a gradient caused by the misalignment is responsible for the drift, excluding the spontaneous motion due to the localized structure's internal degrees of freedom which is described in models of bistable lasers [Fedorov 2000, Rosanov 2002]. Hence we finally interpret the periodic pulsing described above in terms of periodic nucleation and motion of localized structures in presence of a gradient and a local inhomogeneity.

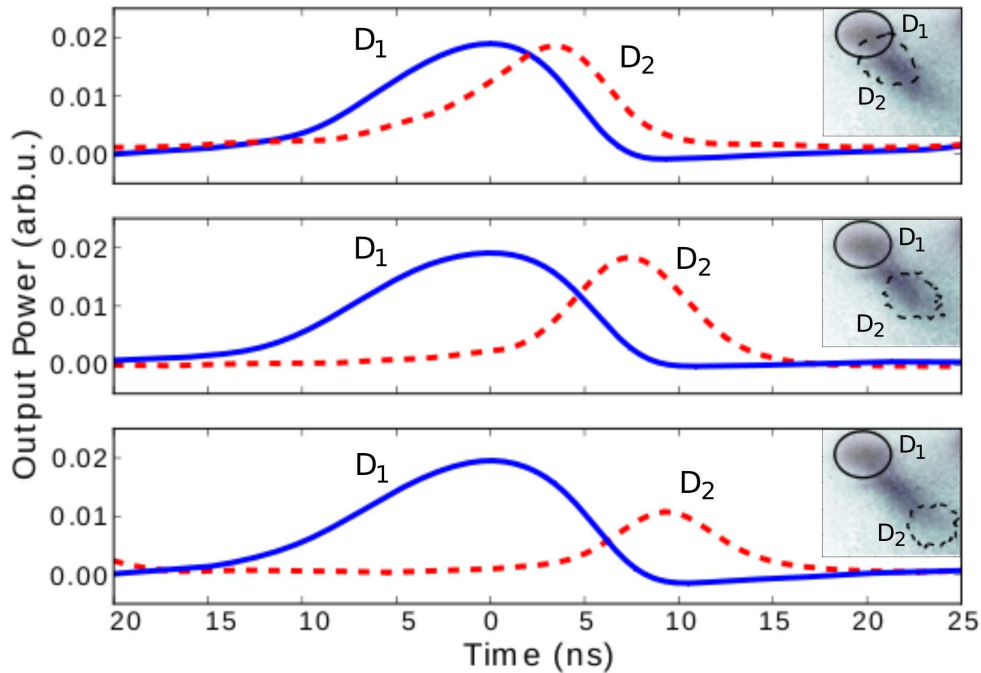


Figure 4.12: Signals acquired simultaneously in two regions of the transverse plane (D_1 , D_2). The position of D_2 is moved along the bright structure as shown in the insets. The delay between the two signals increases with the distance between the two detectors.

4.3.1 Drift-induced excitable localized structures

According to the physical interpretation, we conclude that the previously described noised triggered pulses (see Fig.4.13) are noise generated excitable localized structures. The excitability is proved by the characteristics of the bifurcation (discussed

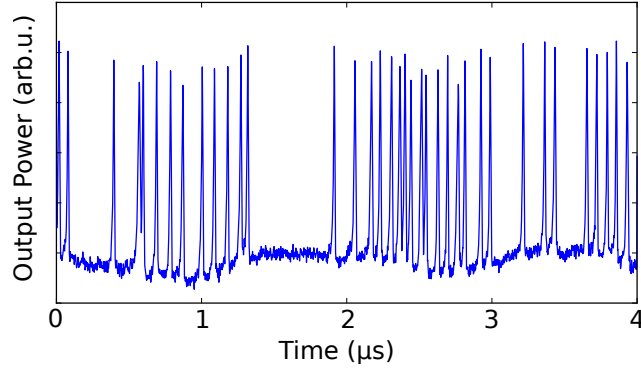


Figure 4.13: Part of the time trace used to trace the histogram a) of Fig. 4.9. It shows local emission of noise triggered pulses that can be described as noise generated localized structures. The visible low frequency modulation comes from the detection.

in sec. 4.2.1), and by the deterministic way by which the system comes back to the nonlasing stable state.

The mechanism that induces the excitability is the drift due to external gradients. The structure nucleates on the local inhomogeneity (D_1), an external gradient makes it drift, subsequently the structure reaches D_2 quitting the region detected by D_1 that comes back to the trivial state. In the end the localized structure dies on another inhomogeneity that makes it unstable.

The described phenomenon exhibits a well-defined trajectory in both the local time-traces (the pulse duration is given by the drift velocity) and in space (the spatial trajectory is defined by the region of drift).

In the following we show that the spatial trajectory of localized structures depends on the parameters. We calculate the time-averaged power measured in both detectors (see Figs. 4.14) for the same data as Fig. 4.6 but for only two values of I_2 : 10.5 mA (left panel) and 1.9 mA (right panel). In both panels, the time-averaged power detected in the region D_1 , which is where the nucleation takes place, is quite high even at the onset of lasing (lower values of I_1). It increases slowly reaching its maximum when the fully periodic regime is achieved (higher values of I_1). On the other hand the power detected in D_2 begins from a value very close to zero and, as the current is increased, it grows linearly until it reaches the same value of D_1 . The fact that the average detected power is equal in both detectors confirms the spatial dynamics observed in the periodic regime: localized structures are nucleated in D_1 and then drift through D_2 . According to this interpretation, the fact that the averaged power in D_2 diminishes as I_1 decreases, indicates that the distance covered by the drifting localized becomes shorter. The shorter distance is obtained for lower

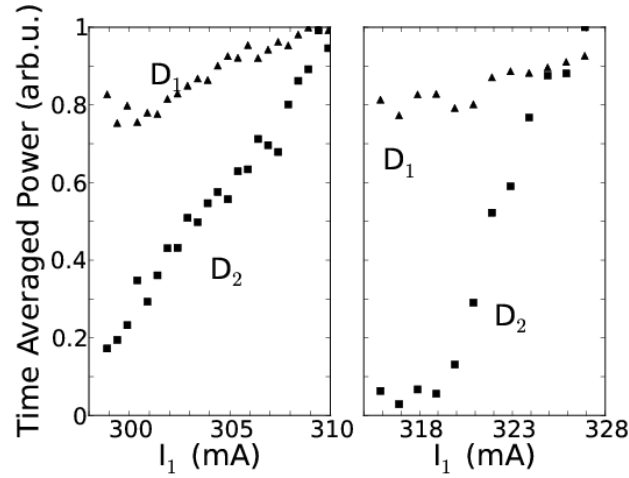


Figure 4.14: Time averaged power detected in two regions of the space D_1 and D_2 as function of I_1 . All the curves are normalized respect to the maximum value. Left: $I_2 = 10.5$ mA. Right: $I_2 = 1.9$ mA.

current of the absorber ($I_2 = 1.9$ mA). For these parameters only the tails of the localized structure are detected in D_2 (see Fig.4.15).

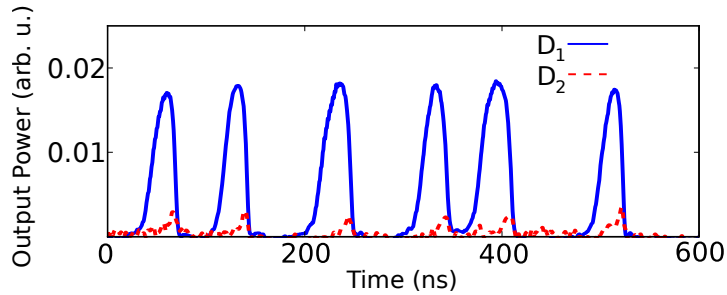


Figure 4.15: Sample of a time traces recorded in two different points in the space: D_1 (blue straight line) and D_2 (red dashed line). $I_1 = 316.9$ mA, $I_2 = 1.9$ mA.

In order to check the determinism of the trajectory, we study the dependence of the correlation of signal D_1 and D_2 on the parameters. If the correlation is high it means that each LS generated in D_1 , decays in the same way. As an indicator we use the value of the maximum of the cross-correlation function (see as an example of the cross correlation function, the dashed curve in Fig. 4.11). From Fig. 4.16 we notice that in all the four curves, the correlation between the two signal never goes close to zero and that only in few cases it is lower than the 60%. Thus the signals corresponding to two different region of the space keep a high correlation all over the considered parameters range. The drop of correlation is partially explained by

the loss of power and by the change of the pulse shape (including only the tails of the LS) in the signal D_2 . Another phenomenon can be at the origin of the decrease of correlation and it is illustrated in the next section.

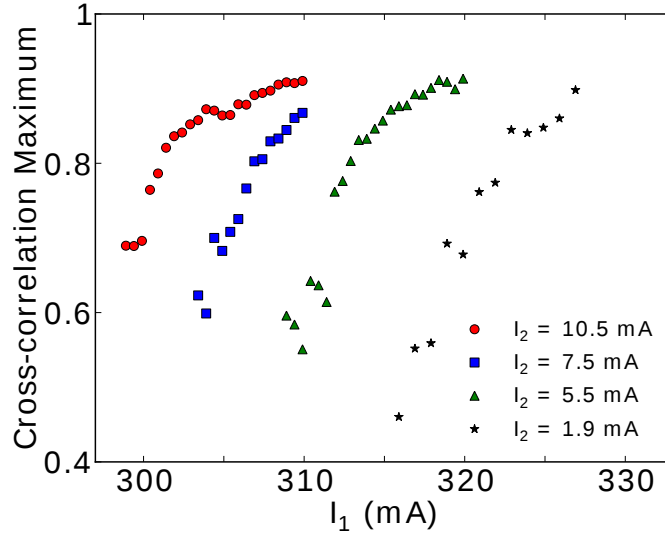


Figure 4.16: Maximum value of the cross-correlation between the signals measured in two different regions of the space: D_1 and D_2 placed as shown in Fig. 4.10. The system parameters are the same as in Figs. 4.6.

4.3.2 Oscillating localized structures

For low amplifier bias current values, (that is when the average period is large and not well defined) time series sometimes present an unexpected dynamical feature, shown on Fig. 4.17. During the interval from 30 to 150 ns, the power measured in D_1 oscillates around some value without ever reaching the background level (the non lasing solution) and correspondingly the power observed in D_2 oscillates without ever reaching the maximum value corresponding to the presence of a localized state. This can be explained by a localized structure which is oscillating around the pinning position. The amplitude of these oscillations increases until at time about 200 ns the localized structure detaches and fully passes in front of D_2 , restoring the regime of mostly periodic nucleation and drift observed previously.

The number of back and forth oscillation events compared to the number of regular drift events seems to depend on the particular configuration. For example they are quite rare in the case of Fig.4.9 indeed they do not clearly appear in the histograms (slight shoulder on the left part of histograms b) and c). While they contribute to reduce the correlation in the case of Fig.4.16.

Localized structures behave as “Aristotelian particles” which means that their velocity (instead of acceleration) is proportional to the external forces (i.e. to an

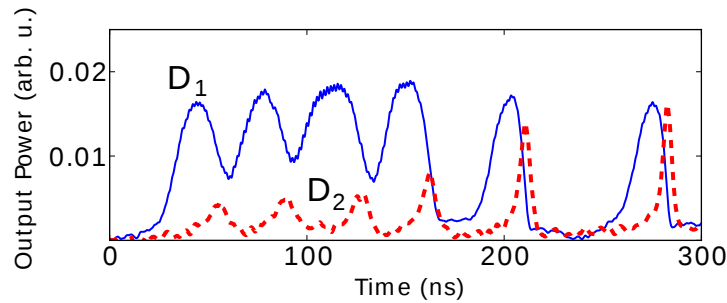


Figure 4.17: Spatially resolved dynamics in two points of space. Localized states oscillate back and forth before drifting away. $I_1 = 298.8$ mA, $I_2 = 10.5$ mA.

applied spatial gradient). Contrary to conservative solitons, their inertia (that is the tendency of a particle to resist any change in its motion) is completely hidden by dissipation [Longhi 1997]. The “Aristotelian” or overdamped character of the LS’s motion has been explained in models of nonlinear optical resonators with driving fields [Firth 1996, Maggipinto 2000].

In [Maggipinto 2000], authors study theoretically the stability of the LS solution with respect to perturbations by evaluating the linearized operator describing deviations from the exact stationary state. Since the LS is a stable solution, all the eigenvalues of this operator have large negative real part, except the ones associated with neutral modes, whose values are zero. Therefore, only the projection of the perturbation on the neutral modes is relevant for the dynamics of LS since the projections on the other modes are strongly damped. The only neutral mode, in the case of driven systems, is the one corresponding to the translational symmetry of the system, thus the effect of any perturbation is to induce a simple translation of the LS, revealing its robustness. When a spatial gradient (for instance in the phase of the driving field) is applied, the LS drifts along the gradient and its velocity results proportional to the gradient itself (see also [Firth 1996]).

Clearly, the back and forth motion of the localized structure which we observed in our system (Fig. 4.17) departs from this “Aristotelian particle” description of localized structure under perturbations. It is understandable that this inertial-like behavior occurs at the very edge of the localized structure’s stability domain where the effects of perturbations are less damped [Maggipinto 2000], and therefore in the parameter range in which the periodicity breaks up and the dynamics is strongly influenced by noise.

4.4 Conclusions

We have shown that the destabilization of the nonlasing solution in a system of coupled broad-area lasers in an absorber-amplifier configuration can occur via stochastic or periodic emission and drift of localized structures. Since this limit cycle

arises with a finite amplitude and zero frequency, the corresponding bifurcation possesses the characteristics required for the generation of excitable localized structures [Izhikevich 2000].

We claim that the randomly emitted pulses, which we have locally measured, are noise triggered excitable localized structures. The excitable behaviour is induced by a local defect, which allows for the nucleation, and by the drift and annihilation which allow the system to relax into its initial resting state. This mechanism for excitability is also discussed by a recent numerical paper: [Parra-Rivas 2013]; and it strongly differs from the case studied in [Gomila 2005] where the excitable localized structures decay on the same spot where they appear.

In addition to noise-triggered excitable localized structures, we have also observed oscillations of localized states around a pinning site. In [Parra-Rivas 2013] authors have observed similar small-amplitude oscillations when the parameters are close to threshold and for large values of the inhomogeneity. This dynamics, which departs from the “Aristotelian particle” description of localized structure’s motion, shows the limits of the low-dimensional description of the nucleation and drift of laser localized states.

Excitable Localized Structures: Numerical Simulations

Contents

5.1	Model and dynamical equations	68
5.2	Self-pulsing cavity solitons	69
5.2.1	Characteristics of the dynamics	71
5.3	Excitable localized structures	72
5.3.1	Response to different perturbations	77
5.4	Conclusions	78

In this chapter, the topic of excitable localized states in a semiconductor laser with saturable absorber (LSA) is considered numerically. Excitable localized structures were first predicted to exist in an optical cavity filled with a Kerr medium which is a system that does not show excitable behavior without spatial extension [Gomila 2005]. In that instance, a local excitable behavior has been observed in presence of an instability of a localized structure. For certain values of the control parameter the LS becomes Hopf unstable, its intensity starts to oscillate while it remains localized in the same region of space [Firth 2002]. As the control parameter is further increased, the limit cycle (originated in the Hopf bifurcation) undergoes a saddle-loop bifurcation which leads to excitability.

The same kind of bifurcation has been remarked in models of laser with saturable absorber without spatial dependence [Plaza 1997, Dubbeldam 1999]. In [Plaza 1997], the system dynamics evolves through the following different regimes by changing the ratio of the characteristic times of the two system variables: non-zero stationary stable output, oscillations around non-zero value (Q-switching-like oscillations [Erneux 1988]) and excitability.

On the other hand LSAs are also able to host localized structures (or cavity solitons) provided that the Fresnel number is high. In lasers with saturable absorber, the formation of CSs was first studied theoretically in the limit of fast materials [Fedorov 1992, Vladimirov 1999, Fedorov 2000]. The existence of laser localized structures in slow materials, such as VCSELs, was demonstrated numerically in models such as [Bache 2005] and [Prati 2007].

In order to look for excitable localized structures, we use the model described in [Bache 2005] and we analyse the response to a local perturbation out of the stability domain of localized structures. The model consider both the passive and active

material to be in the same cavity. Therefore they are more suitable for describing the experiment of the VCSEL with intracavity saturable absorber ([Elsass 2010a]) than the experiment with two VCSELs coupled face-to-face which is studied in this thesis and whose functioning is also based on saturable absorption.

5.1 Model and dynamical equations

The dynamical equations which we analyze are the same as the ones studied in [Bache 2005].

$$\dot{F} = [(1 - i\alpha)D + (1 - i\beta)d - 1]F + i\nabla_{\perp}^2 F \quad (5.1a)$$

$$\dot{D} = -b_1 \left[D(1 + |F|^2) - \mu \right], \quad (5.1b)$$

$$\dot{d} = -b_2 \left[d(1 + s|F|^2) + \gamma \right], \quad (5.1c)$$

The adimensional variables F , D and d are respectively the slow envelop of the electric field, the carrier density of the amplifier medium and the carrier density of the absorber medium. The laplacian operator ∇_{\perp}^2 is the sum of the second partial derivatives respect to the transverse coordinates: $\partial_{xx}^2 + \partial_{yy}^2$ and it represents diffraction in the paraxial approximation. The parameters α , β are the linewidth enhancement factors describing the semiconductor materials; μ and γ are the pump parameters for the active and passive medium; b_1 and b_2 are the ratio of the photon lifetime to the carriers lifetimes for active and passive material, s is the saturation parameter.

The time is rescaled to the cavity lifetime and the transverse coordinates x and y to the diffraction length. This means that, for VCSELs, a time unit (t.u.) is of the order of 10 ps and the spatial unit (s.u.) is of few microns.

In our analysis, contrary to [Bache 2005], the linewidth enhancement factor of the passive medium β is taken different from zero for a more realistic assumption. We also define the quantity r as the ratio between the carrier lifetime of the active and passive material: $r = \frac{\tau_{amp}}{\tau_{abs}} = \frac{b_2}{b_1}$. The parameters r and μ will vary in our studies while the other parameters are kept fixed:

$$\gamma = 0.5, \quad s = 10, \quad \alpha = 2, \quad \beta = 0.2, \quad b_1 = 0.01. \quad (5.2)$$

The dynamical equations are integrated with a split-step method which uses the Runge-Kutta algorithm to solve the non-linear part of the equations and the Fourier transform (FFTW) to integrate the laplacian. The spatial grid is 128×128 pixels wide with periodic boundary conditions.

The consolidated technique to excite CSs in the position (x_0, y_0) is to inject a suitable field for a short period τ_{inj} . We use a field of the form:

$$F_{inj} = |F_{inj}| e^{i(\phi_{inj} + \omega_{inj}t)} e^{-\frac{((x-x_0)^2 + (y-y_0)^2)}{2\sigma_{inj}^2}}. \quad (5.3)$$

That is a field with Gaussian profile in space. $|F_{\text{inj}}|$ is the amplitude; σ_{inj} , the width; ϕ_{inj} , the phase; (x_0, y_0) , the center and ω_{inj} is the frequency. We choose the injection parameters as in [Bache 2005]:

$$x_0 = y_0 = 0, \quad \phi_{\text{inj}} = 0, \quad \omega_{\text{inj}} = 0, \quad \sigma_{\text{inj}} = 3, \quad |F_{\text{inj}}| = 1.5, \quad \tau_{\text{inj}} = 100. \quad (5.4)$$

The position $(x_0, y_0) = (0, 0)$ corresponds to the center of the grid while the frequency $\omega_{\text{inj}} = 0$ corresponds to the cavity resonance.

The peak intensity of the stable CS obtained for $r = 0.45$ is plotted as function of the active material μ in figure 5.1. The homogenous plane-wave solution is also shown for comparison. We were able to switch-on CS in the interval: $1.43 \leq \mu \leq 1.475$. For those values of μ , CSs coexist with the stable homogenous non-lasing solution. For lower values, the CS solution does not survive and the system evolves towards the non-lasing stable state. While for higher values, we find a spatiotemporal turbulence which, for long times, evolves into a regime insufficiently sampled over the numerical grid (the same behaviour was found in [Bache 2005]).

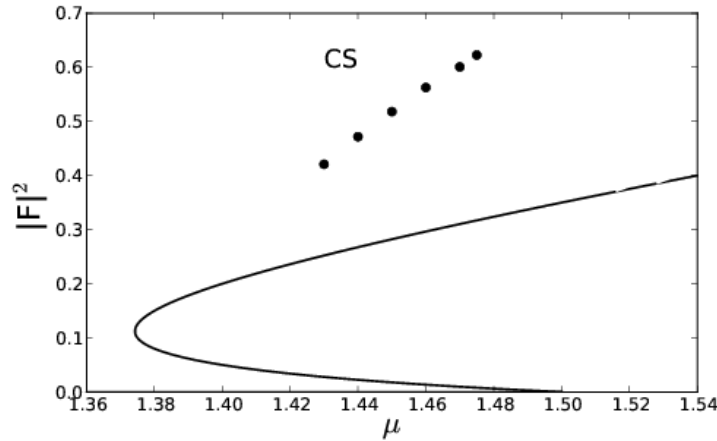


Figure 5.1: Peak intensity of stable stationary cavity solitons (●) for different values of μ , together with the homogenous steady state solution for the intensity $|F|^2$ (solid line). The system parameters are those in Eq. (5.2) with $r = 0.45$. The CSs are switched-on by the injected field in Eq. (5.3) with parameters as in Eq. (5.4). The homogeneous steady state is computed setting the derivatives in the dynamical equations (Eqs. (5.1)) equal to zero. The laser threshold is $\mu = 1.5$.

5.2 Self-pulsing cavity solitons

The stability of CSs depends on our free parameters r and μ .

The stability analysis of the CS solution as function of r and μ has been studied in [Prati 2010] with the model for semiconductor LSA that includes the carrier radiative recombination [Prati 2007]. In [Prati 2010] it is shown that the CS solution has

a C-shape as function of the pump μ . The lower branch is always unstable while the upper branch stability depends on the parameter r . For a given value of μ , the stationary CSs are stable in the interval $r_{\min} < r < r_{\max}$ (see Fig. 5.2) which is below the region where the lasing homogeneous solution is Hopf unstable (upper part of Fig. 5.2). The authors investigate the regime for small values of r ($r < r_{\min}$), they show that there is a drift instability that gives rise to spontaneously moving solitons.

We are interested in the instability that occurs for big values of r . As r is increased, the amplitude of a cavity soliton starts oscillating, the oscillations grow until they reach a critical value after which the amplitude drops down to zero.

We show that there is a range of the parameter r for which these oscillations are stable while remaining localized in space in coexistence with the homogenous non-lasing solution. The stability diagram in the r - μ plane for our equations is displayed

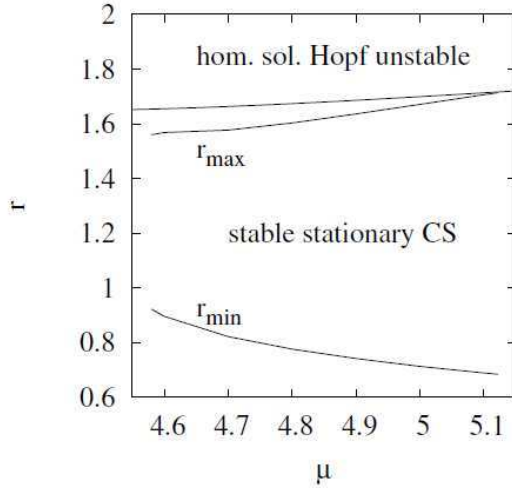


Figure 5.2: Stability diagram of the stationary CS in the plane of the pump parameter (μ) and of the ratio of carrier lifetimes in the active and in the passive medium (r) plane. Stationary CS are stable in the region between the two curves r_{\min} and r_{\max} . The figure is reproduced from [Prati 2010] where the drift instability is studied in the region $r < r_{\min}$.

on the left hand side of Fig. 5.3.

Simulations were done keeping the same parameters (Eq. (5.2)) and for values of μ in the interval $1.43 \leq \mu \leq 1.475$. The boundaries are obtained by observing the different equilibrium states resulting from the simulations.

Stationary CSs are stable in the grey region, beyond the black lines they become unstable and decay into the non-lasing state through a transient of amplitude oscillations which we have previously described. Above $r \approx 0.54$ the homogenous lasing solution is Hopf unstable. This line is traced according to the condition for Hopf instability demonstrated in [Erneux 1988] and also reported on [Bache 2005]: the upper branch is unstable for $\mu < \mu_H$ with $\mu_H = r^2 \gamma s$; which in term of r becomes $r > \sqrt{\mu/\gamma s}$.

Below the red line ($r \approx 0.05$) we also find spontaneously moving CSs which we do not report on in this thesis. We focus our attention on the self-oscillating CS (OCS) instead. Their stability domain is in the region between the black lines which is zoomed-in on the right hand side of Fig. 5.3.

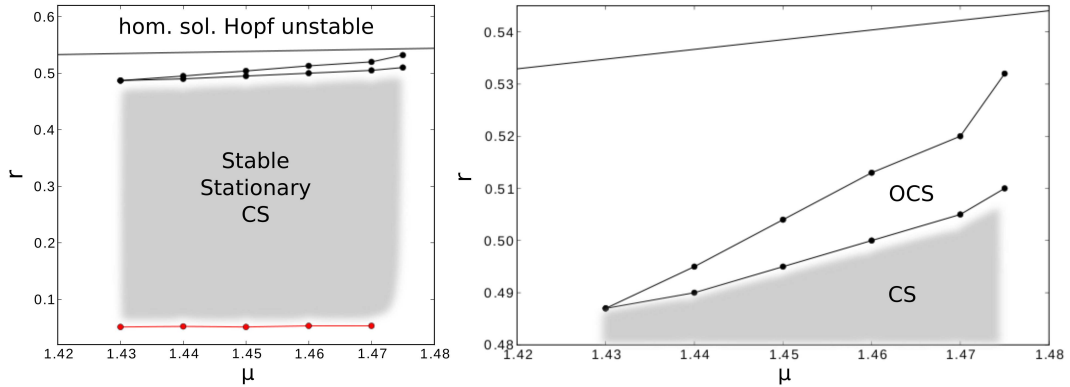


Figure 5.3: Left: stability diagram of the CS solution in the r - μ plane; stationary CSs are stable in the grey region; below that region, the CSs drift on the transverse plane. Right: Zoom of the upper part of the diagram showing the stability domain of the self-oscillating cavity solitons (OCS); below the displayed lower boundary, cavity solitons are stationary; beyond the upper boundary, they decay into the non-lasing state through a transient that consists in increasing-amplitude oscillations.

5.2.1 Characteristics of the dynamics

We characterize the CS's oscillations by measuring the period, the maximum value and the minimum value of the peak oscillations as function of r . The values measured for $\mu=1.45$ are shown in Fig. 5.4. Both the amplitude of the peak oscillations (top) and the period (bottom) increase with r .

For values from 0.48 to 0.492, the cavity soliton is stationary so the intensity is constant. For bigger r the peak intensity, through a transient of increasing-amplitude oscillations, reaches a Q-switching pulsing regime: the intensity is close to zero for most of the time except for short periodic intervals i.e. the pulse width (see inset of Fig. 5.4). The maximum pulse amplitude is eight times the intensity of a stationary CS for $\mu = 1.45$ and it grows as μ increases. The maximum value reached is fourteen times the stationary CS intensity for $\mu = 1.475$.

On the other hand the period behaves in a similar way for different values of μ : it is around 150 t.u. at the onset of the oscillations and it increases abruptly over 300 t.u. when r approaches the upper boundary for the existence of OCS (the last point in Fig. 5.4 is $r = 0.504055$). For higher values of r , the period of the oscillations increases even more but it never reaches a stationary value. After some oscillations (tens in the proximity of the critical value), the OCS switches-off spontaneously. Hence we observe a local bifurcation from an oscillation (OCS) to a fixed point (homogeneous non-lasing state), so our system is a candidate for exhibiting excitability [Izhikevich 2000]. In the next section we effectively demonstrate the existence of a localized excitability.

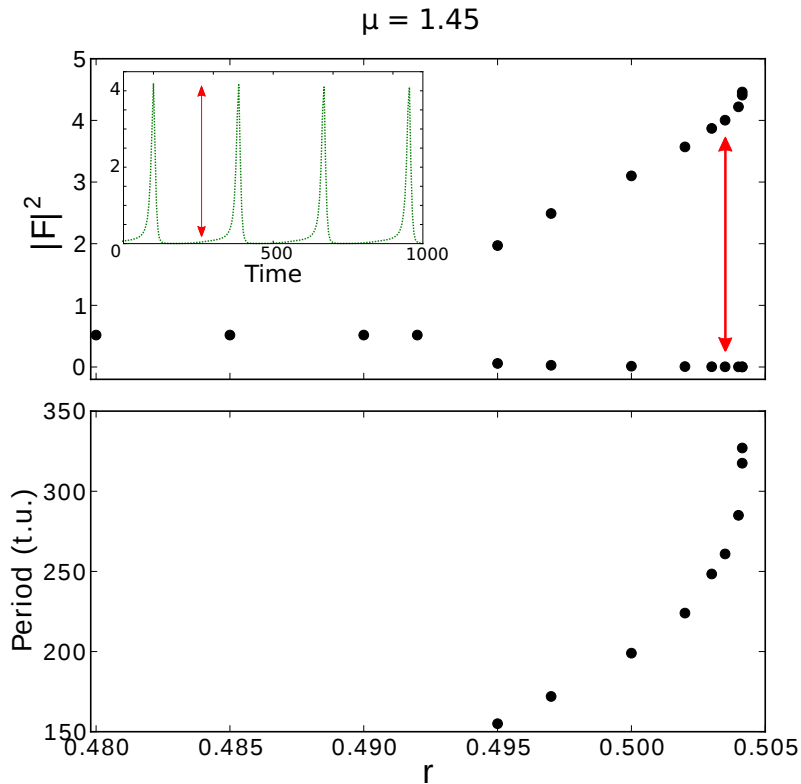


Figure 5.4: Top: maximum and minimum value of the peak-intensity of an oscillating CS as function of r for $\mu = 1.45$. Inset is the time trace for $r = 0.504$. Bottom: corresponding period of the intensity oscillation. Other parameters as in Eq. (5.2).

5.3 Excitable localized structures

Excitability is a feature of a non-linear dynamical system defined by the response to an external perturbation. Perturbations smaller than a characteristic threshold are exponentially damped and the system keeps its stable state. If the perturbation exceeds this threshold, the system performs a large excursion in the phase space before coming back to its initial resting state.

We apply a perturbation to the zero-intensity homogenous solution and we compare the response of the system for three different values of r . One value is within the stability domain of stationary CSs, one within the stability domain of OCSs and another one outside of both stability domains. The three initial conditions are pointed out in the stability diagram on the right hand side of Fig. 5.5.

We use the same perturbation as in Eq. (5.3), the parameters are reported in the caption of Fig. 5.5.

On the left hand side of Fig. 5.5 we display the evolution of the peak intensity in the central point of the applied perturbation. The three different initial conditions

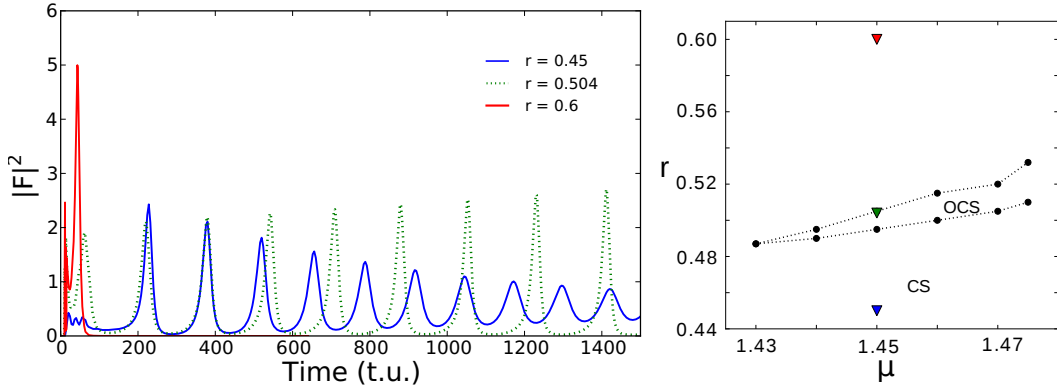


Figure 5.5: Response of system to a local gaussian perturbation for three different values of r : 0.45 (blue), 0.504 (green), 0.6 (red); and $\mu = 1.45$. Left: time evolution of the intensity in the central point of the applied perturbation. Right: three initial conditions (∇) located in the $r - \mu$ plane in comparison with the stability diagram of CS and OCS. Parameters of the perturbation are: $\sigma_{inj} = 3$, $|F|^2 = 2.5$, $\tau_{inj} = 50$ t.u. for $r = 0.45$ and $\tau_{inj} = 5$ t.u. for $r = 0.504, 0.6$; $\omega_{inj} = 0$.

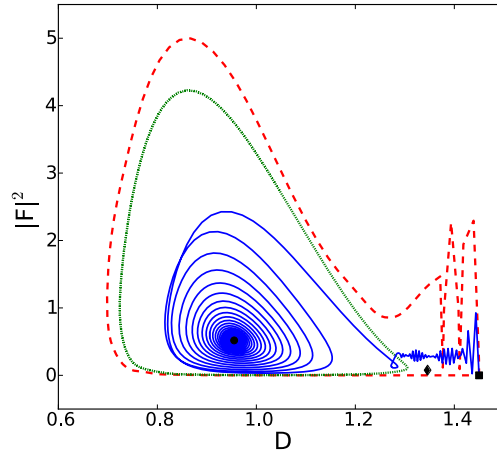
give three different behaviors: i) for $r=0.45$ (blue straight line), the system reaches, through damped oscillations, the CS solution (the process takes about 5000 t.u.) ; ii) for $r=0.504$ (green dotted line), the system goes towards the OCS solution through growing oscillations; iii) for $r=0.6$ (red line), the system emits a short pulse and go back to the zero-intensity solution.

In Fig. 5.6 we illustrate the corresponding trajectories in phase space. We choose to project the phase space onto the $|F|^2 - D$ plane. In cases i) and ii) the system has two attractors: the non-lasing state (black square) and the CS (black circle) in case i); the non-lasing state and the limit cycle i.e. the OCS solution (green dotted lines) in case ii). The system can go from one attractor to the other provided that the applied perturbation makes it go over the saddle point (black diamond). The saddle point corresponds to the unstable CS and it defines the threshold for the perturbation. Its value is reconstructed graphically by measuring the separatrix of the time evolution of both variables (intensity and carrier density of the amplifier) during the switch-on process. When varying the perturbation energy around the threshold value, the separatrix is where the transition from relaxing to the non-lasing solution to the switching to the CS solution takes place.

Eventually the phase portrait in case iii) (red dotted line) presents a geometry typical of excitability. Indeed the system, once it has overtaken the saddle, performs a large trajectory around the limit cycle which is no longer stable and it finally comes back to the stable non-lasing state.

In order to demonstrate that the phenomenon observed in case iii) is an excitable cavity soliton, we investigate the dependence of the response on the injected pulse amplitude and we compare the spatial profile of the emitted pulse with the stationary CS profile.

Figure 5.6: Phase space: intensity ($|F|^2$) vs amplifier carrier-density (D). The trajectories correspond to the simulations of Fig.5.5. The system, initially in the stable non-lasing state (■), goes to the stable CS solution (●) through damped oscillations for $r = 0.45$ (blue straight line), provided the perturbation takes the system beyond the unstable CS (◆). For $r = 0.504$ the system is in a stable limit cycle (green dotted line). For $r = 0.6$, the system performs a large trajectory in the phase space before coming back to the initial stable state (red dashed line).



We notice that, in case iii) ($r = 0.6$), the response to a perturbation can be of two kinds according to the perturbation strength: after a weak perturbation the peak intensity makes a small hump before relaxing to zero (Fig. 5.7 a)); after a strong perturbation a pulse, like the one previously described, is emitted (Fig. 5.7 b)).

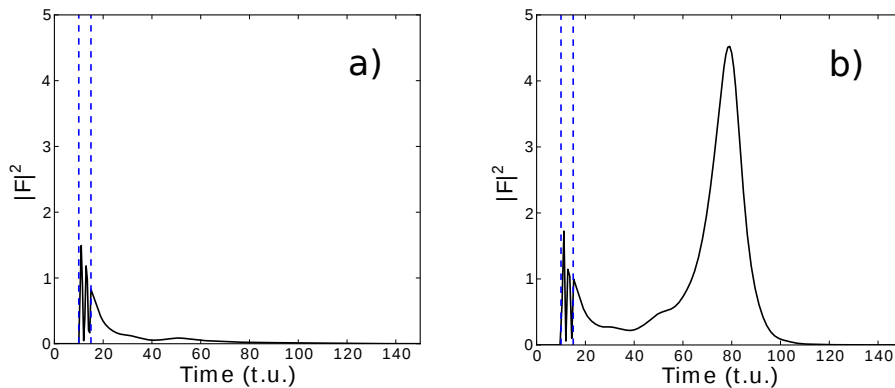


Figure 5.7: Time evolution of the peak intensity in response to a perturbation. For weak perturbations ($|F_{inj}| = 1.7$) the system relaxes into the non-lasing state (a); for strong perturbations ($|F_{inj}| = 2.4$) it performs a large excursion before coming back to non-lasing state (b). The intensity oscillations during the injection (within the blue dashed lines) are attributed to the beating between the perturbation frequency and the CS frequency. $\mu = 1.45$ and $r = 0.6$.

The peak intensity of the emitted pulse as function of the amplitude of the injected perturbation ($|F_{inj}|$), together with the delay between the injected pulse and the pulse emission are depicted in Fig. 5.8. We observe an abrupt transition from quasi-zero intensity to a high intensity response which reveals a threshold-like behaviour. Moreover, the delay becomes larger for amplitudes closer to threshold and

it decreases as the amplitude is increased. This slowing down of the dynamics is also a typical behaviour in the proximity of a threshold. For values of $|F_{inj}|$ above threshold, the pulses are all similar and the peak intensity slightly increases with the perturbation amplitude. The existence of a threshold and the deterministic orbit of the emitted pulse make the observed temporal response consistent with excitability. The class of excitability, according to the classification adopted in neuroscience [Hodgkin 1948, Izhikevich 2007], is not easily determined by the present analysis. There are signatures of class I excitability since the limit cycle seems to disappear through a saddle-loop bifurcation. Indications of this bifurcation come from the fact that the limit cycle in Fig. 5.6 is closed to the collision with the unstable CS, and that its period increases abruptly in the proximity of the bifurcation (see lower panel of Fig. 5.4). But, there is no evidence of class I excitability because the period does not diverge. This ambiguity reveals the complexity of our model. A stability analysis of the CS solution would allow to identify the correct bifurcation diagram that would explain the observed dynamical scenario.

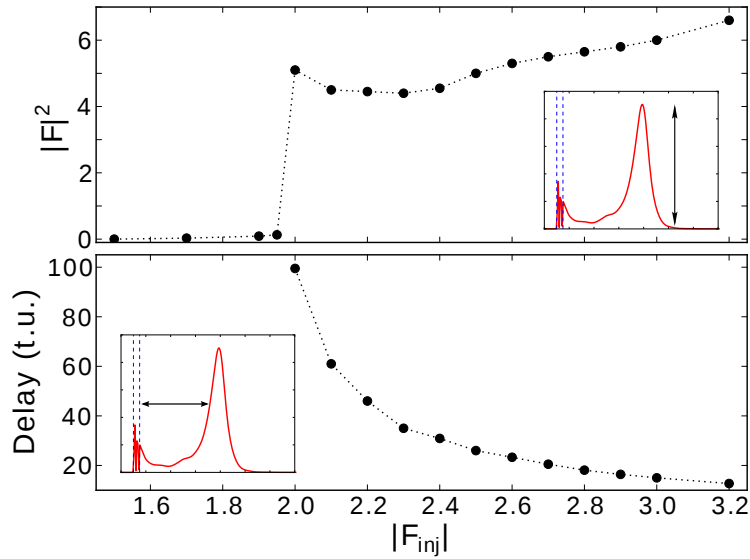


Figure 5.8: Top: amplitude of pulse emitted by the system in response to a perturbation (see inset) as function of the amplitude of the injected-beam $|F_{inj}|$. Bottom: corresponding delay time of the emitted pulse calculated from the end of the injected pulse (see inset). A threshold-like behavior is clearly observed. The parameters of the system are: $\mu = 1.45$, $r = 0.6$ while the other perturbation parameters are: $\tau_{inj} = 5$ t.u. (blue dashed lines in the insets), $\sigma_{inj} = 3$.

The excitable behaviour is found for all the considered values of the pump parameter: $1.43 \leq \mu \leq 1.475$ at $r = 0.6$. The excitability threshold decreases as the current is increased as shown in Fig. 5.9. This can be understood from the fact that for higher pumping of the amplifier, the unstable CS get closer to the

non-lasing solution (they collide at the laser threshold).

The new and interesting aspect is that the excitable behavior is confined in a region

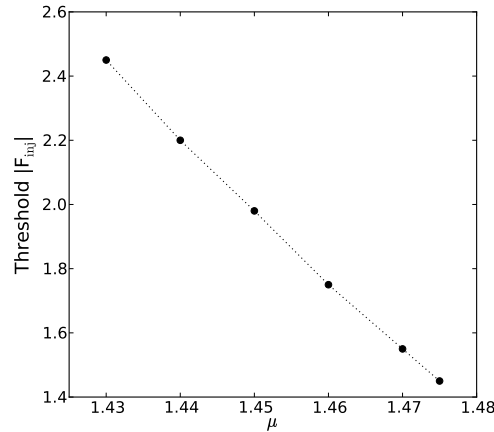


Figure 5.9: The excitability threshold as function of the pump parameter μ ; $r = 0.6$. Parameters of the injection are $\tau_{inj} = 5$ and $\sigma_{inj} = 3$.

of the transverse plane that matches the stationary CS profile. Therefore we claim that we are observing excitable CSs (or excitable localized structures) to distinguish our case from the plane-wave excitable behaviour reported in lasers with saturable absorber [Dubbeldam 1999, Plaza 1997]. In Fig. 5.10 we report the spatial profiles corresponding to the maximum peak intensity of all the three cases analyzed in Figs. 5.5, 5.6. Stationary, oscillating and excitable CSs have the same spatial shape.

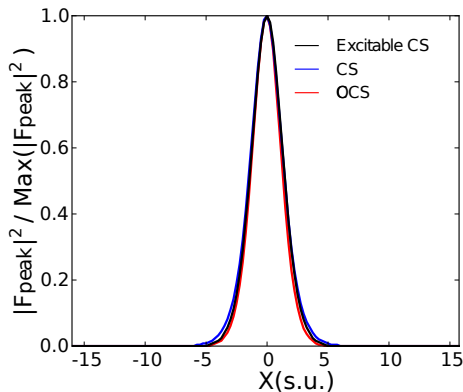


Figure 5.10: Spatial profile obtained by cutting the intensity distribution along a line including the the maximum value of the peak intensity of the stationary ($r = 0.45$), oscillatory ($r = 0.504$) and excitable ($r = 0.6$) CSs. The curves are normalized to their maximum value. No matter what is the temporal behavior, the light emission is localized in the same spatial profile.

5.3.1 Response to different perturbations

In the following we analyze the effect of the spatial width and of the frequency of the perturbation on the excitable response.

First we inject three Gaussian-shaped pulses with different widths: $\sigma_{\text{inj}} = 4, 3, 2$; the field amplitude is adjusted to be at the excitability threshold. The temporal profile of the pulse is square and it is kept constant: $\tau_{\text{inj}} = 5$ t.u. The intensity profile is reported on the left column of Fig.5.11. The narrower is the Gaussian pulse, the more powerful it should be in order to excite the response of the system. Thus the injected energy

$$E_{\text{inj}} = \pi |E_{\text{inj}}|^2 \sigma_{\text{inj}}^2 \tau_{\text{inj}}$$

seems to be the important quantity that determines the threshold. Though we also notice that, when the pulse is larger, the energy that is required to reach the excitability threshold is higher. This suggests that there should be a critical value of the width for which it becomes impossible to trigger excitable CSs. The energies corresponding to the considered perturbations are: $E_{\text{inj}} = 643.4$ for $\sigma_{\text{inj}} = 4$ and $E_{\text{inj}} = 565.5$ for $\sigma_{\text{inj}} = 3, 2$. The time traces and spatial profiles of the system responses are illustrated for comparison in the central and right columns of Fig.5.11.

The temporal behaviours are all quite similar: the peak intensity of the pulse is slightly bigger than 5 and its HWHM is of 13 t.u., only the delay time seems to depend on the perturbation: it grows as the perturbation shrinks. On the other hand, we know that the time delay changes a lot as the perturbations gets close to threshold (as it is observed in the lower panel of Fig. 5.9); then the difference in the delay time can be due to the precision used to determined the threshold which is $\delta|F_{\text{inj}}| = 0.1$.

At last we observe that the spatial profiles at the peak maximum are the same in the three cases. Hence we have shown that excitable localized structures in a laser with saturable absorber can be triggered by input pulses with different widths in contrast to studies about their counterparts in Kerr cavities which use as addressing beam a pulses of a specific form: the one of the unstable localized structure [Gomila 2005, Gomila 2007, Jacobo 2008].

In a second time, we change the injected frequency ω_{inj} , we keep the same injection time as before and we set $\sigma_{\text{inj}} = 3$. So that we can compare the threshold energy for two different frequencies of the perturbation. In the case of stationary CS, the injection at the cavity soliton frequency (ω_{CS}) allows to reduce the energy threshold for the switching respect to the injection at the cavity frequency ($\omega_{\text{inj}} = 0$) [Mahmoud Aghdami 2008]. We show that also in the case of excitable CSs, the energy is significantly reduced.

On the left panel of Fig. 5.12, the spatial intensity profile of the perturbation at threshold is depicted. Compared to the perturbation with the same width and at the cavity frequency (central row of Fig.5.11), it is much weaker. The corresponding energy is $E_{\text{inj}} = 11.1$ that is about fifty times smaller than the threshold previously calculated.

The resulting excitable CS has the same properties as the excitable CS triggered

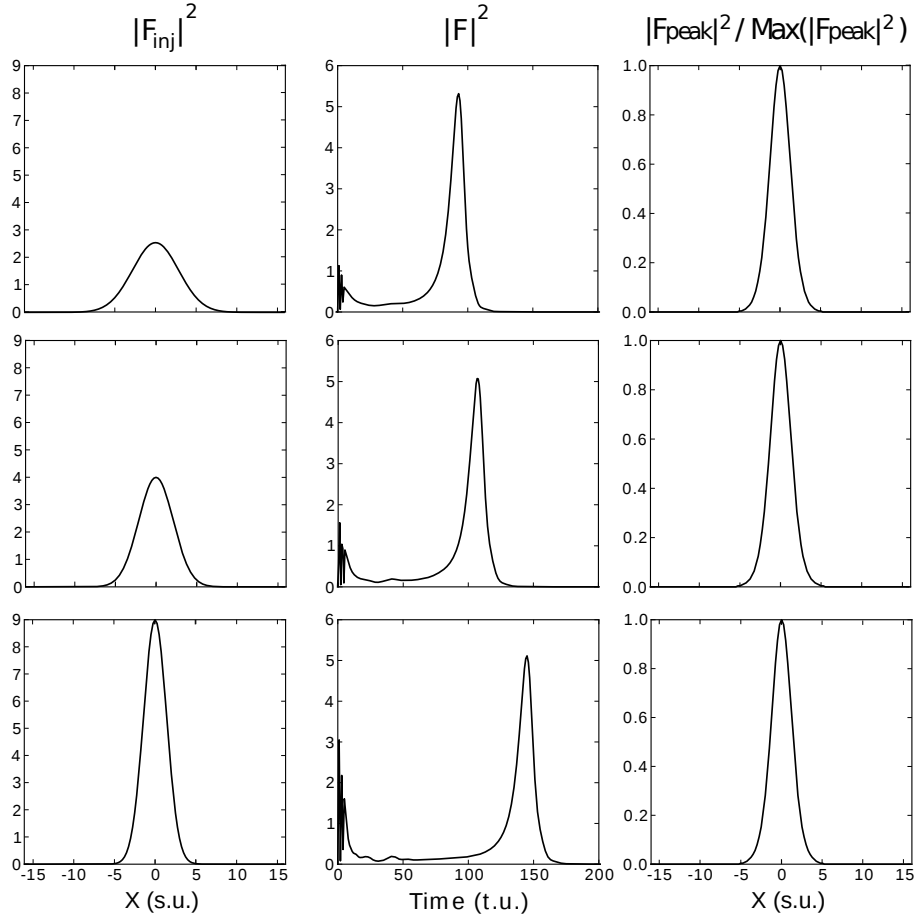


Figure 5.11: Three different injected pulses and the resulting responses. Left column: spatial intensity profiles of the injected Gaussian pulses. Centre column: time evolution of the peak intensity from the beginning of the injection. Right column: normalized spatial intensity profile corresponding to the peak of the excitable response. The injection parameters are: $\sigma_{inj} = 4$ and $|F_{inj}| = 1.6$ (top); $\sigma_{inj} = 3$ and $|F_{inj}| = 2$ (center); $\sigma_{inj} = 2$ and $|F_{inj}| = 3$ (bottom). For all of them $\tau_{inj} = 5$, $\omega_{inj} = 0$.

by a pulse at the cavity frequency as it can be seen from the temporal and spatial profiles on the central and right panels of Fig. 5.12.

5.4 Conclusions

We have studied numerically the stability of cavity solitons in a VCSEL with saturable absorber using the ratio of the carrier lifetimes in the passive and in the active material (r), as control parameter. In a certain parameter region, CSs that develop a Q-switching instability (Oscillatory Cavity Solitons), are found to be stable and to coexist with the homogeneous non-lasing solution.

Beyond the bifurcation from the OCS regime to the non-lasing solution, we have

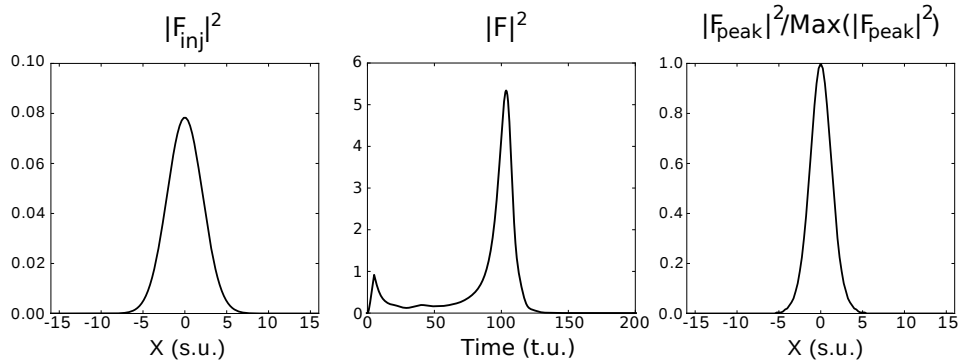


Figure 5.12: Excitable response for $\omega_{inj} = \omega_{CS}$. Left: spatial intensity profile of the injected Gaussian pulse. Centre: time evolution of the intensity from the beginning of the injection. Right: normalized spatial profile corresponding to the peak of the excitable response. The other injection parameters are: $\sigma_{inj} = 3$ and $|F_{inj}| = 0.28$, $\tau_{inj} = 5$.

demonstrated the existence of excitable laser cavity solitons. They appear as a short laser pulse localized in space, they arise from the stable non-lasing state in response to a local perturbation that exceeds a characteristic threshold. After the emission of the pulse, the system is back to the non-lasing stable state. The spatial profile of the emitted pulse matches the profile of stable CSs found in the same system.

Excitable localized structures have been already predicted in an optical cavity filled with a Kerr medium [Gomila 2005]. They represent a new tool in the all-optical processing of information [Jacobo 2010]. We have shown that excitable laser CSs can also be used for pulse reshaping by proving that the shape of the output does not depend on the input. The output also does not depend on the input frequency. We were able to trigger an excitable excitable localized structures with input pulses at the cavity frequency and at the CS frequency. Injection at the CS frequency allows to reduce the energy of the trigger pulse of a factor fifty respect to the injection at the cavity frequency. The results about excitability obtained in our analysis could be reproduced using the pump μ as bifurcation parameter by fixing the value of r in the range of stability of the Oscillatory CSs. A similar bifurcation from periodic oscillations to non-lasing solution would be observed as one decreases the pump parameter. This could be more realistically realized in experiments where the characteristic lifetimes of the system can not be changed.

We already looked for excitable localized structures in the experiment with two coupled VCSELs by studying the response of the system to a local perturbation, when the the pump parameter is set below the stability domain of the CS (see sec. 3.4). The behaviour of the system could not be identified as excitability since no bifurcation to (or from) an oscillating regime was observed. This difference from the numerical analysis is plausibly due to the characteristic lifetimes of the experiment.

Indeed the experiment studied in this thesis differs from the above model since it

has a long external cavity (≈ 30 cm) which allow multimode dynamics and which makes the photon lifetime much longer¹ compared to the photon lifetime in a single VCSEL (10 ps) which is used in our model. Moreover, since the roles of the amplifier and of the absorber are played by identical devices, the carrier lifetime of the absorber and of the amplifier are the same. Therefore in the experiment r is fixed and equal to one whereas in the numerical simulations is always smaller than one.

¹The photon lifetime of a single cavity is proportional to the cavity length, L , and inversely proportional to the logarithm of the cavity mirrors reflectivity, R : $\tau_{ph} = -L/(c \ln(R^2))$. If we consider that, in the compound cavity, the dominant losses are given by the beam-splitter, whose reflectivity is $R \approx 0.8$, the photon lifetime can be reasonably estimated between 1 to 10 ns.

Control of Excitable Pulses in an Optically Injected VCSEL

Contents

6.1	Experimental Set-up	82
6.2	Response to a perturbation	83
6.3	Threshold-like behaviour	85
6.4	Conclusions	86

In this chapter we consider the excitable dynamics in a different system without spatial dependence. The studied system is an optically injected semiconductor laser. In this configuration two lasers (a master and a slave) are coupled in such a way that the light from the master is injected into the cavity of the slave and not vice versa. When the frequencies of the two lasers are sufficiently close, the master field may force the slave field to oscillate at the same frequency and at a fixed relative phase, provided that the injection level is sufficiently high. This system is rich in non-linear dynamics such as multistability, chaos and the focus of our investigations: excitability.

As we have already discussed in the previous chapters, excitability refers to the response of a system to perturbations from a steady state. The excitability in this kind of systems has been so far claimed by analyzing the bifurcation from resting state to periodic emission of pulses [Goulding 2007] and by the observation of random emission of pulses interpreted as noise triggered excitable pulses [Kelleher 2009, Kelleher 2011b]. In [Goulding 2007] authors show that the observed phenomenon can be explained in terms of excitability described by the Adler model [Adler 1973]. In the Adler model, which describes the phase locking of two oscillators, an excitable event consists in a 2π -rotation of the slave phase. This phase change during noise-triggered pulses has been experimentally measured [Kelleher 2009]. More recent works report on multipulse regimes [Kelleher 2011a] and on the evolution of interspike statistics as function of the injection strength [Kelleher 2011b]. Nevertheless excitability, as by definition, have not been demonstrated, since no perturbation has been applied in the system yet.

We study, for the first time at our knowledge, the response to an external perturbation, obtained by modulating the phase of the master field. The experimental set-up is described in the next section. The features of the observed excitable pulses

together with the conditions at which they appear are discussed in sec. 6.2. Finally we study the evolution of the system response under variation of the perturbation's amplitude.

6.1 Experimental Set-up

The experimental set-up is sketched in Fig. 6.1. The MASTER is a tunable edge-emitter semiconductor laser while the SLAVE is a mono-mode small-area VCSEL. An optical isolator (OI) is placed in front of the MASTER in order to preserve the unidirectionality of the coupling.

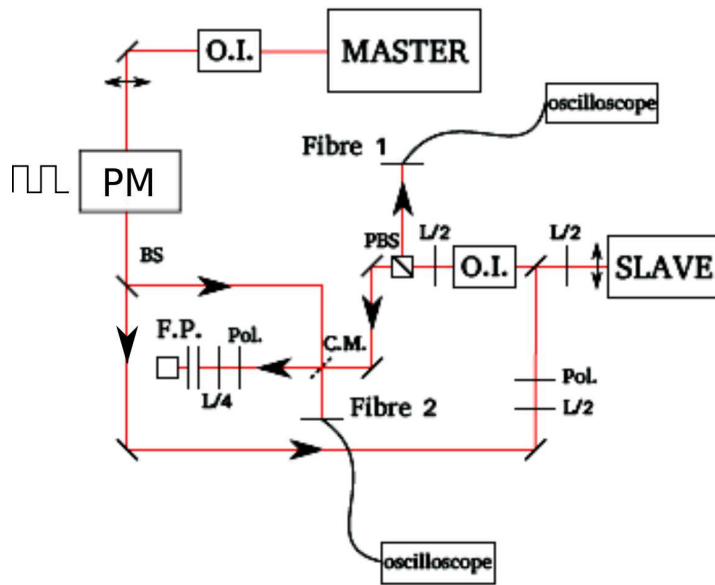


Figure 6.1: Sketch of the experimental set-up adopted to study excitability in a laser with optical injection. PM, phase modulator; OI, optical isolator; FP, Fabry-Perot interferometer; BS, beam splitter; PBS, polarizing beam-splitter; CM, clipping mirror; Pol, polarizer; L/2, half wave plate.[Courtesy of Bruno Garbin, adapted from [Garbin 2012]].

The frequency of the master is kept fixed, we use two parameters in order to achieve the synchronization and to look for the excitable regime: i) the slave current I_S and ii) the injection strength. The slave bias controls the emitted frequency and the power. The slave's threshold is at about $I_S = 0.2$ mA, the emission is linearly polarized until $I_S = 1.8$ mA. Its wavelength at threshold is 978.85 nm for the operating temperature, and it increases as the current is increased with a rate of 0.45 nm/mA. In terms of frequency it corresponds to 140 GHz/mA. The strength of the injection is controlled by turning the half-wave plate in front of the polarizer which is oriented parallel to the main polarization of the SLAVE, just before the beam-splitter.

The phase of the master field can be modulated by applying a square wave voltage into the phase modulator (PM in Fig. 6.1). This means that the phase undergoes

to periodic and abrupt changes with amplitude $\Delta\phi$, which depends on the voltage amplitude. The phase kicks are alternately positive and negative according to the derivative of the square wave and they represent the perturbation. The duration of the perturbation is given by the rise-time of the function generator which is 100 picoseconds. The maximum value of the phase jump that we can achieve is limited by the maximum voltage amplitude provided by our function generator and it is $2/5\pi$.

The signal from the slave goes into two branches of detection in order to monitor the dynamics. In one branch we measure the spectrum with a Fabry-Perot interferometer. The resolution is about 650 MHz. In the other branch we measure the time traces with a resolution of 6 GHz. Both measurements can be done simultaneously.

6.2 Response to a perturbation

In order to find the excitable regime, we look at the spectrum. The excitable regime is in proximity of the locking region for a low level of injection. If we look at the signal from the Fabry-Perot, it is found that when the two lasers are not interacting because their spectra are far apart, the power of the master should be about the 5% of the power of the slave. We consider the master red-tuned compared to the slave (positive detuning). The typical behaviour as I_S is increased is the following: as the frequencies of the two fields get closer, a non-linear interaction takes place and other frequencies appear in the spectrum, the corresponding time-trace reveals a periodic behaviour; for a certain value of the current, the two frequencies lock and the dynamics becomes stationary. The synchronization persists for some values of I_S until the slave is too blue tuned (negative detuning) and the two fields suddenly unlock. As the current is diminished, an hysteresis cycle between locked and unlocked state becomes visible at the edges of the locking region (for both positive and negative detuning). The two cycles may not be symmetric and their widths depend on the injection strength.

The excitable behaviour can be found by perturbing a stationary stable state in the proximity of a bifurcation to a limit cycle. Hence we apply a perturbation when the lasers are synchronized for a value of I_S close to the frequency unlocking. Let us consider the case of positive detuning that is for lower values of I_S . We set the amplitude of the perturbation at its maximum and the period at 30 ns, an example of the resulting temporal dynamics is reported on Fig. 6.2. The system responds in a binary way to the perturbations: when the perturbation is suitable it emits a sub-nanosecond pulse (the zoom of a pulse is depicted in the inset in Fig. 6.2) otherwise it stays in its stationary state. In the figure the pulse is emitted only for positive phase variation, $\Delta\phi$. Because of the noise fluctuations some perturbations may not be effective as the one at 50 ns.

The conditions for excitability described above can be reached for different sets of parameters, for instance by fixing a different master frequency so that the locking occurs at different I_S . We checked that the dynamics does not depend on the

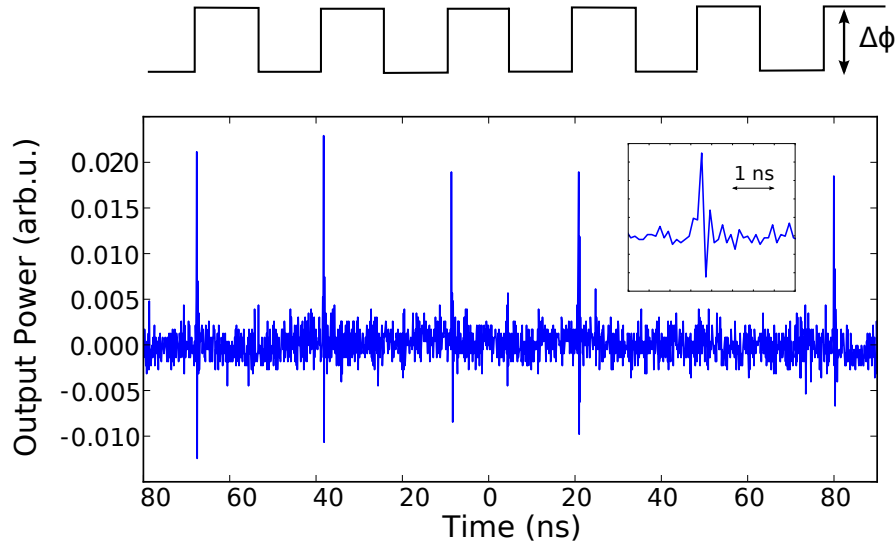


Figure 6.2: Temporal response of the system to a periodic perturbation of the phase $\Delta\phi$. The phase modulation is drawn on top of the figure, its period is 30 ns. The system responds with the emission of pulses all similar to each other (see inset), when the phase kick is suitable (positive in this case and strong enough) or it does not respond (a pulse is missed at 50 ns). $I_S = 1.095$ mA.

polarization.

In Fig. 6.3 we show the evolution of the spectrum as I_S is decreased in order to point out the value at which excitability occurs. The frequency of the master is set to zero. Until $I_S \approx 2.03$ the lasers are unlocked, one harmonic resulting from the interaction

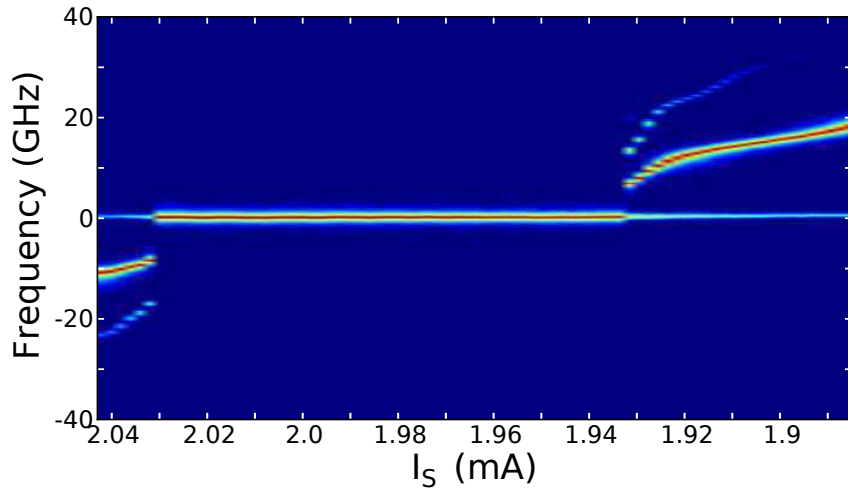


Figure 6.3: Evolution of the spectrum as the current of the slave I_S is decreased. The frequency of the master is set to zero. Excitability occurs at $I_S = 1.935$, close to the locking-unlocking transition. The color scale is logarithmic.

is visible; between 2.03 and 1.93 we recognize the locking region. Beyond 1.93 the lasers are again unlocked and from 1.9 they do not interact anymore. Excitable pulses appear at $I_S = 1.935$. In the next section we study the dynamics for these parameters as function of the amplitude of the perturbation.

6.3 Threshold-like behaviour

In order to be definitely sure that the observed dynamics is excitability it is important to establish the presence of a threshold for the perturbation.

For low amplitudes of the perturbation, the response of the system is not visible (top trace of Fig. 6.4); as $\Delta\phi$ is increased, some of the perturbations start to be effective and are able to trigger pulses (central trace); for higher values almost the totality of the applied perturbations is able to trigger a pulse (bottom trace).

We perform statistics of the amplitude of the emitted pulses over five-thousands perturbations for several values of $\Delta\phi$. The results are illustrated in Fig. 6.5.

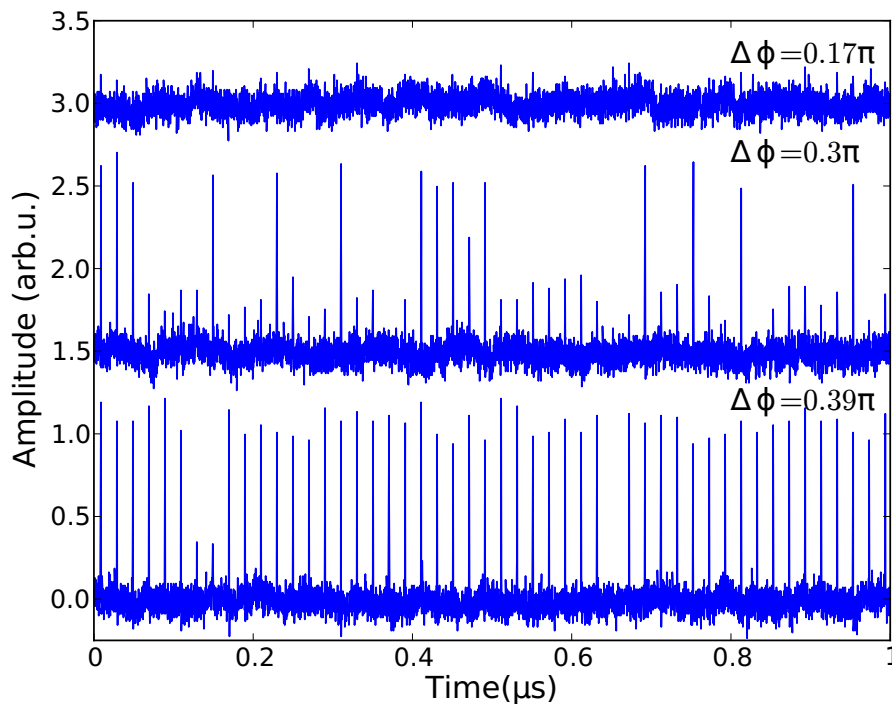


Figure 6.4: Time traces corresponding to periodic perturbations with different amplitudes $\Delta\phi$: below threshold $\Delta\phi = 0.17 \pi$ (top), very close to threshold $\Delta\phi = 0.3 \pi$ (center) and above threshold $\Delta\phi = 0.39 \pi$ (bottom). The signal is normalized respect to the mean value of the excitable pulses. The traces are shifted vertically of 1.5 for clarity. $I_S = 1.935$.

For low values of $\Delta\phi$, the average amplitude is of the order of the detection noise. Then, it increases slightly and linearly up to $\Delta\phi \approx 0.27\pi$. In the interval $0.27\pi < \Delta\phi < 0.32\pi$, the mean peak amplitude has a big excursion. On the other hand the standard deviation reaches a maximum within the same interval. This means that the perturbation has reached a critical value that takes the system close to a separatrix where it is sensitive to fluctuations: either it emits a weak pulse or a strong one (as we can see from the central time trace of Fig. 6.4). We locate the excitable threshold at $\Delta\phi \approx 0.3\pi$.

Beyond this range, the peak amplitude does not depend critically on the perturbation and it does not show big fluctuations.

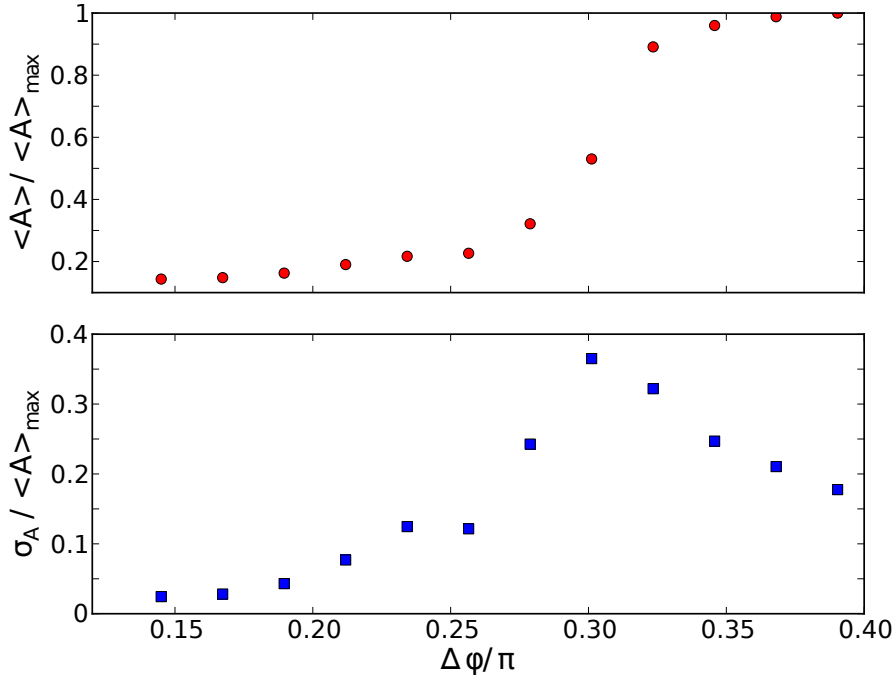


Figure 6.5: Top: mean value of the peak amplitude of the system response as function of $\Delta\phi$. Bottom: corresponding standard deviation. Both curves are normalized respect to the average peak amplitude of the excitable pulses obtained for $\Delta\phi_{\text{MAX}} = 0.39\pi$.

6.4 Conclusions

A laser with optical injection is expected to be able to show excitability [Coullet 1998]. Differently from the studies that have been performed so far in this kind of systems, we experimentally demonstrate the excitability by applying a perturbation. We show that excitable pulses can be triggered by perturbations obtained by modulating the phase of the injection. Moreover the statistics of the

peak amplitude as function of the perturbation amplitude confirms the threshold-like behaviour of the phenomenon. For perturbations lower than the critical value $\Delta\phi \approx 0.3\pi$, the system responds with weak pulses. For bigger values, it emits strong pulses whose average amplitude does not depend critically on the perturbation's one.

Conclusions and Perspectives

The research carried out during the three years of my PhD concerns excitability and laser localized structures (LLS). We studied the separate and simultaneous occurrence of these two nonlinear phenomena in semiconductor-based system.

On the one hand, we looked for excitability in a small-area VCSEL with optical injection (chapter 6). Many theoretical and experimental studies claim that this kind of system can be excitable. None has demonstrated excitability by analyzing the response to an external perturbation. We demonstrated the excitability by performing an experiment which shows the possibility to control the excitable pulses by a phase perturbation, provided that the perturbation is stronger than a certain threshold. Therefore, from a phenomenological point of view, the response of this system to an external perturbation, is analogue to that of a neuron. The experimental system is relatively simple to handle, and thanks to the control that we achieved on the output pulses, it can be used to build more complex experiments such as: the realization of an optical neuronal network, by interconnecting two or more of such devices, and the realization of an optical buffer.

On the other hand, we realized a cavity soliton laser in order to study the properties of coherence and mutual coherence of LLS (chapter 2). Our cavity soliton laser consists in two mutually coupled broad-area VCSELs, placed face-to-face at a distance of thirty centimeters, and its functioning is based on saturable absorption. LLS are localized structures arising from the spontaneous emission noise of the system, thus their phase and frequency are not determined by an external driving field. For what concerns the frequency of LLSs, mode hops between different longitudinal modes of the compound cavity and multi-mode emission have been observed. We also reported on phase hops induced by small changes of the system parameters. Because of the phase profile which has a diameter three times bigger than the intensity profile, interaction between two distant structures is possible. We reported on in-phase and out-of-phase locking between two different localized structures. However, the spatial disorder, caused by defects in the material or in the alignment, plays an important role in the interaction between different structures and it can prevent their locking. Because of that, two LSs that are in the range of the phase interaction (at a distance smaller than three times the LS diameter), may emit on different and very distant longitudinal modes and therefore they appear mutually incoherent.

There is an important thing to be checked in perspective of applications: the control

of LSs by an external beam. We studied the characteristics of the control beam that allow for the most efficient switching with the available power (chapter 3). The switch-on process is favored by parallel polarization respect to the LS's one and by blue-tuned wavelength compared to the LS's one. The necessary energy is of few picojoules. Whereas The switch-off process is favored by crossed polarization and a wavelength that matches the LS's one; moreover, it requires more energy: tens of picojoules. Even though the different characteristics of the writing and erasing beam raise interesting questions about the physical phenomenon occurring during the switching, they limit the ease of use of the control beam which is fundamental for applications. It would be possible to control LSs with the same beam if more power were provided.

Our investigations went beyond the study of LSs in their stable stationary regime with the aim of searching for excitable localized structures. The existence of excitable localized structures was first predicted in a paradigmatic model for a nonlinear cavity. The system described by that model is not excitable, but when spatially extended, it hosts LSs which can exhibit excitable behaviour. This excitability mediated by localized structures was found close to the bifurcation that annihilates the limit cycle constituted by the oscillating localized structure. Excitable localized structures are very interesting for applications since they offer both the parallel mode of operation of localized structures and the threshold-like response of excitable systems.

We numerically demonstrated the existence of excitable localized structures in a model for semiconductor laser with intracavity saturable absorber (chapter 5) by studying the response to a perturbation. The perturbation was applied out of the stability domain of the localized structure. The stationary LS may become unstable as the ratio between the carrier lifetime of the active and of the passive material is changed. For certain values, when the carrier lifetime of the absorber is reduced, we observed oscillating localized structures. In this case the mechanism that originates the limit cycle is the Q-switching instability. Excitable localized structures exist after the bifurcation that annihilates the limit cycle represented by the Q-switched LS.

We showed that excitable localized structures can be used for pulse reshaping since the spatial and temporal shape of the output pulse does not depend on the ones of the input. Future works will involve the analysis of the interactions between different excitable LSs.

We also studied experimentally the response of the system to a local perturbation when the non-lasing solution is stable and the LS is unstable (sec. 3.4 in Chapter 3). Two kinds of responses are distinguishable: after weak or not well-tuned perturbations the system remains in its stable state; after strong and well-tuned perturbations the system locally emits light whose intensity and spatial profile match the LS's ones, and then it decays on the non-lasing state again. We

showed that the events of the latter kind possess features typical of excitability such as threshold-like behaviour and a certain determinism in the return trajectory (the minimal and typical lifetime is about 100 nanoseconds). Nonetheless that cannot be interpreted as excitable behaviour since the emitted pulses were not all identical. Moreover, the excitable response to an external perturbation results from the vicinity in the parameters space to a bifurcation which creates (or annihilates) a limit cycle. Such a bifurcation of a limit cycle, whose features could fit the ones of the observed response, could not be identified.

Differently from the one found in the numerical analysis, the Localized structure of the experiment does not undergo a Q-switching instability, this is probably due to the time scales of the experiment, which do not match the ones of model. As we discussed in the conclusive section of Chapter 5, the main difference consists in the photon lifetime, which in the experiment is about a thousand times the one used in the numerical simulations, because of the long cavity length. Moreover, the carrier lifetimes of the experiment are fixed by the VCSELs constructor. Since the numerical simulations show that an excitable CS occurs for a saturable absorber which is faster compared to the one which gives stable stationary CSs, the employment of a faster saturable absorber in the experiment could be useful for future investigations.

Then, in our experimental search for excitable localized structures, we followed a different approach: we looked for a bifurcation to/from a limit cycle.

We reported on a localized emission of periodic bursts which occurs when the system is misaligned (chapter 4). The bursts are composed of fast pulses (linked to the longitudinal modes interaction) with a slow periodic envelope (the minimum period observed is twenty nanoseconds). We focused our analysis on the slow envelope dynamics. The transition from non-lasing state to periodic emission of pulses occurs through an infinite period and non-zero amplitude bifurcation; in addition, a random emission of pulses with Kramer statistics is observed close to this bifurcation. We showed that this phenomenon can be explained by the nucleation and drift of a localized structure in presence of a defect and a gradient. Since the observed bifurcation has the characteristics required for the generation of excitability, we believe that the observed random generated pulses are noise-triggered excitable localized structures whose excitability is induced by inhomogeneities and drift.

In order to effectively demonstrate the excitability, an external short perturbation should be applied.

In the switch-on transient and in the above described bursts, we could observe unstable trains of short pulses separated by the cavity round trip time. In the future, it will be worth analyzing this fast dynamics which clearly indicates a multimode regime. If a stable phase relationship could be established between the different modes, mode-locking would be realized and the three-dimensional (in space and in time) localization of light would be possible. It is known that the carrier life-

time of the saturable absorber plays an important role in stabilizing mode-locking [Kurtner 1998]. In particular, a fast saturable absorber makes mode-locking more stable against multiple pulse breakup than a slow saturable absorber. Therefore, in order to achieve stable mode-locking with our set-up, one could replace the VCSEL acting as saturable with a faster semiconductor saturable absorber.

A.1 Resonant Saturable Absorber Mirror

This appendix aims to illustrate some features of Resonant Saturable Absorber Mirrors (RSAM).

A RSAM is composed of a semiconductor saturable absorber in between two Bragg reflectors (see Fig.A.1). Hence it is in principle analogous with a VCSEL pumped below transparency as L_2 . The behaviour of a RSAM will be useful to understand the response of L_2 to the WB injection. In particular we are interested in the qualitative dependence of reflectivity on wavelength (Fig. A.2 left) and intensity (Fig.A.2 right).

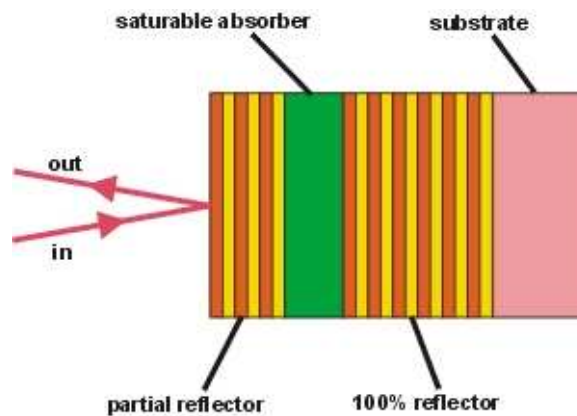


Figure A.1: Scheme of a Resonant Saturable Absorber Mirror (RSAM). Image from <http://www.batop.com>.

For a given value of saturation, the reflection is lower at resonance (1064 nm in Fig.A.2, left) and higher for other wavelengths (up to 100% when the incoming radiation is out of the resonance bandwidth). Moreover, for a given wavelength within the resonance bandwidth, the reflection increases as the absorber comes closer to saturation. Indeed, the RSAM has a low reflectance for weak optical signals and high reflectance for high power signals that are able to saturate the device (see right hand side of Fig.A.2).

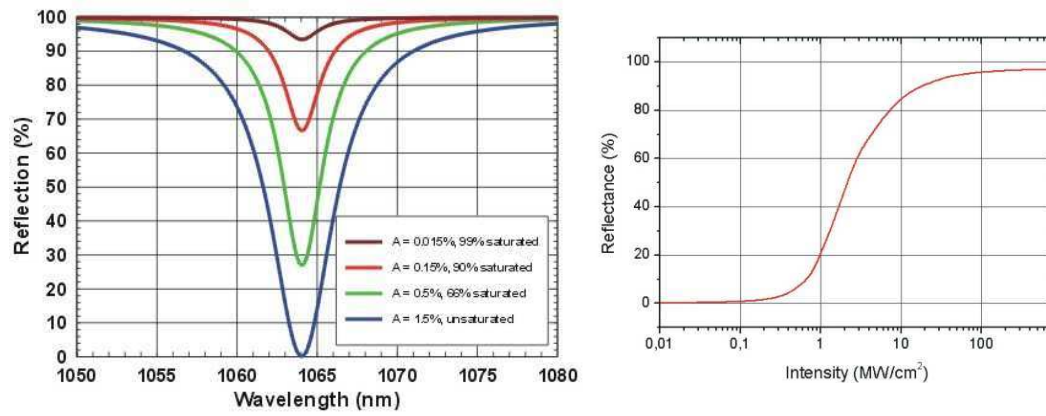


Figure A.2: Left: resonance bandwidth of a RSAM for different saturation levels. Reflection is low within the resonance bandwidth and it increases as the the saturation level increases. Right: reflectance of a RSAM for orthogonal injection at resonance as function of the incident pulse intensity. Images from <http://www.batop.com>

Bibliography

- [Ackemann 2001] T. Ackemann and M. Sondermann. *Characteristics of polarization switching from the low to the high frequency mode in vertical-cavity surface-emitting lasers*. Appl. Phys. Lett., no. 78, page 3574, 2001. (Cited on page 41.)
- [Ackemann 2009] T. Ackemann, W. J. Firth and G. L. Oppo. *Chapter 6 Fundamentals and Applications of Spatial Dissipative Solitons in Photonic Devices*. In Advances in Atomic Molecular and Optical Physics, , volume 57, pages 323 – 421. Academic Press, 2009. (Cited on pages 3 and 23.)
- [Adler 1973] R. Adler. *A study of locking phenomena in oscillators*. Proceedings of the IEEE, vol. 61, pages 1380–1385, 1973. (Cited on page 81.)
- [Astrov 1997] Yu. A. Astrov and Yu. A. Logvin. *Formation of Clusters of Localized States in a Gas Discharge System via a Self-Completion Scenario*. Phys. Rev. Lett., vol. 79, pages 2983–2986, Oct 1997. (Cited on page 1.)
- [Bache 2005] M. Bache, F. Prati, G. Tissoni, R. Kheradmand, L.A. Lugiato, I. Protosenko and M. Brambilla. *Cavity soliton laser based on VCSEL with saturable absorber*. Appl. Phys., vol. B, no. 81, pages 913–920, 2005. (Cited on pages 9, 67, 68, 69 and 70.)
- [Barbay 2006] S. Barbay, L. Leroy I. Sagnes Y. Meñesguen X. Hachair and R. Kuszelewicz. *Incoherent and coherent writing and erasure of cavity solitons in an optically pumped semiconductor amplifier*. Optics Letters, vol. 31, pages 1504–1506, 2006. (Cited on pages 32 and 40.)
- [Barbay 2011] S. Barbay, R. Kuszelewicz and A. M. Yacomotti. *Excitability in a semiconductor laser with saturable absorber*. Optics Letters, vol. 23, no. 23, pages 4476–4478, 2011. (Cited on pages 32 and 48.)
- [Barland 2002] S. Barland, J. R. Tredicce, M. Brambilla, L. A. Lugiato, S. Balle, M. Giudici, T. Maggipinto, L. Spinelli, G. Tissoni, Thomas Knoedl, M. Miller and R. Jager. *Cavity solitons as pixels in semiconductor microcavities*. Nature, vol. 419, pages 699–702, 2002. (Cited on pages 3 and 31.)
- [Barland 2003] Stéphane Barland, Oreste Piro, Massimo Giudici, Jorge R. Tredicce and Salvador Balle. *Experimental evidence of van der Pol–Fitzhugh–Nagumo dynamics in semiconductor optical amplifiers*. Phys. Rev. E, vol. 68, page 036209, Sep 2003. (Cited on page 8.)
- [Belousov 1959] B.P. Belousov. *A periodic reaction and its mechanism*. In Collection of short papers on radiation medicine for 1958. Med.Publ., Moscow, 1959. (Cited on page 4.)

- [Brambilla 1996] M. Brambilla, L. A. Lugiato and M. Stefani. *Interaction and control of optical localized structures*. EPL (Europhysics Letters), vol. 34, no. 2, page 109, 1996. (Cited on page 32.)
- [Brambilla 1997] M. Brambilla, L. A. Lugiato, F. Prati, L. Spinelli and W. J. Firth. *Spatial Soliton Pixels in Semiconductor Devices*. Phys. Rev. Lett., vol. 79, pages 2042–2045, Sep 1997. (Cited on page 3.)
- [Brunstein 2012] Maia Brunstein, Alejandro M. Yacomotti, Isabel Sagnes, Fabrice Raineri, Laurent Bigot and Ariel Levenson. *Excitability and self-pulsing in a photonic crystal nanocavity*. Phys. Rev. A, vol. 85, page 031803, Mar 2012. (Cited on page 8.)
- [Caboche 2009] E. Caboche, S. Barland, M. Giudici, J. Tredicce, G. Tissoni and L. A. Lugiato. *Cavity-soliton motion in the presence of device defects*. Phys. Rev. A, vol. 80, page 053814, Nov 2009. (Cited on pages 23 and 59.)
- [Coullet 1998] P. Coullet, D. Daboussy and J. R. Tredicce. *Optical excitable waves*. Phys. Rev. E, vol. 58, pages 5347–5350, Nov 1998. (Cited on page 86.)
- [Coullet 2004] P. Coullet, C. Reira and C. Tresser. *A new approach to data storage using localized structures*. Chaos, vol. 14, page 193, 2004. (Cited on page 3.)
- [Davidenko 1992] J.M. Davidenko, A.M. Pertsov, R. Salomonsz, W.T. Baxter and J. Jalife. *Stationary and drifting spiral waves of excitation in isolated cardiac muscle*. Nature, vol. 355, pages 349–351, 1992. (Cited on page 4.)
- [Dubbeldam 1999] Johan L. A. Dubbeldam, Bernd Krauskopf and Daan Lenstra. *Excitability and coherence resonance in lasers with saturable absorber*. Phys. Rev. E, vol. 60, pages 6580–6588, Dec 1999. (Cited on pages 32, 67 and 76.)
- [Eguia 2000] M. C. Eguia and G. B. Mindlin. *Distribution of interspike times in noise-driven excitable systems*. Phys. Rev. E, vol. 61, pages 6490–6499, Jun 2000. (Cited on page 57.)
- [Elsass 2010a] T. Elsass, K. Gauthron, G. Beaudoin, I. Sagnes, R. Kuszelewicz and S. Barbay. *Control of cavity solitons and dynamical states in a monolithic vertical cavity laser with saturable absorber*. The European Physical Journal D - Atomic, Molecular, Optical and Plasma Physics, vol. 59, pages 91–96, March 2010. (Cited on page 68.)
- [Elsass 2010b] T. Elsass, K. Gauthron, G. Beaudoin, I. Sagnes, R. Kuszelewicz and S. Barbay. *Fast manipulation of laser localized structures in a monolithic vertical cavity with saturable absorber*. Applied Physics B: Lasers and Optics, vol. 98, pages 327–331, 2010. 10.1007/s00340-009-3748-9. (Cited on pages 4 and 32.)
- [Erneux 1988] T. Erneux. *Q-switching bifurcation in a laser with saturable absorber*. J. Optic. Soc. Am. B, vol. 5, page 1063, May 1988. (Cited on pages 67 and 70.)

- [Faraday 1831] M. Faraday. *On the forms and states assumed by fluids in contact with vibrating elastic surfaces*. Phil. Trans. R. Soc. Lond., vol. 52, pages 319–340, 1831. (Cited on page 1.)
- [Fauve 1990] S. Fauve and O. Thual. *Solitary waves generated by subcritical instabilities in dissipative systems*. Phys. Rev. Lett., vol. 64, pages 282–284, Jan 1990. (Cited on page 16.)
- [Fedorov 1992] S. V. Fedorov and N. N. Rosanov. *Diffraction switching waves and autosolitons in a laser with saturable absorption*. Optics and Spectroscopy, vol. 72, pages 782–785, 1992. (Cited on page 67.)
- [Fedorov 2000] S. V. Fedorov, A. G. Vladimirov, G. V. Khodova and N. N. Rosanov. *Effect of frequency detunings and finite relaxation rates on laser localized structures*. Phys. Rev. E, vol. 61, pages 5814–5824, May 2000. (Cited on pages 60 and 67.)
- [Firth 1996] W. J. Firth and A. J. Scroggie. *Optical Bullet Holes: Robust Controllable Localized States of a Nonlinear Cavity*. Phys. Rev. Lett., vol. 76, pages 1623–1626, Mar 1996. (Cited on pages 3 and 64.)
- [Firth 2002] W.J. Firth, G.K. Harkness, A. Lord, J.M. McSloy, D. Gomila and P. Colet. *Dynamical properties of two-dimensional Kerr cavity solitons*. J. Optic. Soc. Am. B, vol. 19, page 747, April 2002. (Cited on page 67.)
- [Garbin 2012] Bruno Garbin. *étude des rogue waves dans le laser à signal injecté*. Master’s thesis, Université de Nice Sophia Antipolis, June 2012. (Cited on page 82.)
- [Gaspard 1990] Pierre. Gaspard. *Measurement of the instability rate of a far-from-equilibrium steady state at an infinite period bifurcation*. The Journal of Physical Chemistry, vol. 94, no. 1, pages 1–3, 1990. (Cited on page 56.)
- [Genevet 2008] P. Genevet, S. Barland, M. Giudici and J. R. Tredicce. *Cavity Soliton Laser Based on Mutually Coupled Semiconductor Microresonators*. Phys. Rev. Lett., vol. 101, page 123905, Sep 2008. (Cited on pages 4, 9, 11, 13, 14, 16, 32, 33 and 38.)
- [Genevet 2009a] P. Genevet. *Laser à Solitons et Vortex Localisés*. PhD thesis, Université de Nice Sophia Antipolis, 2009. (Cited on pages 11, 22, 38 and 48.)
- [Genevet 2009b] P. Genevet, S. Barland, M. Giudici and J. R. Tredicce. *Stationary localized structures and pulsing structures in a cavity soliton laser*. Phys. Rev. A, vol. 79, page 033819, Mar 2009. (Cited on pages 11, 13 and 22.)
- [Genevet 2010a] P. Genevet, S. Barland, M. Giudici and J. R. Tredicce. *Bistable and Addressable Localized Vortices in Semiconductor Lasers*. Phys. Rev. Lett., vol. 104, page 223902, Jun 2010. (Cited on page 14.)

- [Genevet 2010b] P. Genevet, L. Columbo, S. Barland, M. Giudici, L. Gil and J. R. Tredicce. *Multistable monochromatic laser solitons*. Phys. Rev. A, vol. 81, page 053839, May 2010. (Cited on pages 17 and 45.)
- [Genevet 2010c] P. Genevet, M. Turconi, S. Barland, M. Giudici and J. R. Tredicce. *Mutual coherence of laser solitons in coupled semiconductor resonators*. The European Physical Journal D - Atomic, Molecular, Optical and Plasma Physics, vol. 59, pages 109–114, 2010. 10.1140/epjd/e2010-00138-0. (Cited on pages 17, 22 and 25.)
- [Giudici 1997] M. Giudici, C. Green, G. Giacomelli, U. Nespolo and J. R. Tredicce. *Andronov bifurcation and excitability in semiconductor lasers with optical feedback*. Phys. Rev. E, vol. 55, pages 6414–6418, Jun 1997. (Cited on page 8.)
- [Gomila 2005] Damià Gomila, Manuel A. Matías and Pere Colet. *Excitability Mediated by Localized Structures in a Dissipative Nonlinear Optical Cavity*. Phys. Rev. Lett., vol. 94, page 063905, Feb 2005. (Cited on pages 8, 51, 65, 67, 77 and 79.)
- [Gomila 2007] Damià Gomila, Adrian Jacobo, Manuel A. Matías and Pere Colet. *Phase-space structure of two-dimensional excitable localized structures*. Phys. Rev. E, vol. 75, page 026217, Feb 2007. (Cited on pages 50 and 77.)
- [Gorecka 2006] J. Gorecka and J. Gorecki. *Multiargument logical operations performed with excitable chemical medium*. J. Chem. Phys., vol. 124, page 084101, 2006. (Cited on page 5.)
- [Goulding 2007] D. Goulding, S. P. Hegarty, O. Rasskazov, S. Melnik, M. Hartnett, G. Greene, J. G. McInerney, D. Rachinskii and G. Huyet. *Excitability in a Quantum Dot Semiconductor Laser with Optical Injection*. Phys. Rev. Lett., vol. 98, page 153903, Apr 2007. (Cited on pages 8 and 81.)
- [Gray 2012] R.A. Gray, J. Jalife, Panfilov A., W.T. Baxter, C. Cabo, Davidenko J.M. and A.M. Pertsov. *Nonstationary Vortexlike Reentrant Activity as a Mechanism of Polymorphic Ventricular Tachycardia in the Isolated Rabbit Heart*. Circulation, vol. 91, pages 2454–2469, 2012. (Cited on page 4.)
- [Grelu 2012] P. Grelu and N. Akhmeidev. *Dissipative solitons for mode-locked lasers*. Nature Photonics, vol. 6, pages 84–92, 2012. (Cited on page 2.)
- [Hachair 2004] Xavier Hachair, Stéphane Barland, Luca Furfaro, Massimo Giudici, Salvador Balle, Jorge R. Tredicce, Massimo Brambilla, Tommaso Maggipinto, Ida M. Perrini, Giovanna Tissoni and Luigi Lugiato. *Cavity solitons in broad-area vertical-cavity surface-emitting lasers below threshold*. Phys. Rev. A, vol. 69, page 043817, Apr 2004. (Cited on pages 3 and 31.)

- [Hänggi 1990] Peter Hänggi, Peter Talkner and Michal Borkovec. *Reaction-rate theory: fifty years after Kramers*. Rev. Mod. Phys., vol. 62, pages 251–341, Apr 1990. (Cited on page 57.)
- [Hodgkin 1948] A.L. Hodgkin. *The local electric changes associated with repetitive action in a non-medullated axon*. J. of Physiology, vol. 107, pages 165–181, 1948. (Cited on pages 6 and 75.)
- [Hodgkin 1952] A.L. Hodgkin, A.F. Huxley and B. Katz. *Measurements of current-voltage relations in the membrane of the giant axon of loligo*. Journal of Physiology, vol. 116, pages 341 – 347, 1952. (Cited on page 4.)
- [Izhikevich 2000] M. Izhikevich. *Neural excitability, spiking, and bursting*. International Journal of Bifurcation and Chaos, vol. 10, pages 1171–1266, 2000. (Cited on pages 65 and 71.)
- [Izhikevich 2007] M. Izhikevich. MIT press, 2007. (Cited on pages 8, 56 and 75.)
- [Jacobo 2008] Adrian Jacobo, Damià Gomila, Manuel A. Matias and Pere Colet. *Effects of a localized beam on the dynamics of excitable cavity solitons*. Phys. Rev. A, vol. 78, page 053821, Nov 2008. (Cited on pages 8 and 77.)
- [Jacobo 2010] A. Jacobo, D. Gomila, P. Colet and M.A. Matias. *All optical logical operation using excitable cavity solitons*. Photonics Society Winter Topicals Meeting Series (WTM), vol. 10, pages 122–123, 2010. (Cited on pages 51 and 79.)
- [Jacobo 2012] A. Jacobo, D. Gomila, M.A. Matias and P. Colet. *Logical operations with localized structuresgomi*. New Journal Physics, vol. 14, page 013040, 2012. (Cited on page 9.)
- [Kelleher 2009] B. Kelleher, D. Goulding, S. P. Hegarty, G. Huyet, Ding-Yi Cong, A. Martinez, A. Lemaitre, A. Ramdane, M. Fischer, F. Gerschütz and J. Koeth. *Excitable phase slips in an injection-locked single-mode quantum-dot laser*. Opt. Lett., vol. 34, no. 4, pages 440–442, Feb 2009. (Cited on page 81.)
- [Kelleher 2011a] B. Kelleher, C. Bonatto, G. Huyet and S. P. Hegarty. *Excitability in optically injected semiconductor lasers: Contrasting quantum-well- and quantum-dot-based devices*. Phys. Rev. E, vol. 83, page 026207, Feb 2011. (Cited on page 81.)
- [Kelleher 2011b] B. Kelleher, D. Goulding, G. Huyet, E. A. Viktorov, T. Erneux and S. P. Hegarty. *Dimensional signature on noise-induced excitable statistics in an optically injected semiconductor laser*. Phys. Rev. E, vol. 84, page 026208, Aug 2011. (Cited on page 81.)

- [Keller 2006] U. Keller and A.C. Tropper. *Passively modelocked surface-emitting semiconductor lasers*. Physics Reports, vol. 429, pages 67–120, 2006. (Cited on page 21.)
- [Kerner 1994] B.S. Kerner and V.V. Osipov. Kluwer academic publishers, 1994. (Cited on page 1.)
- [Koga 1980] S. Koga and Y. Kuramoto. *Localized patterns in reaction-diffusion systems*. Progress of Theoretical Physics, vol. 63, pages 106–121, 1980. (Cited on page 1.)
- [Kramers 1940] H.A. Kramers. *Brownian motion in a field of force and the diffusion model of chemical reactions*. Physica, vol. 7, no. 4, pages 284 – 304, 1940. (Cited on page 57.)
- [Kuhnert 1989] L. Kuhnert, K.I. Agladze and V.I. Krinsky. *Brownian motion in a field of force and the diffusion model of chemical reactions*. Nature, vol. 337, pages 337 – 339, 1989. (Cited on page 5.)
- [Kurtner 1998] F.X. Kurtner, J.A. der Au and U. Keller. *Mode-locking with slow and fast saturable absorbers-what's the difference?* Selected Topics in Quantum Electronics, IEEE Journal of, vol. 4, no. 2, pages 159–168, 1998. (Cited on page 92.)
- [Kuszelewicz 2000] R. Kuszelewicz, I. Ganne, I. Sagnes, G. Sleky and M. Brambilla. *Optical Self-Organization in Bulk and Multiquantum Well GaAlAs Microresonators*. Phys. Rev. Lett., vol. 84, pages 6006–6009, Jun 2000. (Cited on page 23.)
- [Larotonda 2002] Miguel A. Larotonda, Alejandro Hnilo, Jorge M. Mendez and Alejandro M. Yacomotti. *Experimental investigation on excitability in a laser with a saturable absorber*. Phys. Rev. A, vol. 65, page 033812, Feb 2002. (Cited on page 32.)
- [Laughlin 1983] D. W. Mc Laughlin, J. V. Moloney and A. C. Newell. *Solitary Waves as Fixed Points of Infinite-Dimensional Maps in an Optical Bistable Ring Cavity*. Phys. Rev. Lett., vol. 51, pages 75–78, Jul 1983. (Cited on page 1.)
- [Lioubashevski 1999] O. Lioubashevski, Y. Hamiel, A. Agnon, Z. Reches and J. Fineberg. *Oscillons and Propagating Solitary Waves in a Vertically Vibrated Colloidal Suspension*. Phys. Rev. Lett., vol. 83, pages 3190–3193, Oct 1999. (Cited on pages 1 and 2.)
- [Longhi 1997] S. Longhi. *Perturbation of parametrically excited solitary waves*. Phys. Rev. E, vol. 55, pages 1060–1070, Jan 1997. (Cited on page 64.)
- [Lugiato 2003] L.A. Lugiato. *Introduction to the Special Issue on Cavity Solitons*. IEEE J. Quantum Electron., vol. 39, page 193, 2003. (Cited on page 13.)

- [Maggipinto 2000] T. Maggipinto, M. Brambilla, G. K. Harkness and W. J. Firth. *Cavity solitons in semiconductor microresonators: Existence, stability, and dynamical properties*. Phys. Rev. E, vol. 62, pages 8726–8739, Dec 2000. (Cited on page 64.)
- [Mahmoud Aghdami 2008] K. Mahmoud Aghdami, F. Prati, P. Caccia, G. Tissoni, L. A. Lugiato, R. Kheradmand and H. Tajalli. *Comparison of different switching techniques in a cavity soliton laser*. The European Physical Journal D - Atomic, Molecular, Optical and Plasma Physics, vol. 47, pages 447–455, 2008. 10.1140/epjd/e2008-00069-3. (Cited on pages 32, 49 and 77.)
- [Marino 2005] Francesco Marino and Salvador Balle. *Excitable Optical Waves in Semiconductor Microcavities*. Phys. Rev. Lett., vol. 94, page 094101, Mar 2005. (Cited on page 8.)
- [Michealis 1998] D. Michealis, U. Peschel and F. Lederer. *Incoherent switching between multistable cavity solitons in a semiconductor optical resonator*. Optics Letters., vol. 23, pages 337–339, Sep 1998. (Cited on page 32.)
- [Parra-Rivas 2013] P. Parra-Rivas, D. Gomila, M. A. Matías and P. Colet. *Dissipative Soliton Excitability Induced by Spatial Inhomogeneities and Drift*. Phys. Rev. Lett., vol. 110, page 064103, Feb 2013. (Cited on page 65.)
- [Paulau 2012] P. V. Paulau, C. McIntyre, Y. Noblet, N. Radwell, W. J. Firth, P. Colet, T. Ackemann and G.-L. Oppo. *Adler Synchronization of Spatial Laser Solitons Pinned by Defects*. Phys. Rev. Lett., vol. 108, page 213904, May 2012. (Cited on pages 26 and 27.)
- [Pedaci 2005] F. Pedaci, G. Tissoni, S. Barland, M. Giudici and J. R. Tredicce. *Mapping local defects of extended media using localized structures*. Applied Physics Letters, vol. 93, page 111104, Sept. 2005. (Cited on page 3.)
- [Pedaci 2006] F. Pedaci, P. Genevet, S. Barland, M. Giudici and J. R. Tredicce. *Positioning cavity solitons with a phase mask*. Applied Physics Letters, vol. 89, page 221111, 2006. (Cited on page 3.)
- [Pedaci 2008] F. Pedaci, E Barland S.and Caboche, P. Genevet, M. Giudici, J.R. Tredicce, T. Ackemann, A.J. Scroggie, W.J. Firth, G.L. Oppo, G. Tissoni and R. Jäger. *All-optical delay line based on semiconductor cavity solitons*. Applied Physics Letters, vol. 92, page 011101, 2008. (Cited on page 3.)
- [Plaza 1997] F. Plaza, M. G. Velarde, F. T. Arecchi, S. Boccaletti, M. Ciofini and R. Meucci. *Excitability following an avalanche-collapse process*. EPL (Europhysics Letters), vol. 38, no. 2, page 85, 1997. (Cited on pages 8, 32, 67 and 76.)
- [Prati 2007] F. Prati, P. Caccia, G. Tissoni, L.A. Lugiato, K. Mahmoud Aghdami and H. Tajalli. *Effects of carrier radiative recombination on a VCSEL-based*

- cavity soliton laser*. Applied Physics B, vol. 88, pages 405–410, 2007. (Cited on pages 67 and 69.)
- [Prati 2010] F. Prati, G. Tissoni, L. A. Lugiato, K. M. Aghdami and M. Brabilla. *Spontaneously moving solitons in a cavity soliton laser with circular section*. The European Physical Journal D - Atomic, Molecular, Optical and Plasma Physics, vol. 59, pages 73–79, 2010. (Cited on pages 69 and 70.)
- [Radwell 2010] N. Radwell, C. McIntyre, A.J. Scroggie, G.L. Oppo, W.J. Firth and T. Ackemann. *Switching partial dissipative solitons in a VCSEL with frequency selective feedback*. The European Physical Journal D - Atomic, Molecular, Optical and Plasma Physics, vol. 59, pages 121–131, 2010. (Cited on page 39.)
- [Rosanov 1990] N. N. Rosanov and G.V. Khodova. *Diffractional autosolitons in nonlinear interferometers*. J. Opt. Soc. Am. B, vol. 7, pages 1057–1065, 1990. (Cited on page 1.)
- [Rosanov 2002] N.N. Rosanov. Springer, 2002. (Cited on pages 23 and 60.)
- [Steinbeck 1995] O. Steinbeck, A. Tóth and K. Showalter. *Navigating complex labyrinths: optimal paths from chemical waves*. Science, vol. 267, pages 868 – 871, 1995. (Cited on page 5.)
- [Strogatz 1994] S. Strogatz. Nonlinear dynamics and chaos. Addison-Wesley Reading MA, 1994. (Cited on page 56.)
- [Tanguy 2007] Y. Tanguy, T. Ackemann and R. Jäger. *Characteristics of switching dynamics in a semiconductor-based cavity-soliton laser*. Optics Express, vol. 15, pages 16773–16780, 2007. (Cited on page 39.)
- [Tanguy 2008a] Y. Tanguy, T. Ackemann, W. J. Firth and R. Jäger. *Realization of a Semiconductor-Based Cavity Soliton Laser*. Phys. Rev. Lett., vol. 100, page 013907, Jan 2008. (Cited on page 4.)
- [Tanguy 2008b] Y. Tanguy, N. Radwell, T. Ackemann and R. Jäger. *Characteristics of cavity solitons and drifting excitations in broad-area vertical-cavity surface-emitting lasers with frequency-selective feedback*. Phys. Rev. A, vol. 78, page 023810, Aug 2008. (Cited on pages 21 and 24.)
- [Taranenko 1997] V. B. Taranenko, K. Staliunas and C. O. Weiss. *Spatial soliton laser: Localized structures in a laser with a saturable absorber in a self-imaging resonator*. Phys. Rev. A, vol. 56, pages 1582–1591, Aug 1997. (Cited on page 33.)
- [Umbanhowar 1996] P.B. Umbanhowar, F. Melo and L. Harry. *Localized excitations in a vertically vibrated granular layer*. Nature, vol. 382, pages 793–796, 1996. (Cited on pages 1 and 2.)

- [Vahed 2011] H. Vahed, R. Kheradmand, H. Tajalli, G. Tissoni, L. A. Lugiato and F. Prati. *Phase-mediated long-range interactions of cavity solitons in a semiconductor laser with a saturable absorber*. Phys. Rev. A, vol. 84, page 063814, Dec 2011. (Cited on pages 16, 17, 25 and 27.)
- [van Exter 1997] M. P. van Exter, A. K. Jansen van Doorn and J. P. Woerdman. *Electro-optic effect and birefringence in semiconductor vertical-cavity lasers*. Phys. Rev. A, vol. 56, pages 845–853, Jul 1997. (Cited on page 41.)
- [Vladimirov 1999] A. G. Vladimirov, S. V. Fedorov, N. A. Kaliteevskii, G.V. Khodova and N.N. Rosanov. *Numerical investigation of laser localized structures*. Journal of Optics B, vol. 1, pages 101–106, 1999. (Cited on page 67.)
- [Vladimirov 2001] A. G. Vladimirov, G. V. Khodova and N. N. Rosanov. *Stable bound states of one-dimensional autosolitons in a bistable laser*. Phys. Rev. E, vol. 63, page 056607, Apr 2001. (Cited on page 25.)
- [Winfree 1972] A.T. Winfree. *Spiral waves of chemical activity*. Science, vol. 175, pages 634–636, 1972. (Cited on page 4.)
- [Winfree 1973] A.T. Winfree. *Scroll-shaped waves of chemical activity in three dimensions*. Science, vol. 181, pages 937–939, 1973. (Cited on page 4.)
- [Yacomotti 1999] A. M. Yacomotti, M. C. Eguia, J. Aliaga, O. E. Martinez, G. B. Mindlin and A. Lipsich. *Interspike Time Distribution in Noise Driven Excitable Systems*. Phys. Rev. Lett., vol. 83, pages 292–295, Jul 1999. (Cited on page 57.)
- [Yacomotti 2004] A. M. Yacomotti, L. Furfaro, X. Hachair, F. Pedaci, M. Giudici, J. Tredicce, J. Javaloyes, S. Balle, E. A. Viktorov and Paul Mandel. *Dynamics of multimode semiconductor lasers*. Phys. Rev. A, vol. 69, page 053816, May 2004. (Cited on pages 21 and 24.)
- [Zhabotinsky 1964] A.M. Zhabotinsky. *Periodical oxidation of malonic acid in solution (a study of the Belousov reaction kinetics)*. Biofizika, vol. 9, pages 306–311, 1964. (Cited on page 4.)
- [Zhabotinsky 1973] A.M. Zhabotinsky and A.N. Zaikin. *Autowave processes in a distributed chemical system*. J. Theor. Biol., vol. 40, pages 45–61, 1973. (Cited on page 4.)